

Design of Quasi-periodic and Aperiodic Array Lattices to Improve Array Antenna Performance

by

PRATIK MEVADA
(201721006)

A Thesis Submitted in Partial Fulfilment of the Requirements for the Degree of

DOCTOR OF PHILOSOPHY

to

DHIRUBHAI AMBANI INSTITUTE OF INFORMATION AND COMMUNICATION TECHNOLOGY

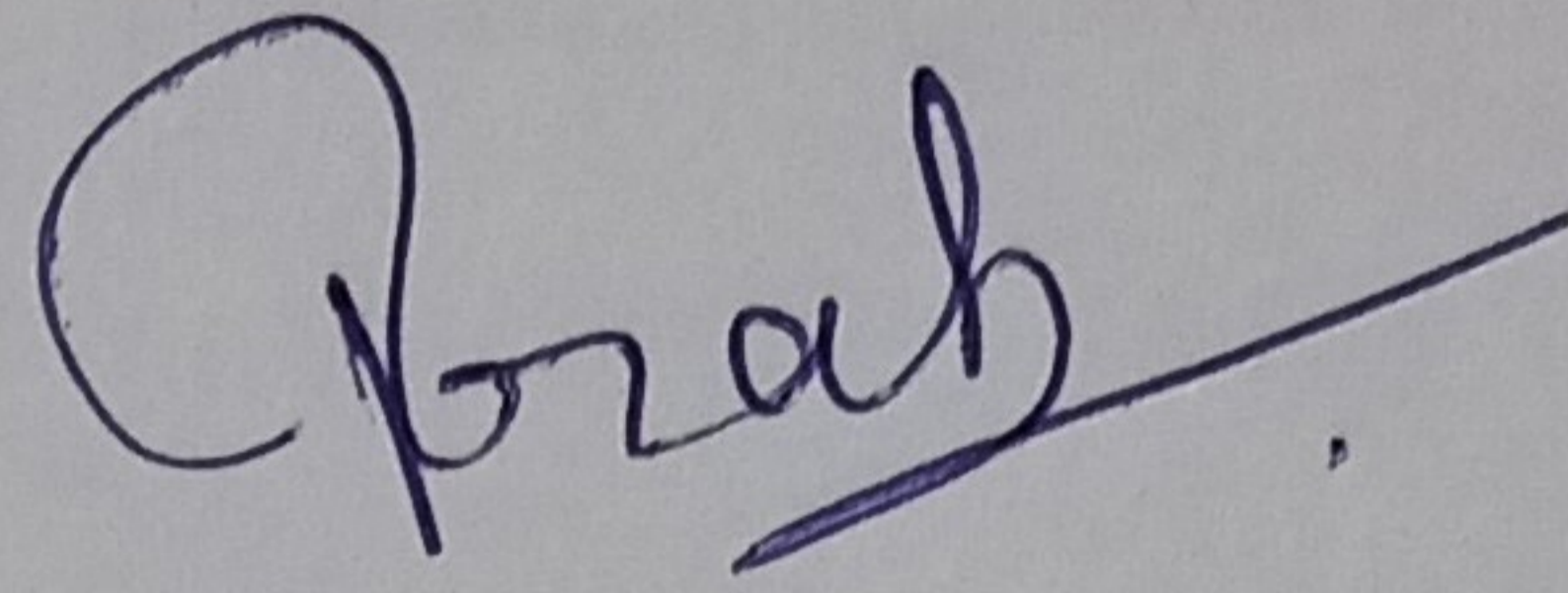


March, 2023

Declaration

I hereby declare that

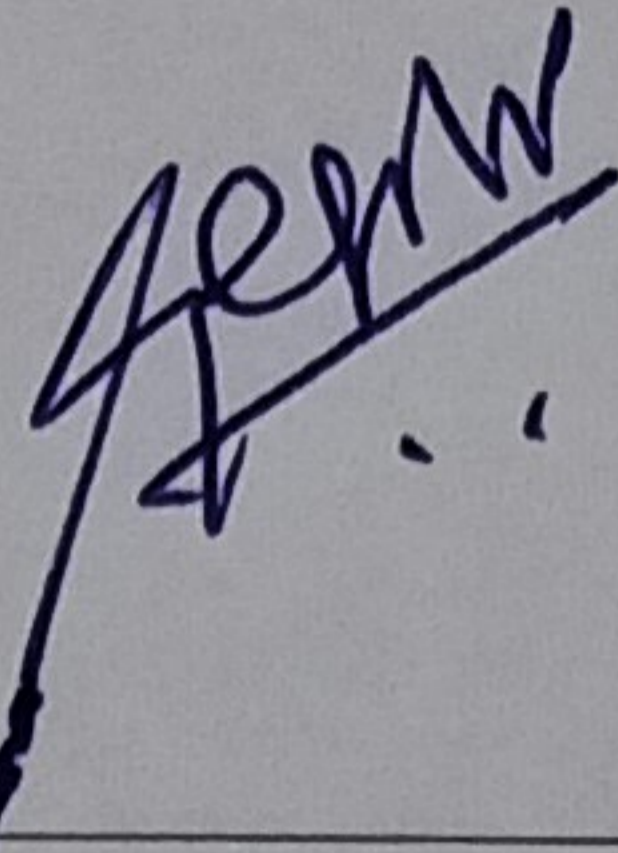
- i) the thesis comprises of my original work towards the degree of Doctor of Philosophy at Dhirubhai Ambani Institute of Information and Communication Technology and has not been submitted elsewhere for a degree,
- ii) due acknowledgement has been made in the text to all the reference material used.



Pratik Mevada

Certificate

This is to certify that the thesis work entitled DESIGN OF QUASI-PERIODIC AND APERIODIC ARRAY LATTICES TO IMPROVE ARRAY ANTENNA PERFORMANCE has been carried out by PRATIK MEVADA for the degree of Doctor of Philosophy at *Dhirubhai Ambani Institute of Information and Communication Technology* under our supervision.



Prof. Dr. Sanjeev Gupta
Thesis Supervisor

Acknowledgment

I am incredibly thankful to my guide and mentor, Prof. Dr. Sanjeev Gupta, Dhirubhai Ambani Institute of Information and Communication Technology (DA-IICT), Gandhinagar, for his noble guidance and support with full encouragement and enthusiasm. Without his constant encouragement and freedom of work, this work could not have been possible to complete.

I would also like to thank my committee members, Prof. Dr. Deepak K. Ghodgaonkar, Prof. Dr. Rajib Lochan Das and Prof. Dr. Hemant Patil, for their time and for offering fruitful reviews, comments and recommendations, which have lifted the quality of my work.

I am extremely grateful to Shri. Nilesh Desai, Director, Space Applications Centre (SAC), Ahmedabad, for allowing me to pursue the Ph.D.

I gratefully recognize the help, support, constant encouragement and motivation of Dr. Milind Mahajan, Group Direction (GD), Antenna Systems Group (ASG) at SAC, Ahmedabad and Prof. Dr. Soumyabrata Chakrabarty, Indian Institute of Technology, Gandhinagar. I would also like to express my sincere thanks to Dr. Vijay Kumar Singh and Shri. Sanjeev Kulshrestha from SAC, Ahmedabad, for their critical insights and constant moral support. I can't thank enough my colleague at SAC, ISRO for helping and supporting me during the course.

Most importantly, I am grateful for my family's unconditional, unequivocal, and loving support.

Many thanks go to all those who are unnamed and who undoubtedly influence on me and thus, the creation of this work.

PRATIK MEVADA

Contents

Abstract

List of Tables

List of Figures

1	Introduction	
1.1	Introduction of Beam Steerable Aperiodic Array Antenna.....	1
1.2	Motivation	2
1.3	Aims and Objectives	3
1.4	Organization of the thesis	4
2	Literature Survey	5
3	Aperiodic Beam Steerable Array Antennas based on Strip-Projection (SP) Based Method	
3.1	Introduction	12
3.2	Effect of Aperture Tapering	12
3.3	Effect of aperiodicity in the periodic arrays	14
3.4	Pinwheel based aperiodically clustered array	17
3.5	Strip projection (SP) method based aperiodic array antenna	22
3.5.1	Design of Aperiodic Linear Array Antenna	23
3.5.2	Design of Aperiodic Planar Array Antenna	31
3.6	Design of Quasi-periodic Planar Array Antenna using Projected Polyhedron based Approach	45
4	Application of Projection Based Aperiodic Arrays	

Application A	Design of Interferometric Array for Radio Astronomy	
4.1	Introduction	55
4.2	Application of Directly Projected Polyhedron based projection method in Radio Astronomy	56
4.3	Application of Stereographically project Polyhedron based Strip projection method in Radio Astronomy	60
Application B	Direction of Arrival (DoA) using MVDR technique using proposed Aperiodic Array	67
5	Conclusion and Future Work	
5.1	Conclusion	70
5.2	Future Work	73
	References	74
	List of Publications	80
	Annexure A List of Element Locations in the Proposed Aperiodic Planar Array	81

Abstract

The thesis addresses one of the possible solutions to the grating lobe occurrence in the beam steerable periodic arrays for large angular beam scans. The controlled aperiodicity has been introduced to the periodic array to achieve the same and the object is set to design the beam steerable array antenna offering improvement in the peak SLL performance with beam scan and reducing the number of array elements. The designs of such aperiodic and quasi-periodic array antennas have been carried out using the innovative strip projection (SP) based method. The strip projection method uses the area of rotated higher dimensional lattice and projects it to lower dimensions to generate an aperiodic array. The designs of aperiodic linear and planar arrays have been carried out to achieve $\pm 30^\circ$ conical beam scan range with peak SLL ≤ -10 dB over -90° to 90° angular range. The novelty of the proposed SP method is that the number of optimization variables is fixed and independent of the size of the aperiodic array. The reported techniques to generate the aperiodic arrays lack in this aspect. The proposed method facilitates a significant reduction of the design efforts, especially in the case of the larger beam-steerable arrays. The proposed method is relatively straightforward to implement compared to the reported algorithms.

The performance of the aperiodic linear array antenna has been compared with the aperiodic arrays designed using evolutionary optimization algorithms, namely, genetic algorithm (GA), particle swarm optimization (PSO) and Jaya algorithms and it is found that the proposed design method is comparatively more efficient and faster. The aperiodic array lattice is also populated with X-band electromagnetically coupled patch antenna integrated with a phase shifter and simulated. The aperiodic patch array antenna has been fabricated and characterized in the anechoic chamber. The comparison of the measured and simulated results is presented. In measurement, a significant improvement of 5.72dB in peak SLL is achieved at $\pm 30^\circ$ beam scan angle.

The design of an aperiodic planar array antenna has been carried out for a $15\lambda \times 15\lambda$ aperture size. The optimized array has 21.9% less elements than the conventional periodic rectangular lattice. The Pinwheel based aperiodic array lattice has also been designed for the same beam scan requirement and presented for comparison. It is observed that the peak SLL

performance is maintained at $<-11.63\text{dB}$ and $<-12.70\text{dB}$ over the 0° - 30° beam scan range by the proposed aperiodic array and Pinwheel based array, respectively. Moreover, both types of lattice have been populated with S-band cubic-shaped dielectric resonator (DR) antenna element and their simulations have been carried out using a 3D electromagnetic solver. For the quantification of the aperiodicity in the structure, position standard deviation (σ_0) is also defined and computed.

The projection concept is generalized and implemented to design a quasi-periodic beam steering array antenna by projecting the vertices of co-centric polyhedrons on the 2D aperture plane. The modelling and design of quasi-periodic array lattice are carried out by projecting the vertices of co-centric polyhedrons, namely dodecahedrons and icosahedrons, on the aperture plane. The angular orientation of the polyhedrons is optimized to achieve a 4.2dB peak SLL improvement for a $\pm 30^\circ$ beam scan. The optimized array lattice is populated with cubic shaped DR based elements and integrated with a Voronoi based metallic fence and decoupling network (DCN) for mutual coupling improvement between the elements. The polyhedron projection based concept has been extended to design interferometric arrays for radio astronomy. The stereographic projection has been used for the projection of vertices of the rotated polyhedron and forms the aperiodic array, whose performance is subsequently evaluated for radio interferometric imaging. The necessary test framework for imaging of 1" sample image using the designed array lattice has been developed in Matlab and the array lattice has been optimized to achieve the maximum fidelity index (FI). The various cases of the aperiodic array with various combinations of polyhedrons have been evaluated and compared with the *Giant Metrewave Radio Telescope* (GMRT) array. The aperiodic array generated by the three co-centric polyhedrons, i.e., dodecahedron, octahedron and tetrahedron, is proved to have a better fidelity index (FI) over the various declinations (δ). In addition, the projection based aperiodic array antenna has also been evaluated for minimum variance distortionless response (MVDR) type of beamformer, which is a widely used technique in various fields like communication, radar, acoustics, and sonar. Matlab codes are developed to implement DoA estimation using the MVDR technique and applied to the conventional periodic and proposed aperiodic linear arrays. It is shown that aperiodicity in the element position has eliminated the unwanted lobes in the detection range.

List of Tables

3.1	List of excitation distribution given to 8 element linear array	13
3.2	Comparison of aperture tapering methods for 10^0 beam scan	14
3.3	Farfield Performance of 8 x 8 Array with subarray displacement	16
3.4	Comparison of Antenna Parameters for 10^0 Scan	22
3.5	Comparison of Antenna Parameters for 20^0 Scan	22
3.6	No. of Objective Function Evaluations and Peak SLL for Optimization Algorithms	27
3.7	Farfield parameters of aperiodic and periodic arrays at 30^0 beam scan	40
3.8	Best-fit equations for computation of number of elements	41
3.9	Summary of the proposed aperiodic array and published array designs	42
3.10	Comparison between the proposed aperiodic and periodic array	44
3.11	No. of vertices of the polyhedrons	45
3.12	Summary of the quasi-periodic arrays	53
3.13	No. of elements in array for co-centric platonic solids	54
4.1	Various Cases of Polyhedron Combinations	63

List of Figures

2.1	Various methods and their brief description to generate the array layout	9
3.1	16 element linear array antenna with 8 sub-arrays (All dimensions are in mm.)	12
3.2	(a) Aperture distribution with symmetric linear tapering and (b) its farfield parameters for various tapers	13
3.3	(a) Aperture distribution with symmetric raised cosine type tapering and (b) its farfield parameters for various cosine powers	13
3.4	(a) Aperture distribution with (cos + sin) type asymmetric tapering and (b) its farfield parameters for various 'A' values	14
3.5	Array lattice generated with/without displacement of quadrants in 8 x 8 array antenna formed with 2 x 2 subarray, 3 x 3 subarray and 4 x 4 subarray	15
3.6	UV radiation pattern of 8 x 8 array with/without displacement of quadrant's and formed with 2 x 2 subarray, 3 x 3 subarray and 4 x 4 subarray	16
3.7	Principle plane radiation pattern of 8 x 8 array with/without displacement of quadrant's and formed with 2 x 2 subarray, 3 x 3 subarray and 4 x 4 subarray, for 10 ⁰ beam scan	17
3.8	Generation of Pinwheel lattice and computation of the farfield pattern of isotropic sources placed at the vertices of the triangles in the lattice	18
3.9	Periodic 8 x 8 array antenna and its subarraying	19
3.10	(a) 10 ⁰ and (b) 20 ⁰ scanned radiation patterns of periodically subarrayed 8 x 8 Array Antenna	19
3.11	Various possible offsets applied to an 8 x 8 array antenna placed on Pinwheel type pattern.....	20
3.12	Peak SLL in 3D radiation pattern w.r.t displacements, for (a) 10 ⁰ and (b) 20 ⁰ beam scans	21
3.13	Pinwheel clustering of 8 x 8 array elements for displacement (a) (X_offset = 3.76, Y_offset = 2.99) for 10 ⁰ beam scan and (b) (X_offset = 3.36, Y_offset = 1.15) for 20 ⁰ beam scan	21
3.14	3D radiation patten of 8 x 8 array antenna for (a) conventional rectangular clustering and (b) Pinwheel type clustering, for 10 ⁰ beam scan	22
3.15	Modeling of aperiodic array lattice using SP method	23
3.16	Sample aperiodic linear arrays for $\theta_{Rot} = 0^0, 30^0, 45^0$	24

3.17	(a) Variation of peak SLL w.r.t θ_{Rot} for various w_h and (b) Variation of number of elements w.r.t θ_{Rot} for various w_h	25
3.18	Element locations in the optimized linear aperiodic array and conventional periodic array	26
3.19	Far-field radiation pattern of aperiodic linear array and periodic linear array for -30° beam scan	26
3.20	Comparison of (a) directivity variation, (b) beamwidth variation and (c) peak SLL variation, w.r.t scan angle for proposed aperiodic array and periodic array....	26
3.21	Far-field principle plane cuts of aperiodic array for various beam scans	27
3.22	Comparisons of far-field pattern of aperiodic linear arrays generated by GA, PSO, Jaya algorithms and proposed SP method	27
3.23	(a) X-Band Electromagnetically coupled (EMCP) microstrip single antenna element and (b) its simulated return loss and radiation pattern performance.....	28
3.24	(a) Design of X band high Dk substrate (TMM10i) based phase shifter and (b) its simulated insertion phase and insertion loss performance by varying the width of TMM10i substrate	29
3.25	(a) Simulation model of X-band 21 elements aperiodic array antenna and (b) synthesized phase shifter layouts for various scan angles	30
3.26	(a) Developed aperiodic array integrated with 1:21 equi-phase power divider and 10° phase shifter, and (b) developed phase shifter layers for various beam scans	30
3.27	Comparison of analyzed, simulated and measured (a) gain/directivity variation with beam scan, (b) 0° scan radiation pattern and (c) -30° scan radiation pattern, for X-band 21 elements aperiodic array antenna.....	31
3.28	Modeling of SP method for planar aperiodic array, where rotated 3D lattice (red dots), acceptance domain (yellow box), lattice points enclosed by acceptance domain (green dots)	32
3.29	Variation of No. of Elements, directivity and peak SLL w.r.t W_z for $(W_x, W_y) = (15\lambda, 15\lambda)$ aperture dimension	33
3.30	Aperiodic planar array generated using SP method	34
3.31	(a) Variation of number of element w.r.t χ and (b) Variation of directivity w.r.t χ , for $(15\lambda \times 15\lambda)$ pinwheel based aperiodic array	35
3.32	(a) Construction of pinwheel lattice and (b) designed pinwheel lattice based aperiodic array, for $(15\lambda \times 15\lambda)$ aperture dimension	35
3.33	(a) S-band cubic shaped DR based radiating element, and (b) its simulated return loss and radiation pattern performance	37
3.34	Simulated structures of (a) strip-projected planar aperiodic array and (b) pinwheel lattice based planar aperiodic array	37

3.35	(a) Analyzed and (b) simulated UV radiation patterns of strip-projection method based planar aperiodic array, for -30^0 beam scan	38
3.36	(a) Analyzed and (c) simulated UV radiation patterns of pinwheel lattice based planar aperiodic array, for -30^0 beam scan	38
3.37	Variation of (a) directivity, (b) peak SLL and (c) beamwidth with scan angle for three types of array lattices (PW – Pinwheel based planar aperiodic array, SP – Strip-projection based planar aperiodic array, PR – Periodic planar array)	39
3.38	Distributions of the nearest element spacing for the planar aperiodic array lattices	39
3.39	Element wise active S_{11} of planar aperiodic DR array antenna using (a) the strip projection method and, (b) Pinwheel based method	40
3.40	Comparison of the variation of the number of array elements with aperture size for various types of planar array lattices	41
3.41	Typical layout of RF receiver BF IC	43
3.42	Typical RF block diagram of RF receiver BF IC	43
3.43	Proposed element grouping in the proposed planar aperiodic array antenna, forming a planar quasi-periodic array	44
3.44	Feed network layout of the proposed aperiodic array antenna integrated with RF-ICs	44
3.45	Sample cases of rotation of Dodecahedron and corresponding element positions	45
3.46	(a) Geometry of co-centric dodecahedron and icosahedron and (b) projection of vertices of co-centric polyhedrons on XY plane and corresponding array element positions ($\alpha_d = 0.25$, $\beta_{x,d} = 319.7^0$, $\beta_{y,d} = 218.9^0$, $\beta_{z,d} = 0^0$, $\alpha_i = 0.18$, $\beta_{x,i} = 0^0$, $\beta_{y,i} = 102.1^0$, $\beta_{z,i} = 0^0$, d = dodecahedron, i = icosahedron)	46
3.47	Flow chart for array lattice optimization using co-centric polyhedrons based approach	49
3.48	Simulation model of the planar quasi-periodic array of DRA (a) without Voronoi boundary and (b) with Voronoi boundary	50
3.49	System schematic of feed network of quasi-periodic array of DRA	50
3.50	Element wise mutual coupling variation for various conditions of the planar quasi-periodic DRA array	50
3.51	(a) Block diagram of DCN and (b) schematic of simulation model of aperiodic array with DCN	51
3.52	Analyzed UV radiation pattern for (a) ($\theta = 30^0$ and $\phi = 0^0$), (b) ($\theta = 30^0$ and $\phi = 90^0$), and simulated UV radiation pattern for (c) ($\theta = 30^0$ and $\phi = 0^0$), (d)	51

	($\theta = 30^\circ$ and $\varphi = 90^\circ$) , of the planar quasi-periodic DRA array with Voronoi boundary and DCN	
3.53	Simulated beam scan performance of co-centric polyhedrons based quasi-periodic array of DRA for beam scan in (a) $\varphi = 0^\circ$ and (b) $\varphi = 90^\circ$	52
3.54	(a) Quasi-periodic Pinwheel lattice and its analysed beam scan performance for Pinwheel based array lattice for (a) ($\theta = 30^\circ$ and $\varphi = 0^\circ$) beam scan, (b) ($\theta = 30^\circ$ and $\varphi = 90^\circ$) beam scan	52
3.55	Comparison of far-field parameters (gain, beamwidth and peak SLL) for analyzed projected polyhedron based planar lattice and simulated planar quasi-periodic array of DRA with Voronoi boundary and DCN, for beam scan in (solid line – analyzed results, dotted line – simulated results) (a) $\varphi = 0^\circ$; and (b) $\varphi = 90^\circ$	53
4.1	Coordinate definition and observation geometry for radio interferometry	57
4.2	(a) Rotated and scaled co-centric polyhedrons, and (b) planar aperiodic array generated by projection of the vertices	57
4.3	Computed UV Coverage using co-centric Polyhedron (icosahedron and dodecahedron) based Synthesized array for various declinations over 12hr observation	58
4.4	(a) Array Analysis, computation of U-V coverage and its impact on Image and (b) residual image, for co-centric Polyhedron (icosahedron and dodecahedron) based synthesized array	59
4.5	Inner holes in the U-V coverages of various polyhedron based arrays.....	58
4.6	Stereographic projection of vertices of the polyhedrons and formation of planar aperiodic array	61
4.7	Filled inner holes in the U-V coverages of various polyhedron based arrays generated using stereographic projection	62
4.8	Design flow chart of the aperiodic interferometric array using stereographic projection	62
4.9	Array Distribution of GMRT (No. of Array Elements = 30)	63
4.10	Array distributions of (a) case-1, (b) case-2, (c) case-3, (d) case-4, (e) case-5, (f) case-6, (g) case-7, (h) case-8, (i) case-9 and (j) case-10	65
4.11	Fidelity Index for various declination angles for various cases of aperiodic arrays and GMRT array	65
4.12	Histogram of baselines for Case-4 (Dodecahedron + Octahedron + Tetrahedron) and for -50° and 70° declination angles.....	65
4.13	(a) Image sampling and generation using aperiodic array from the case – 4 and (b) residual image, for -50° declination angle	66

4.14	(a) Image sampling and generation using aperiodic array from the case – 4 and (b) residual image, for 70° declination angle	67
4.15	Proposed strip projection based aperiodic linear array and conventional periodic linear array	68
4.16	Angular plot of DoA estimation carried out by the proposed SP based aperiodic array and conventional aperiodic array	69

CHAPTER 1

Introduction

1.1 Introduction of Beam Steerable Aperiodic Array Antenna

Phased array antennas are widely used beam steering antennas, in which each element of the array is excited with a specific phase to generate the farfield beam in the desired direction. Such array antennas are configured and designed with a periodically ordered arrangement of various antenna elements. Based on the required number of transmit-receive modules (TRMs) in communication and radar systems, the number of excitation points in array antennas is limited. Hence, the individual antenna elements are usually combined to form periodic clusters resulting in subarrays. Clustering of antenna elements limits many far field antenna parameters such as,

- It limits the bandwidth performance of the array during beam steering.
- It limits the scanning range as the interelement spacing is increased.
- It generates grating lobes for very small scan angles.

Such limitations can be overcome by using an orderly-disordered arrangement of array elements, i.e., quasi-period array antennas. Quasi-periodic arrangement of array elements can provide sufficiently large controlled degrees of freedom to synthesize the far field radiation patterns. Therefore, such array lattices are recently being studied extensively in the antenna community. Followings are the major advantages achieved with such lattices,

- ✓ To spread out the energy that would otherwise accumulate in grating lobes (GL) due to the wide interelement spacing
- ✓ The possibility of reducing the number of elements in one assigned aperture without a major impact on the beamwidth
- ✓ To reduce the control points in the phased array antenna
- ✓ To reduce the sidelobe level (SLL) without resorting to an amplitude tapering
- ✓ To shape the radiation pattern

1.2 Motivation

The phased array antenna has been one of the widely demanded antennas, especially for currently being developed 5G and MIMO based technology [1]. As the 5G technology offers a variety of applications to the user, it tends to consume large RF and DC power. Moreover, the large beam steerable array antenna offers flexibility to generate number of beams in Tx and Rx. The increase in the number of elements requires large RF power. Therefore, the need is always sustained to reduce the array elements while maintaining the same level of beam steering capabilities.

In spaceborne and airborne based synthetic aperture radar (SAR) systems, the electronically scanned phased array offers wide flexibility to switch between operational modes like stripmap, scanSAR and spotlights [2]. For SAR systems, the increase in the azimuth dimension of the phased array improves the azimuth resolution and the large beam steering capability in elevation direction improves the swath. To meet both requirements, the number of elements required in the phased array system grows and poses various problems related to DC power consumption and dissipation, which effectively leads to thermal related problems during the design and development of the SAR system. Therefore, reducing the number of elements in the array antenna while maintaining a similar scan performance is always in favor of the SAR system designer.

Radio astronomy is one of the dominating fields where the configuration of an array antenna plays a significant role in the imaging the cosmic microwave images [3]. Here, the beam steering is usually implemented using a correlator-based system design. The correlator-based design highly depends on the array configuration. The type of single antenna element is a reflector antenna, whose single structural unit is enormous, difficult to develop and expensive. Therefore, reducing the number of elements in such an array is always demanded.

Another important field of application is the well-known adaptive array antenna, sometimes called a smart antenna. The elements of such an antenna are connected with the signal processor, which optimizes the excitation distribution of the array to form the beam in the source direction and place nulls in the interfering direction. Here, the array lattice plays a significant

role as it mainly governs the maximum range of the estimation of direction of arrival (DoA) and the number of nulls. The conventional periodic array antenna usually limits the same based on the number of elements and selected interelement spacing. However, there is always a requirement to achieve a wider range of DoA estimation for the same number of elements.

The above requirements can be fulfilled using aperiodic or quasi-periodic arrays in place of conventional periodic array antennas. Adding a controlled amount of aperiodicity in the periodic environment significantly reduce the periodic samples to maintain the same array scan performance. This thesis explores the nature of aperiodicity using periodic arrays and proposes a new method to design the aperiodic and quasi-periodic beam steerable array antenna using the strip projection method.

1.3 Aims and Objectives

Followings are the primary aims and objectives which are addressed in detail in this thesis,

- To understand the behavior of aperiodicity in the periodic array environment
- To study various available aperiodic array design techniques
- To develop the new design technique for an aperiodic array offering wide beam scanning ($\geq 30^\circ$) with at least a 20% reduced number of elements
- Practical demonstration of the devised technique using the aperiodic array offering $\geq 30^\circ$ beam scanning capability
- Application of the new design technique for practical systems like radio interferometry and MVDR based beamformer

This thesis comprehensively explores a new strip-projection based technique for designing aperiodic and quasi-periodic beam steerable array antennas offering farfield performance improvement during beam scan. By synthesizing SP based array antenna theory and applying it to the linear and planar array, the aspiration is to propose and develop the most effective technique which reduces the number of control points in the conventional phased array antenna and also achieves the farfield goals with minimum iterations, reducing the design and simulation time significantly. The results will be an innovative aperiodic linear beam steerable antenna

having $\pm 30^\circ$ beam scan capability offering 5.72dB improvement in peak SLL and an innovative aperiodic planar beam steerable antenna having $\pm 30^\circ$ beam scan capability and 21.9% reduction in the number of elements as compared to the conventional phased array antenna. In doing so, this work also paves the way for interferometric arrays and MVDR based beamformers. This thesis will include such applications and the use of SP method for their designs.

1.4 Organization of the thesis

Followings the chapter wise description of the thesis,

- | | |
|-------------|---|
| Chapter - 2 | This chapter describes the historical background of the design of aperiodic arrays and summarizes the reported approach for the design of aperiodic arrays. It also includes a few manuscripts describing the application of aperiodic arrays for radio astronomy. |
| Chapter - 3 | In this chapter, the aperiodicity is discussed in detail using the subarray displacement technique and Pinwheel based clustering of the array. The strip projection-based method has been presented with analysis, simulation and development for linear and planar beam steerable array antenna. The polyhedron-based projection approach has also been described for the quasi-periodic arrays. |
| Chapter - 4 | This chapter mainly focuses on applying the proposed polyhedron-based projection method for the interferometric array design for radio astronomy and aperiodic linear array antenna for MVDR based beam forming. |
| Chapter - 5 | The chapter discusses the conclusion of the work and its future aspects. |

CHAPTER 2

Literature Survey

The research on Aperiodic and quasi-periodic arrays has been initiated in 1956 by H. Unz [4]. H. Unz wrote a technical paper in 1960, describing how the arbitrarily distributed elements can be analysed using the equation for the computation of far-zone radiation pattern [5]. H. Unz mentioned that the general case of the array with arbitrarily placed elements adds one more degree of freedom for the design, in addition to the complex amplitude. During the same year, D. King et al. published a technical paper on a broad-band beam steerable linear array using the unequally spaced array [6]. He mentioned about 2-to-1 bandwidth with beam steering up to $\pm 90^\circ$ with sidelobe level $\leq -5\text{dB}$. They adopted the trial-based method. Looking at the current requirements for communication and remote sensing systems, such performance is inferior. However, they raised one of the important points of unequally space array and that is its usefulness in high-power applications where the conventional aperture tapering causes loss in the aperture efficiency. In 1961, Roger Harrington published a manuscript, describing the use of nonuniform element spacing for the sidelobe level reduction [7]. Roger proposed the perturbation-based approach, where the normalized field pattern equation is modified by considering the periodic elements positioned with small individual perturbations added to their position. Using the simplified version of the field pattern equation, he derived the perturbations such that the sidelobe level is suppressed significantly. The procedure discussed by Roger is relatively simple to implement, but it involves small angle approximations and impulse function to represent sidelobe level and its position. Following such trade to propose the various technique for the design of unequally spaced or aperiodic or quasi-periodic arrays, several manuscripts have been published and the work presented in some of them is described subsequently.

The non-linear aspect of the element position in the equation of array factor ceases the linear synthesis of the element positions and hence, alternative methods are discovered and reported. One of the widely used methods is the use of an optimization algorithm to adjust the element positions as per the desired cost function. Literature is replete with such manuscripts, offering the design of aperiodic arrays using optimization schemes. M. G. Bray et al. have

published a very interesting manuscript, describing the use of the genetic algorithm to optimize an aperiodic linear phased array antenna for suppressing grating lobe level during scanning [8]. The half wave dipole-based element has been used and its driving point impedance has been constrained during optimization, which effectively prevents the occurrence of scan blindness in the desired scan range.

In 2005, V. Pierro et al. presented aperiodic tiling for planar array antennas [9]. The study of various radiation properties of aperiodic tiles like Penrose, Octagonal, Table, Danzer, Binary and Pinwheel has been reported along with the discussion on the basics of aperiodic tiling, their construction rules and algorithms. The authors have presented the maximum directivity and sidelobe level variation of various tiles with frequency. It has also been concluded that aperiodic tiles like Danzer and Pinwheel offer the broadband performance of sidelobes. Although the presented study gives a detailed insight into aperiodic tilings and their radiation based electromagnetic properties, it does not include the design details and procedures for the design of an array antenna using such types of aperiodic tiles. Moreover, the beam steering performance for the presented aperiodic tiling is not included.

Aperiodicity has also been applied for the grouping/clustering of the array antenna, to reduce the number of transmit-receive modules (TRMs) while still maintaining the periodic array performance. In 2009, T. Isernia et al. have proposed Penrose based tiling of the array elements, which forms two types of subarrays, namely, thick and thin tiles [10]. The author has claimed to improve the farfield performance of the array antenna, including the aperture efficiency. The hybrid optimization-based approach has also been discussed where the element positions and their excitation weights are simultaneously optimized to improve the grating lobe level (GLL).

W. Barott and P. Steffes have proposed the genetic algorithm (GA) based optimization for the design of a physically large aperiodic linear array [11]. They have presented the study for the single element based linear array and subarray based linear array. The maximum relative sidelobe level (-RSL) has been computed and its inverse has been used to determine the fitness of the individuals in the GA. The term 'aperture ratio' is defined below. It has been proved that the effect of an array having an aperture ratio $< 40\%$, on SLL, is negligible and it is significant for the array having an aperture ratio $> 80\%$.

$$\textit{Aperture ratio} = \frac{\textit{Minimum spacing between antennas}}{\textit{the average spacing between antennas}}$$

T. Azar has presented a brief tutorial about overlapped subarrays in [12]. Overlapping of subarrays is a very effective approach as it maintains the desired inter-element spacing in the array environment, resulting in reduced GLL. T. Azar has also given a comparison between contiguous arrays and overlapped subarrays. Although overlapped subarray technique seems promising for antenna array designs, it requires a very complex design of the beamformer.

A. Kedar has reported the deterministic approach for the design of linear sparse array using Array Dilation Technique (ADT) [13]. ADT interestingly stretches the element position in the uniform linear array, equivalent to the stretch in an elastic membrane. It has been shown that the nonuniform array designed using ADT achieves lower peak SLL performance with optimal thinning level. The author has presented various case studies with different sizes of linear arrays designed with various dilation parameters, defined as α_j , and presented the farfield performance for 0° and 60° beam scans. However, the ADT method is deterministic in nature, the variation in the α_j results in the variation in the farfield parameter, which effectively calls for the design of a nonuniform array using either parametric study or optimization.

In addition to the approach to alter element positions in the periodic linear or planar arrays as discussed above, the space filling curve-based approach for the design of aperiodic array antennas has also been reported, which includes the extensive works by the research group led by Dr. D. Werner. D. Werner et al. and T. Spence et al. have reported the design of beam steerable fractile based aperiodic array antennas using Peano-Gosper space filling curve [14-15]. However, the required aperture size and the number of elements in the fractile-based arrays are significantly large than the presented aperiodic array design, when the peak directivity and beam scan ranges are compared. T. Spencer with D. Werner has reported the broadband planar array antenna using Penrose and Dazer aperiodic tilings [16]. The authors have achieved a 22:1 bandwidth ratio in terms of SLL and 76% element reduction using two-point optimization of Danzer tiling. The array performance during the beam scan is not studied and presented.

Another interesting approach for the design of an aperiodic array was presented in 1964 by Y. Lo [17]. Y. Lo reported the probability-based approach for the design of an aperiodic array antenna such that it is a statistically optimized case with respect to SLL, i.e., all SLL are of equal

level with uniform probability. He presented extensive mathematics where the radiation pattern function $P(u)$ is treated as the random function which has element position defined with specific probability distribution $g(x)$. He subsequently related the auto-correlation of $P(u)$ with SLL and compute the required number of elements as a function of SLL for a certain probability of success. Moreover, After Y. Lo's work, various other literature has been appeared offering different methods to handle the probability distribution and determine the element spacing for the required farfield performance [18-24]. Here, it is important to note that the accuracy of the results using such a probability-based approach improves with the array size. Therefore, such an approach is mainly suited for very large aperiodic arrays.

Based on the above literature survey, the overview of the various approaches for the design of an aperiodic array antenna is presented in Fig. 2.1, along with the strip projection based method proposed in this thesis. As it can be observed that the proposed method stands out from the other method in terms of the number of the optimization variables which do not depend on the aperture size. In addition, as the immediate application of the proposed projection based method, the interferometric array is also designed and presented. The followings are the few manuscripts describing the various ways to design the same.

Conventionally, "T", "Y" or circular are the shapes that are used for the array configuration. The communication report by Y. Chow in 1970 compared the baseline generated by these array configurations [25]. Y. Chow has concluded that the "Y" type array is a more attractive array configuration when earth rotation synthesis is implemented.

Norman Treloar has examined the various interferometric array configurations intending to design an array that can resolve the fine structure and array for the extended sources [26]. He has studied the non-random arrays like antennas placed on the perimeter of the circle, antennas placed in a "Y" shape and antennas placed in the single armed spirals. He has also studied random arrays like randomly placed antenna elements on the perimeter of the circle, inside the circle and inside an annulus. To resolve the fine structures, he adopted the uniform U-V distribution and generated the array configurations offering the uniform filling factor over the total aperture radius. However, for the extended sources, he mentioned that the short baselines are more helpful and generated the array configurations with a high filling factor in

the proximity of the center area and gradually reduced filling factor over the total aperture radius.

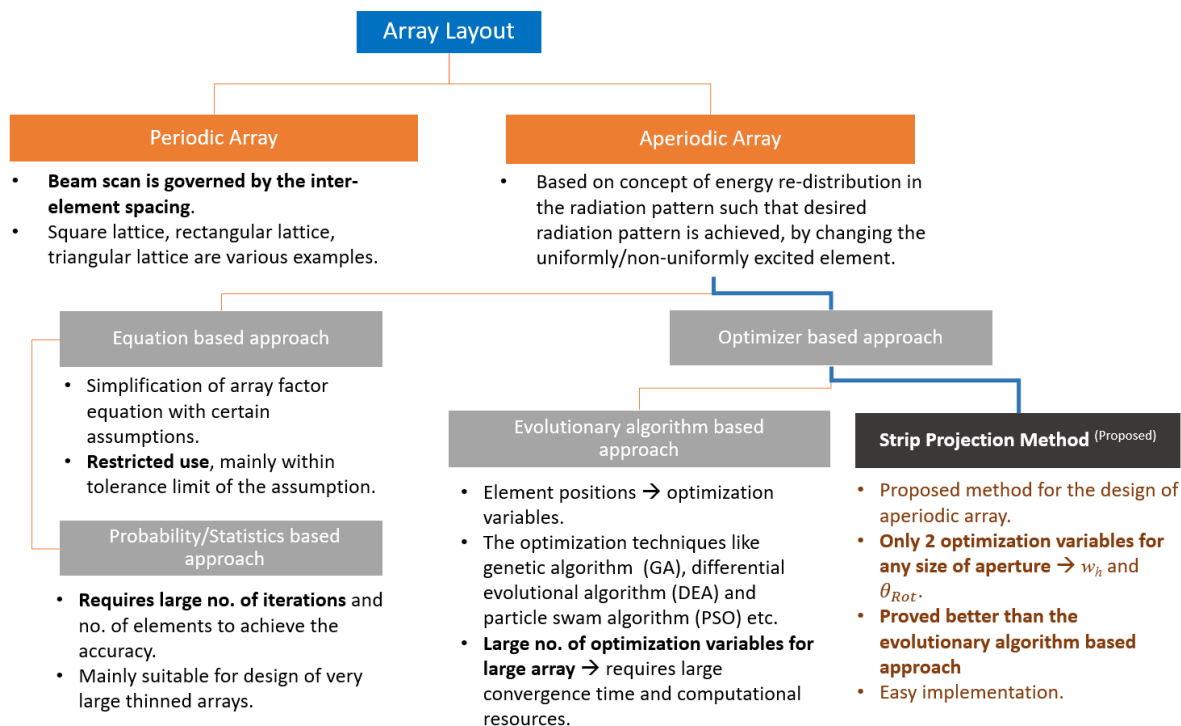


Figure 2.1: Various methods and their brief description to generate the array layout

E. Keto has published the research work on the shape of the interferometric array, carried out for the Smithsonian Astrophysical Observatory’s Submillimetre Array (SMA) project [27]. The author has proposed the array configuration where the antenna elements are placed on Reuleaux Triangle. Such configuration offers uniform U-V sampling, which is required to achieve high resolution with a high signal-to-noise ratio. The author has also applied the self-organizing neural network-based algorithm and proved that the Reuleaux Triangle uniformly samples U-V plane as compared to circular or “Y” shaped configuration.

Y. Su et al. have presented the optimization of the interferometric array configuration using a “sieving” algorithm [28]. In the sieving algorithm, the weight is assigned to U-V points and the least weighted point is removed from the distribution. The algorithm has been applied to generate the gaussian tapered U-V distribution and used for the optimization of the KARST array. The proposed algorithm does the global search for the solution, can handle any size of the interferometric array and is very flexible and expandable.

M. Villiers has described the tomographic projection-based approach for the configuration of the interferometric arrays [29]. Here, the U-V samples are projected into a one-dimensional vector. The projected samples are compared with the ideal distribution and necessary correction is applied to the antenna position to reduce the error between the projected and ideal samples. The iterative implementation of this method offers the desired U-V coverage. The author has applied the proposed approach to the array containing 20 antennas, 100 antennas and 230 antennas, with the aim to synthesize gaussian U-V coverage. The U-V coverage plot, its histogram and point spread function (PSF) have been presented for the above 3 cases, along with their derived observation parameters, by considering the 8-hour observation at -30° site latitude.

N. Patra et al. have reported the study of the possible expansion of the Giant Metrewave Radio Telescope (GMRT) (called EGMRT) by adding the new antennas to the existing array configuration of 30 antennas [30]. The authors have adopted two approaches namely, tomographic projection and random sampling, to form the newly expanded array with the minimum number of antennas for full synthesis observations. Both adopted approaches are based on optimization, where the gaussian distributed U-V distribution has targeted to achieve appropriate full width at half maximum (FWHM) specification. The study has proposed to add 30 new antennas at a short distance and 26 new antennas at a long distance from the GMRT array center, which will result into improvement of the collecting area and the field of view (FOV) by ~ 3 and ~ 30 , respectively.

Aperiodic arrays are also gaining popularity in the field of adaptive beamforming. Such beamforming is widely adopted for radar systems, ultrasound applications and microphone arrays for speech enhancement, as the physics remains the same for applications. In the thesis, the proposed aperiodic linear array has also been evaluated with Minimum Variance Distortionless Response (MVDR) beamforming algorithm. The followings are the briefs about the literature published on a similar topic.

W. Montlouis and P. Cornely have used MVDR based beamformer to estimate the four-dimensional parameters of moving sources, i.e., 2D target location and their respective angular velocities [31]. The author has formulated the weighted least square problem by considering the $M \times N$ rectangular planar array. The authors have also proposed a subspace decomposition-

based approach to reduce the complexity of the computation domain. The authors have addressed the problem of the performance degradation of MVDR beamforming when the source angles are not accurately known. A widely known diagonal loading technique has been applied to improve the same in such a scenario.

In 2000, a new class of beamforming array antenna called Electronically steerable passive array radiator (ESPAR) antenna was proposed by T. Ohira and K. Gyoda [32]. Such an adaptive beamforming antenna is a low-cost solution, which is designed using passive dipole or monopole elements excited using an active element. The passive elements are individually connected with the loads offering variable reactance. Here, the distribution of the reactance of the passive elements forms the desired beam pattern. In 2015, R. Qian et al. presented an exciting study of MVDR based beamforming using such an antenna [33]. In [33], it has been discussed that, as the beamforming depends on the reactance distribution and the ESPAR has single port RF output, the conventional MVDR cannot work. Therefore, the optimization-based approach has been adopted to compute the optimal weight vector, which is mapped on the respective reactance loads of the parasitic elements. The authors have also presented the simulation of the same using 7 passive thin electrical dipoles and for three different scenarios of the direction of arrival and interference.

X. Wang and M. Amin have presented the robust design of a sparse array which provides the optimum array gain within the expected uncertainty in the direction of arrival of the source [34]. The sparse array has been designed by configuring the optimization problem with the aim to minimize the degradation in the output signal-to-noise ratio (SNR) or signal-to-interference plus noise (SINR) ratio. The authors have also included the simulation results of matched and unmatched MVDR beamformers and demonstrated the robustness of the proposed sparse array.

CHAPTER 3

Aperiodic Beam Steerable Array Antennas based on Strip-Projection (SP) Based Method

3.1 Introduction

The work on the aperiodic lattice was initiated long back. Many approaches and techniques are proposed and presented. Majorly the techniques involve either approximation of the array factor equation or the optimization of farfield performance using random optimization algorithms. The main reason that no direct aperiodic array synthesis technique is available is the transcendental nature of array factor w.r.t element position. Moreover, the use of approximated array factor for synthesizing the large array is not feasible and the optimization space increases tremendously for the randomly optimized arrays.

3.2 Effect of Aperture Tapering

It is well reported that the element position governs the grating lobe level (GLL) and location in the beam steerable array antenna. However, there is a common misconception that the grating lobe can be controlled with the array excitation distribution. Therefore, a study has been carried out to show the effect of various types of excitation distributions on the grating lobe performance of an 8-element linear array antenna, where the 2-element linear array is used as the array element (also called subarray). Fig. 3.1 shows the array layout of the same with element numbering and spacing. Here, the operating frequency is 2.2GHz.

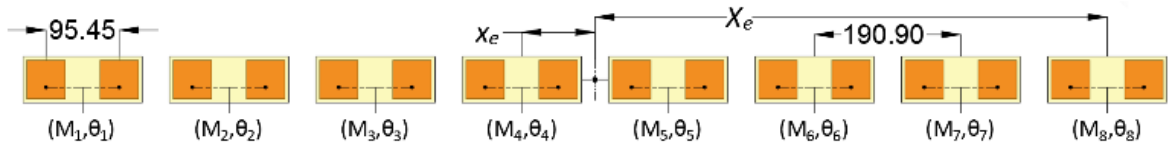


Figure 3.1: 16 element linear array antenna with 8 sub-arrays (All dimensions are in mm.)

Table - 3.1 shows the excitation distribution given to the subarrays and their corresponding mathematic description. Farfield parameters for 10° beam scan have been computed for various control variables in the tapering function. Fig. 3.2, 3.3 and 3.4 presents the aperture distribution plots and corresponding farfield parameter (SLL and GLL) plots for

various cases of the control variables. The comparison list of the farfield parameters is also presented in Table – 3.2. From Fig. 3.2-3.4 and Table – 3.2, it can be concluded that the excitation distribution significantly affects the sidelobe level. However, it does not provide noticeable improvement in the grating lobes. The study can be generalized to any array configuration and its excitation distribution.

TABLE – 3.1: LIST OF EXCITATION DISTRIBUTION GIVEN TO 8 ELEMENT LINEAR ARRAY

Sr. No.	Type of Excitation Distribution	Mathematical Description	Control variable
1	Symmetric Linear Tapering	$M_e = T(x_e) = m x_e + c$, $m = \text{slope}$, $c = \text{intercept}$	T
2	Symmetric Raised Cosine type Tapering	$M_e = T(x_e) = \cos\left(\frac{4\pi x_e}{5 X_e}\right)^q$	q
3	(Cos + Sin) type Asymmetric Tapering	$M_e = T(x_e) = A \cos\left(\frac{4\pi x_e}{5 X_e}\right) + (1 - A) \sin\left(\frac{4\pi x_e}{5 X_e}\right), 0 \leq A \leq 1$	A

Where $T(x_e)$ is called taper function. x_e be the sub-array position in array with respect to (0,0) coordinate. X_e be half dimension of array aperture.

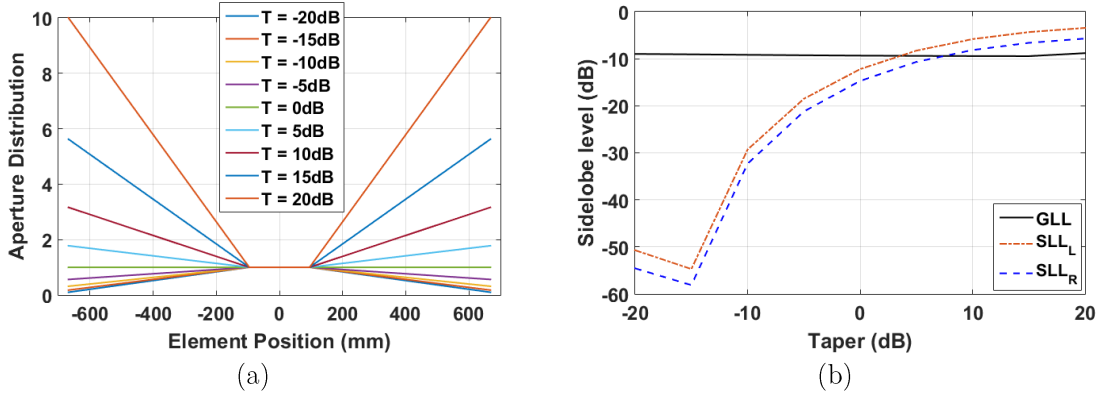


Figure 3.2: (a) Aperture distribution with symmetric linear tapering and (b) its farfield parameters for various tapers

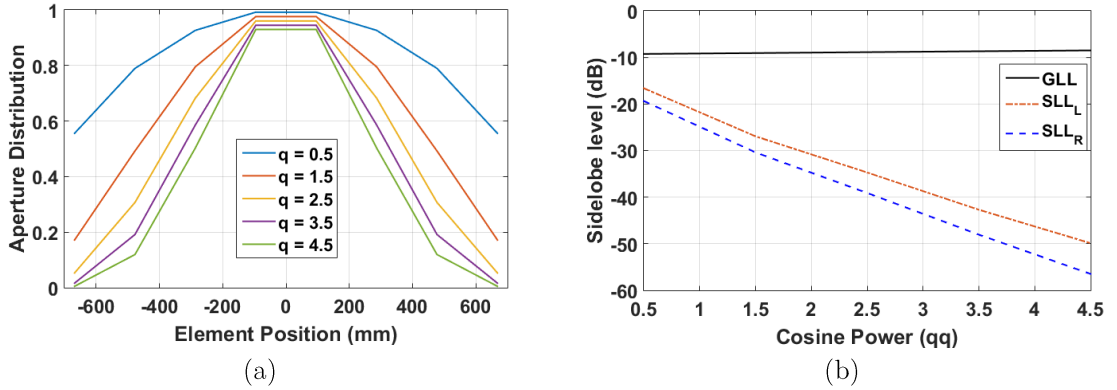


Figure 3.3: (a) Aperture distribution with symmetric raised cosine type tapering and (b) its farfield parameters for various cosine powers

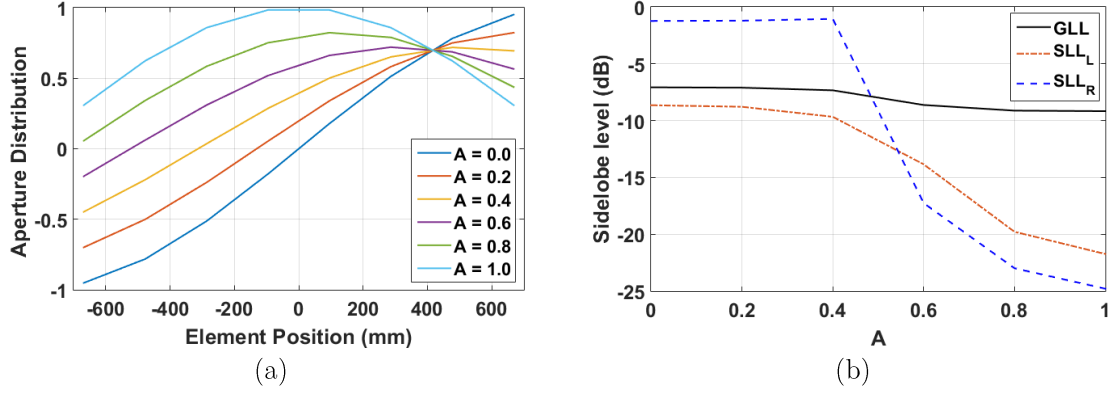


Figure 3.4: (a) Aperture distribution with (cos + sin) type asymmetric tapering and (b) its farfield parameters for various 'A' values

TABLE – 3.2: COMPARISON OF APERTURE TAPERING METHODS FOR 10^0 BEAM SCAN

Aperture Tapering Method	Parameter to control tapering	Range of control parameter	Variation of GLL over given range of control parameter	Variation of SLL over given range of control parameter	
				SLL _L	SLL _R
Symmetric Linear Tapering	Taper $T(x_e)$	-20dB to 20dB	-8.97dB to -8.81dB	-54.7dB to -3.44dB	-58.13dB to -5.71dB
Symmetric Raised Cosine type Tapering	q	0.5 to 4.5	-9.26dB to -8.50dB	-16.63dB to -49.88dB	-19.36dB to -56.48dB
(Cos + Sin) type Asymmetric Tapering	A	0 to 1	-7.07dB to -9.17dB	-8.65dB to -21.74dB	-1.23dB to -24.8dB

3.3 Effect of aperiodicity in the periodic arrays

An understanding of the role of aperiodicity can be obtained by implementing and examining the subarray displacement technique proposed by Y. Krivosheev et al. in [35]. In [35], the subarray displacement of $(d_{\text{elem}}/2)$ is proposed, as shown in Fig. 3.2, where d_{elem} is the inter-element spacing in the periodic array. As per the discussion in [35], the $(d_{\text{elem}}/2)$ displacement of subarray causes the anti-phasing of the field at the location of the nearest neighbor grating lobe, resulting in the grating lobe suppression.

In this thesis, the displacement concept has been generalized and applied to the 8×8 periodic array antenna. Here, the 8×8 array is divided into four quadrants and the half-element displacement is applied in each quadrant as shown in Fig. 3.5. The elements in the array have been configured as the 2×2 , 3×3 and 4×4 sub-arrays made up of the basic

element offering $(\cos \theta)^q$ type of radiation pattern. The inter-element spacing in each subarray is maintained to be 0.6λ .

Fig. 3.5 shows the periodic and displaced array lattices for the three different cases. The array analysis has been carried out for 3 cases and the results are summarized in Table - 3.3. As shown in Table - 3.3, ~ 2 dB improvement in the peak SLL has been achieved in the case of the 8×8 array with a 2×2 subarray when the array is operated for a 10^0 beam scan.

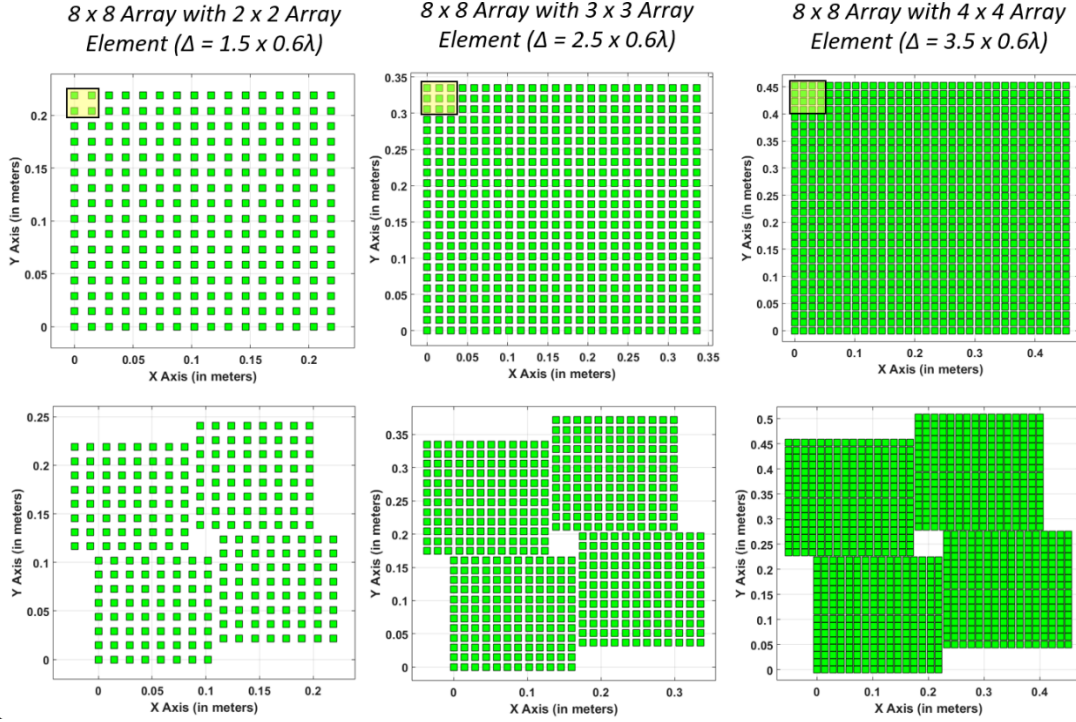


Figure 3.5: Array lattice generated with/without displacement of quadrants in 8×8 array antenna formed with 2×2 subarray, 3×3 subarray and 4×4 subarray

The radiation patterns of periodic arrays and displaced arrays in UV plane are presented in Fig. 3.6. The radiation patterns in the scan plane are also presented in Fig. 3.7. From Fig. 3.6 and 3.7, it can be observed that the displacement of subarrays has caused the null lines to rotate and $(d_{elem}/2)$ displacement has ensured that the rotated null lines pass through the location of the first nearest grating lobe, subsequently dividing it in two halves. As the energy concentrated in the grating lobe is divided into the two lobes, the resulting 2-lobes show at least 3-dB improvement in the grating lobe, equivalently called the peak SLL. In principle, there is no sign of a grating lobe in the scan plane, as can be observed from Fig. 3.7. However, the presence and location of the grating lobe are examined from the UV

radiation patterns. Here, the exact 3-dB improvement is not achieved, as it is shown in Table – 3.3. The same may be attributed to the followings,

1. The subarray pattern weights the location of peak SLL.
2. The displacement is applied by dividing the array in quadrants. Each quadrant contains a 4 x 4 array of sub-arrays. This condition deviates from the proposed in [35].

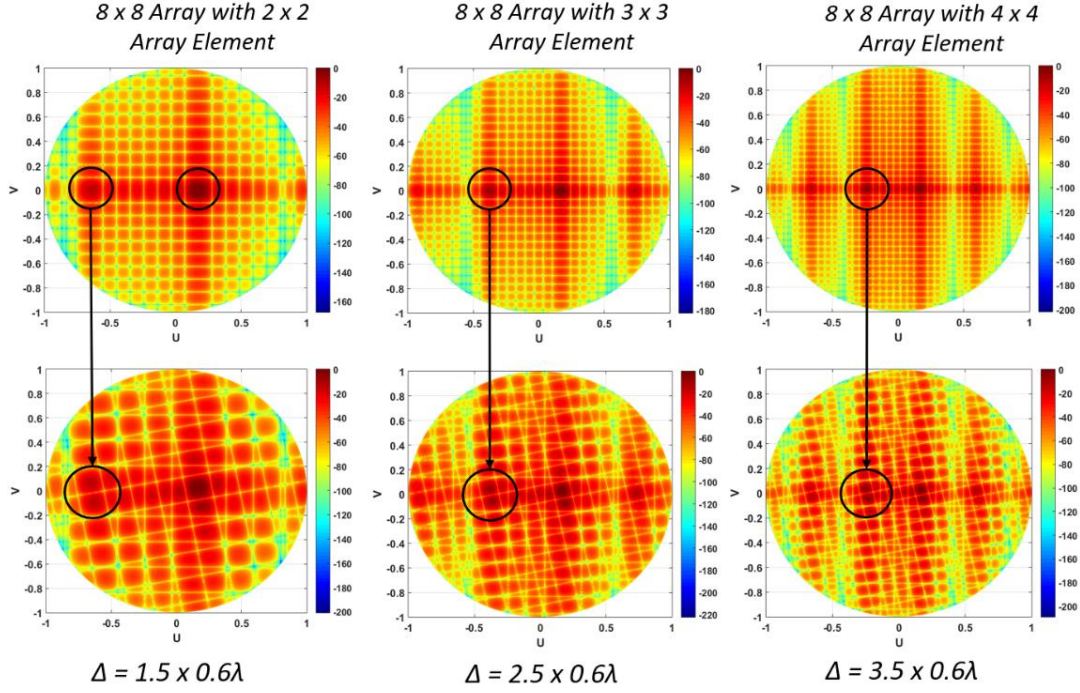


Figure 3.6: UV radiation pattern of 8 x 8 array with/without displacement of quadrant's and formed with 2 x 2 subarray, 3 x 3 subarray and 4 x 4 subarray

TABLE – 3.3: FARFIELD PERFORMANCE OF 8 X 8 ARRAY WITH SUBARRAY DISPLACEMENT

No. of subarrays	8 x 8					
No. of elements in subarray	2 x 2		3 x 3		4 x 4	
Inter-element spacing	0.6λ					
Scan Angle	10°					
Subarray displacement	0	1.5*0.6λ	0	2.5*0.6λ	0	3.5*0.6λ
Directivity	30.23 dB	30.04 dB	32.93 dB	32.33 dB	34.29 dB	33.11 dB
Peak SLL	-11.75 dB	-13.84 dB	-6.825 dB	-8.52 dB	-3.00 dB	-4.15 dB
Difference in Peak SLL	2.09 dB		1.695 dB		1.15 dB	

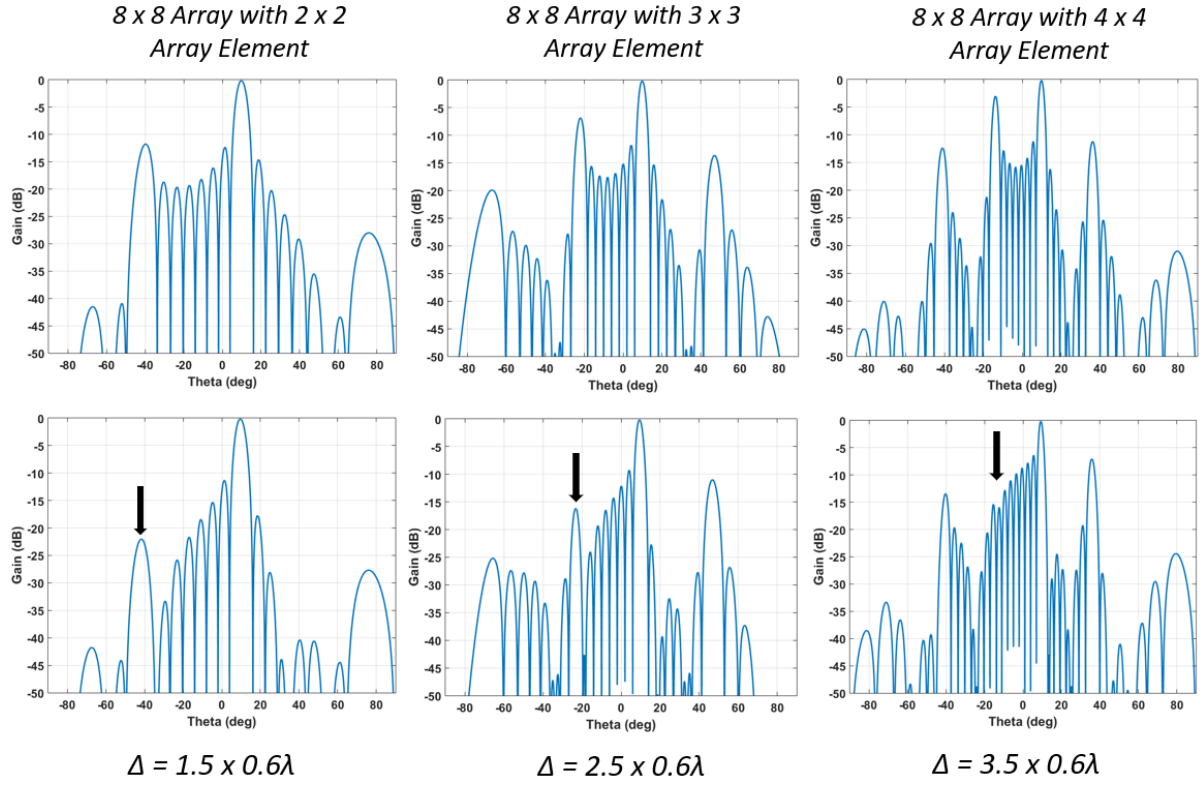


Figure 3.7: Principle plane radiation pattern of 8 x 8 array with/without displacement of quadrant's and formed with 2 x 2 subarray, 3 x 3 subarray and 4 x 4 subarray, for 10^0 beam scan

3.4 Pinwheel based aperiodically clustered array

The aperiodicity can also be introduced for grouping the periodically placed array elements. Such an aperiodic group of elements is called 'clusters' (an alternative way of naming 'subarray,' which is more suitable for the periodic arrays), which results in the improved beam scan range while reducing the number of array elements. In this thesis, one type of such clustering called 'Pinwheel' has been studied and its design process has been explained in detail.

Before initiating the design with the Pinwheel cluster, it is necessary to establish the applicability of such structure to the beam formation in the farfield. M. Marder has presented the manuscript, describing the relation and importance of order and symmetry in the Pinwheel structure [36]. It has been that the aperiodic Pinwheel structure offering finite peaks in their diffraction pattern has a finite degree of order embedded into it [36]. Such property of the Pinwheel structure is the primary inspiration for its use in the electromagnetic array antenna design. Moreover, the diffraction property of the Pinwheel structure has been explicitly established in this thesis. The Pinwheel lattice has been generated by recursive division of a

right angle triangle having $1:2:\sqrt{5}$ side ratio [37]. The section of the generated lattice is selected and the vertices of the triangles in the section are replaced with isotropic radiating sources. The farfield pattern of the same has been computed and plotted in 3D. Fig. 3.8 shows the above-described flow of work. From Fig. 3.8, it can be observed that the finite beam peaks are transpired at some ordered distance, which effectively validates the work presented in [36] and establishes its application for the aperiodic clustering study.

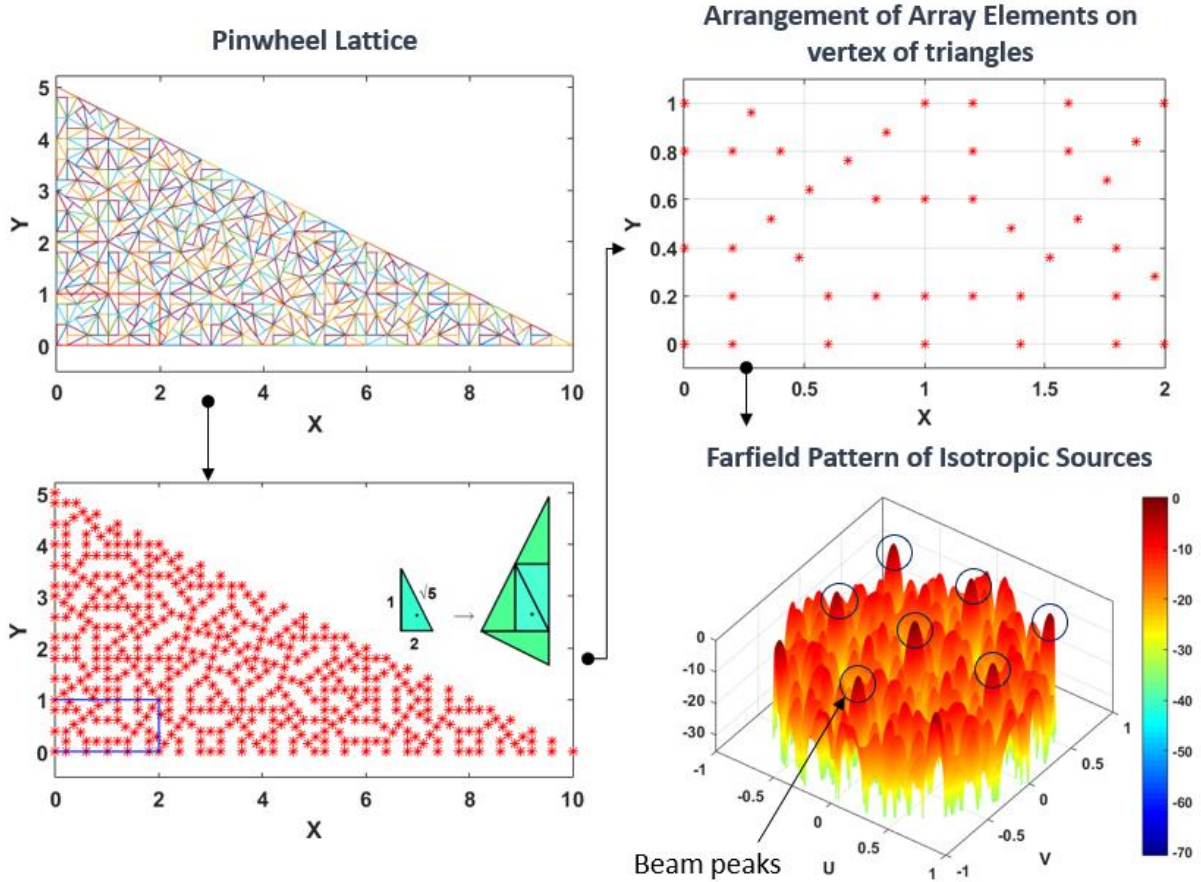


Figure 3.8: Generation of Pinwheel lattice and computation of the farfield pattern of isotropic sources placed at the vertices of the triangles in the lattice

Here, an example of square clustering of an 8×8 array antenna is presented, to discuss scanning characteristics of conventional and aperiodic clustering. S-band Coaxial fed Microstrip Patch Antenna has been designed and arranged in an 8×8 matrix fashion with an inter-element spacing of 0.65λ . The array elements are combined to form 2×2 subarrays and farfield pattern has been computed for 10° and 20° scanned beams. Fig. 3.9 shows the array layout where 2×2 elements are grouped to form a subarray. The farfield radiation patterns for 10° and 20° beam scans are presented in Fig. 3.10. As shown in Fig. 3.10, the 10° scan beam

results in 9.19dB GLL and 20° scan beam results in 1.73dB GLL, which is significant. Such scanning performance is not preferred in practical antenna applications, as a significant amount of radiating energy is wasted in grating lobes and such a high level of grating lobe receives strong interfering signals. These phenomena result in high ambiguity in synthetic aperture radar (SAR) systems and degrade carrier-to-interference ratio in communication systems.

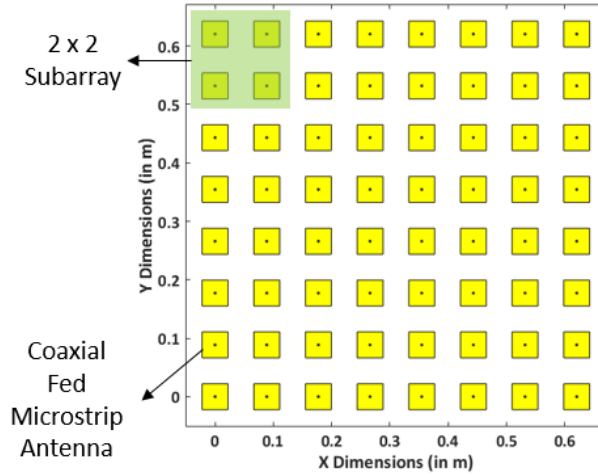


Figure 3.9: Periodic 8 x 8 array antenna and its subarraying

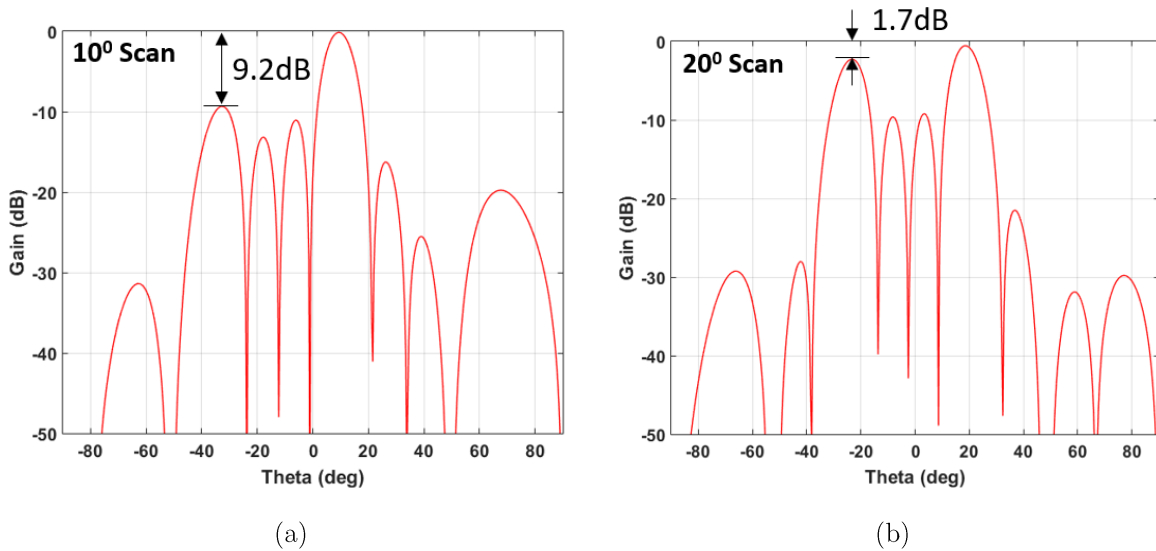


Figure 3.10: (a) 10° and (b) 20° scanned radiation patterns of periodically subarrayed 8 x 8 Array Antenna

As discussed in the previous section, the introduction of aperiodicity in the element position results in GLL improvement for the given scan range. However, in an array environment, the available positional range for perturbation is limited by inter-element spacing and mutual coupling between the array elements. Therefore, in place of changing the physical

location of elements, array elements can be aperiodically clustered to form subarray based on aperiodic tiling patterns. The aperiodic clustering does not strictly produce GL. Hence, it is recommended to look for peak SLL in a 3D radiation pattern as equivalent to GLL in the periodic arrays.

An 8×8 array has been mapped on the Pinwheel pattern to create the Pinwheel clustering, as shown in Fig. 3.11. Here, the location of the 8×8 array on the Pinwheel pattern may be selected by adjusting (X_offset, Y_offset) parameters. The 2D plot of the peak SLL level has been generated by parametric variation of (X_offset, Y_offset) for 10° and 20° beam scans and is presented in Fig. 3.12. The pair (X_offset, Y_offset) has been selected such that the peak SLL is minimum. For 10° beam scan, $(X_offset = 3.76)$ and $(Y_offset = 2.99)$ provides -13.0dB peak SLL. For 20° beam scan, $(X_offset = 3.36)$ and $(Y_offset = 1.15)$ provides -8.3dB peak SLL. Here, 3.8dB and 6.6dB improvements in SLL performance over that of the conventional periodic array have been achieved for 10° and 20° beam scans, respectively. Fig. 3.13 shows clustering of array elements for $(X_offset = 3.76, Y_offset = 2.99)$ and $(X_offset = 3.36, Y_offset = 1.15)$.

Fig. 3.14 shows the UV radiation pattern of the periodically clustered array and Pinwheel based clustered array, for a 10° beam scan. From Fig. 3.14, the phenomena causing the SLL improvement may be understood. From Fig. 3.14, it can be said that the aperiodicity has caused the redistribution of farfield energy. The various antenna farfield parameters of the array without any clustering, with Pinwheel based clustering and 2×2 periodic clustering have been listed in Table – 3.4 and 3.5 for 10° and 20° beam scans, respectively.

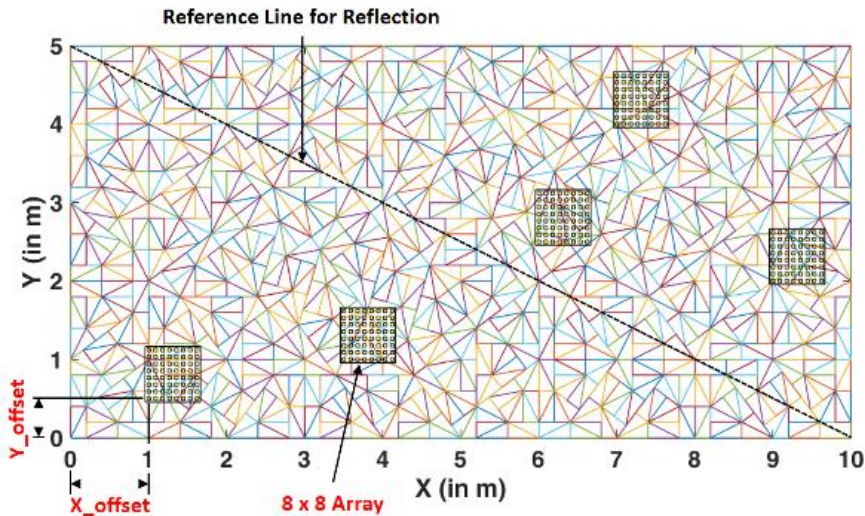
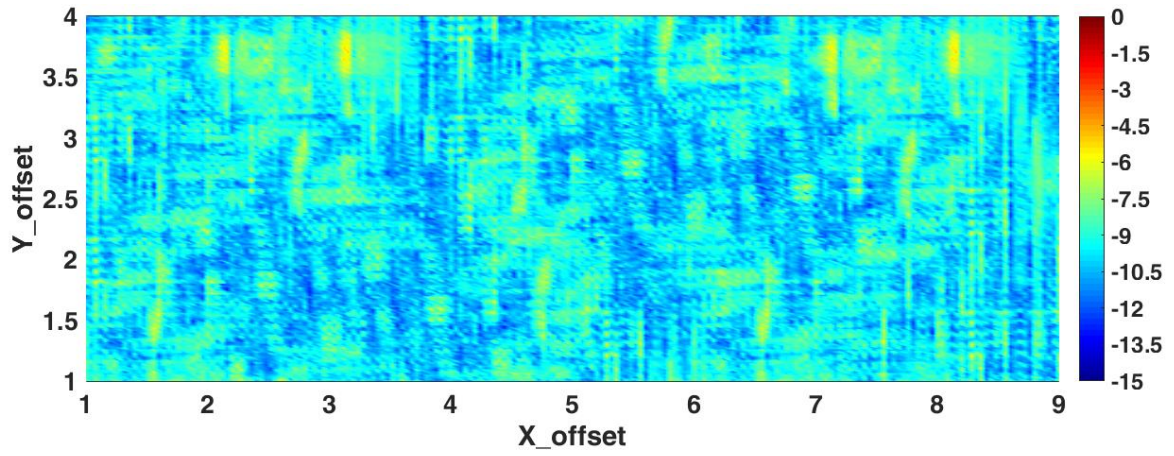
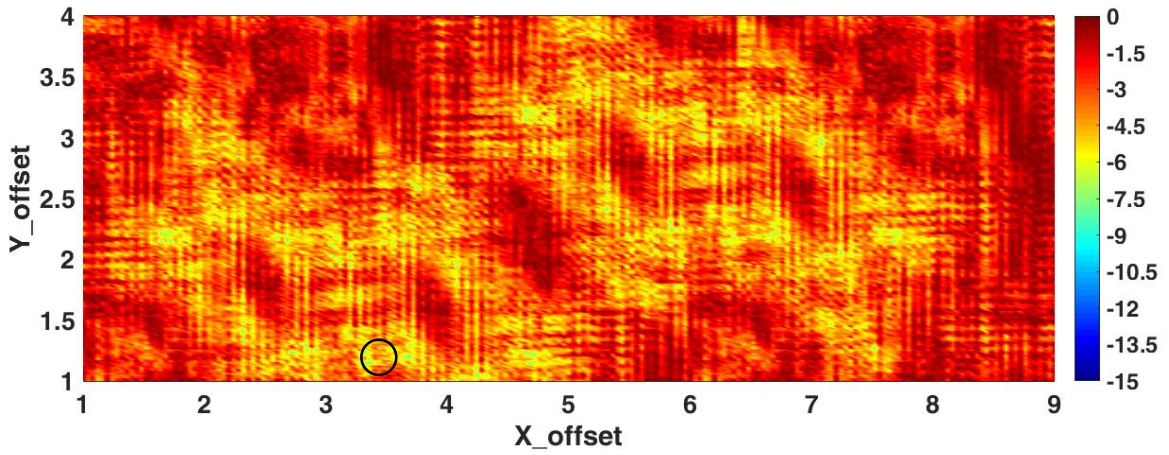


Figure 3.11: Various possible offsets applied to an 8×8 array antenna placed on Pinwheel type pattern

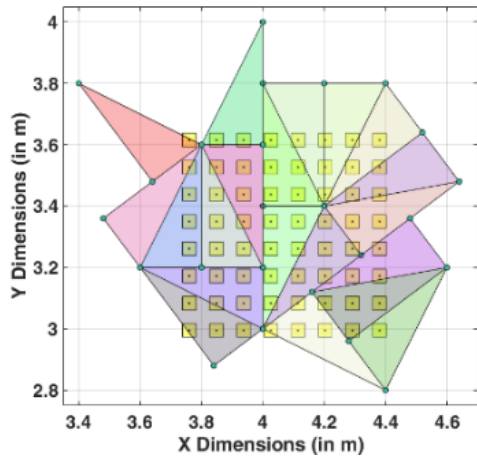


(a)

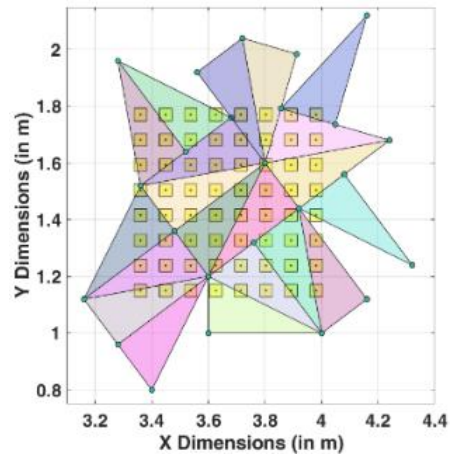


(b)

Figure 3.12: Peak SLL in 3D radiation pattern w.r.t displacements, for (a) 10^0 and (b) 20^0 beam scans

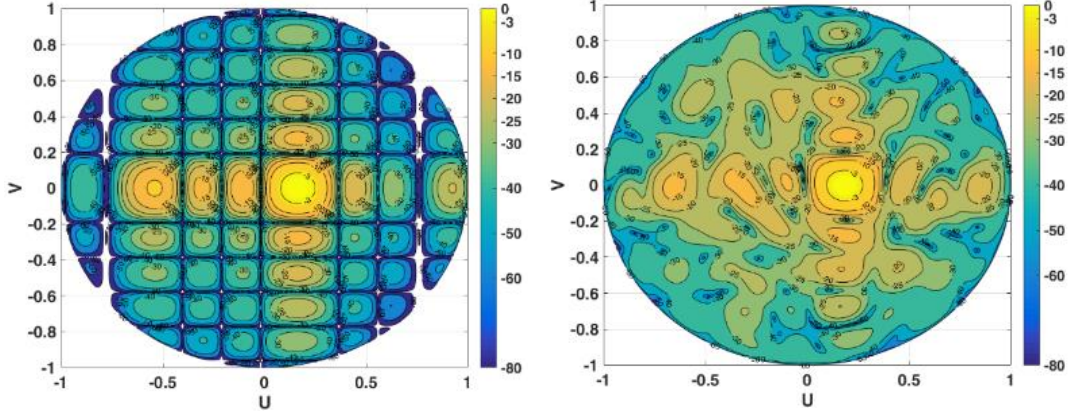


(a)



(b)

Figure 3.13: Pinwheel clustering of 8 x 8 array elements for displacement (a) ($X_{\text{offset}} = 3.76$, $Y_{\text{offset}} = 2.99$) for 10^0 beam scan and (b) ($X_{\text{offset}} = 3.36$, $Y_{\text{offset}} = 1.15$) for 20^0 beam scan



(a) (b)

Figure 3.14: 3D radiation pattern of 8 x 8 array antenna for (a) conventional rectangular clustering and (b) Pinwheel type clustering, for 10^0 beam scan

TABLE – 3.4: COMPARISON OF ANTENNA PARAMETERS FOR 10^0 SCAN

Parameters For 10^0 Scan	Conventional PAA	PAA with 2 x 2 Subarray	X_offset = 3.76, Y_offset = 2.99
No. of TRMs	64	16	20
Worst case SLL	12.7dB	9.2dB	13.0dB
Directivity from array analysis	25.3dBi	24.9dBi	23.7dBi
Simulated Gain	24.9dBi	24.3dBi	23.5dBi
3-dB Beamwidth from analysis	9.9^0	9.9^0	10.2^0
Simulated 3-dB Beamwidth	9.9^0	9.8^0	10.2^0

TABLE – 3.5: COMPARISON OF ANTENNA PARAMETERS FOR 20^0 SCAN

Parameters For 20^0 Scan	Conventional PAA	PAA with 2 x 2 Subarray	X_offset = 3.36, Y_offset = 1.15
No. of TRMs	64	16	20
Worst case SLL	12.2dB	1.7dB	8.3dB
Directivity from array analysis	25.1dBi	23.0dB	21.5dBi
Simulated Gain	24.7dBi	22.6	20.4dBi
3-dB Beamwidth from analysis	10.4^0	10.0^0	9.9^0
Simulated 3-dB Beamwidth	10.1^0	10.1^0	10.1^0

3.5 Strip projection (SP) method based aperiodic array antenna

The strip-projection based technique is the inspiration by the field of crystallography, where quasi-periodic crystals are studied as the projection of one order high dimensional lattice onto the desired dimensional crystal. The concept is profound and will be proved very efficient for the aperiodic and quasi-periodic beam steerable antenna designs. The design of an aperiodic

array antenna is initiated by selecting the one-order higher dimensional periodic lattice of any type like cubic, body-centric, etc. The lattice points of such periodic lattices are projected on the lower dimensional aperture plane. Here, the rotation of periodic lattice w.r.t to the 3-axis of the cartesian coordinate system projects various aperiodic configurations on the aperture plane. The rotation of periodic lattice can be optimized using various optimization techniques to obtain the desired farfield performance over the desired beam scan range. The proposed technique combined with stereographic projection has also been extended to correlation arrays used for radio astronomy. The stereographic projection helps to span the entire aperture plane when the polyhedron vertices are to be projected on the aperture plane.

3.5.1 Design of Aperiodic Linear Array Antenna

Fig. 3.15 shows the modelling scenario for generating an aperiodic linear array using the SP method. Here, the planar triangular periodic lattice in the X-Z plane is filled with elements having 0.7λ inter-element spacing. The acceptance domain (also called window) with dimensions of $(w_l \times w_h)$ has been defined to select the elements from the triangular lattice, which are later, projected onto the X-axis, forming an aperiodic array. In order to vary the aperiodic element distribution on X-axis, the triangular lattice is rotated w.r.t Y-axis (θ_{Rot}), which subsequently alters the number and locations of elements covered in the acceptance domain and hence, forms the variety of aperiodic linear arrays on the X-axis. Fig. 3.16 shows the aperiodic lattices for $\theta_{Rot} = 0^\circ, 30^\circ, 45^\circ$. Here, w_l is decided based on the aperture size requirement and w_h mainly governs the number of elements in the acceptance domain. Therefore, θ_{Rot} and w_h are two parameters that can be tuned or optimized to achieve desired farfield performance with beam scanning.

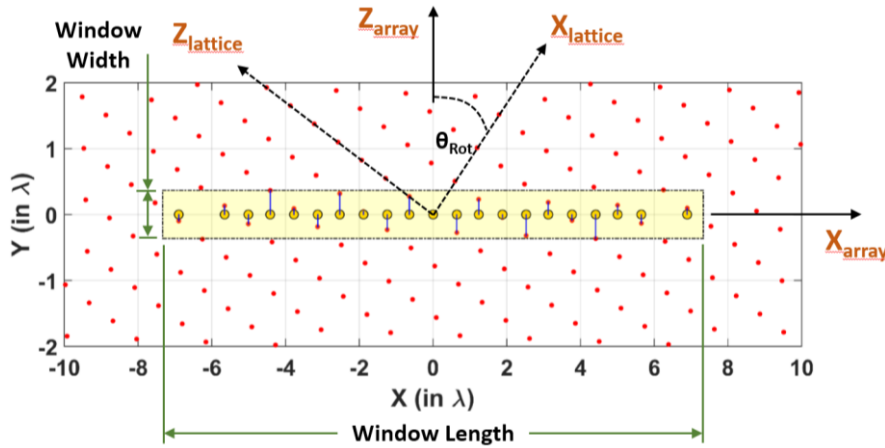


Figure 3.15: Modeling of aperiodic array lattice using SP method

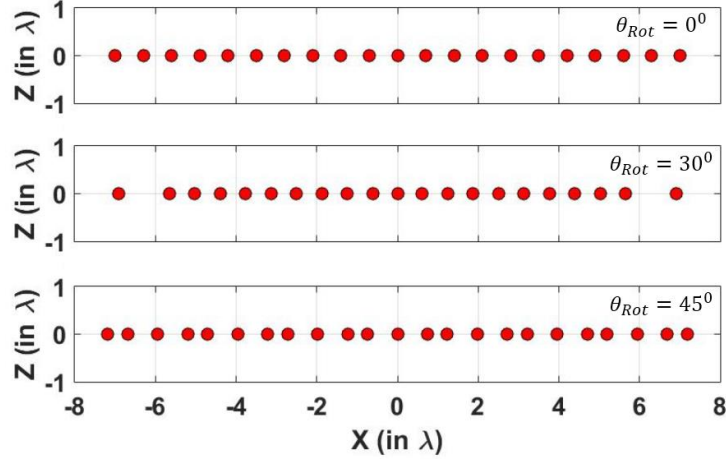


Figure 3.16: Sample aperiodic linear arrays for $\theta_{Rot} = 0^{\circ}, 30^{\circ}, 45^{\circ}$

Following is the brief mathematics carried out to develop and describe the implementation model of the same. Here, the elements in Π are the antenna elements having $\vec{F}(\theta, \varphi)$ radiation pattern. Usually, $\vec{F}(\theta, \varphi)$ is defined as $(\cos \theta)^{1-2}$. Equation (3.1) is used to compute the farfield radiation pattern of the generalized array configuration.

Primitive Vectors

$$\vec{a}_1 = (\cos \alpha, \sin \alpha)$$

$$\vec{a}_2 = \left(\frac{1}{2} \cos \alpha - \frac{\sqrt{3}}{2} \sin \alpha, \frac{1}{2} \sin \alpha - \frac{\sqrt{3}}{2} \cos \alpha \right)$$

$$\text{where } \alpha = 90^{\circ} - \theta_{Rot}$$

Set of planar lattice points

$$\Gamma = \{(m\vec{a}_1 + n\vec{a}_2) | m, n \in \mathbb{Z}\}$$

Acceptance domain

$$\Omega = \left\{ (x, y) \mid |x| \leq \frac{W_l}{2}, |y| \leq \frac{W_h}{2} \right\}$$

Set of projected lattice points on 1D line

$$\Pi = \{(x, 0) | \Gamma(x, y) \in \Omega\}$$

$$\vec{E}(\theta) = \vec{F}(\theta) \cdot \sum_{n=1}^N w_n \cdot e^{-i\vec{k}(\theta) \cdot \vec{x}_n} \quad (3.1)$$

Where,

$\vec{F}(\theta)$ = Element radiation pattern

N = No. of elements in Π

\vec{x}_n = Element position in array (Π_n)

$\vec{k}(\theta)$ = Wave vector $k_0 \cdot \sin(\theta)$

w_n = Excitation of n^{th} element $|w_n|e^{-j\phi_n}$

ϕ_n = Required phase for n^{th} element to scan beam in (θ_0) direction $-\vec{k}(\theta_0) \cdot \vec{x}_n$

k_0 = Wave number ($2\pi/\lambda_0$)

λ_0 = Operating wavelength

In this thesis work, using the SP method, a linear array with a 15λ aperture length is modeled and designed to achieve improved SLL performance for $\pm 30^\circ$ beam scan. As discussed, to achieve the desired performance with beam scan, θ_{Rot} and w_h are optimized. Any optimization algorithm or scheme can be used with a proper objective function definition. As the presented linear array is small, the brute-force search method has been applied. In this method, the θ_{Rot} and w_h are varied in the range of $(0^\circ, 90^\circ)$ and $(0.5\lambda$ to $0.6\lambda)$, respectively. The farfield parameter, especially peak SLL, has been computed for $\pm 30^\circ$ beam scan for all defined cases of θ_{Rot} and w_h . The computed variation of peak SLL and the number of elements is presented in Fig. 3.17. The variation of the peak SLL and the number of array elements have been compared with the conventional 21-element linear array antenna, having 0.7λ inter-element spacing. Such periodic array offers -8.42dB peak SLL for $\pm 30^\circ$ beam scan. Hence, taking -8.42dB peak SLL and 21 number of elements, the θ_{Rot} and w_h are selected from plots in Fig. 3.17, such that peak SLL < -8.42dB with no. of elements ≤ 21 . The obtained optimum θ_{Rot} is 23.15° for ($w_h = 0.55\lambda$). The generated aperiodic array lattice is shown in Fig. 3.18, along with the periodic array.

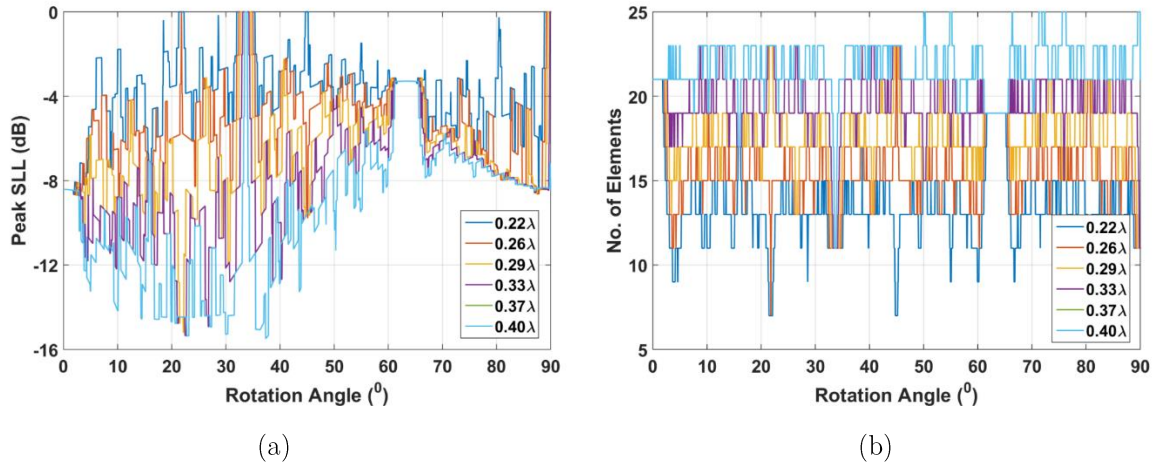


Figure 3.17: (a) Variation of peak SLL w.r.t θ_{Rot} for various w_h and (b) Variation of number of elements w.r.t θ_{Rot} for various w_h

To compare the proposed SP method with the reported optimization schemes for the aperiodic array design, the 21-element aperiodic linear array has also been designed using the optimization algorithms, namely, GA, PSO algorithm and Jaya algorithm. Table – 3.6 lists the no. of variables, the minimum required no. of evaluations and the achieved peak SLL for GA,

PSO and Jaya algorithms, and the proposed SP method. Moreover, Fig. 3.22 shows the comparison plot of far field radiation pattern for the -30° beam scan. From Table – 3.6 and Fig. 3.22, it can be said that the proposed SP method has the advantage over the optimization schemes in terms of no. of function evaluations and achieved peak SLL.

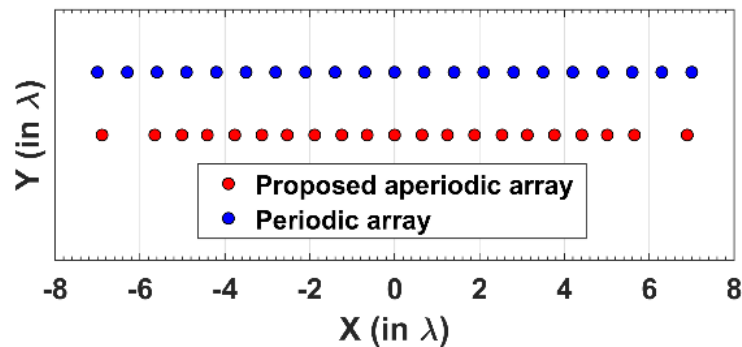


Figure 3.18: Element locations in the optimized linear aperiodic array and conventional periodic array

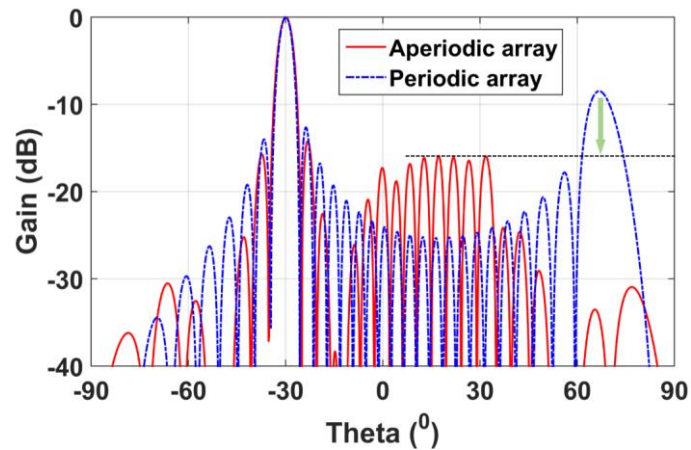


Figure 3.19: Far-field radiation pattern of aperiodic linear array and periodic linear array for -30° beam scan

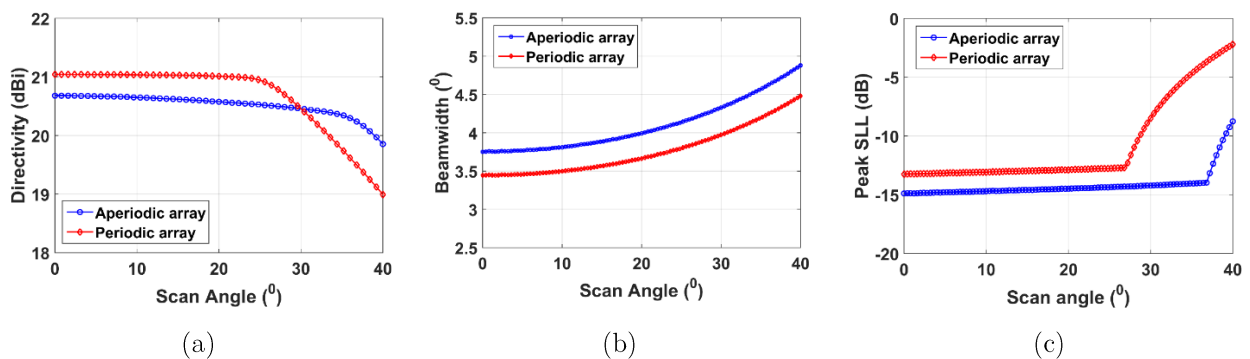


Figure 3.20: Comparison of (a) directivity variation, (b) beamwidth variation and (c) peak SLL variation, w.r.t scan angle for proposed aperiodic array and periodic array

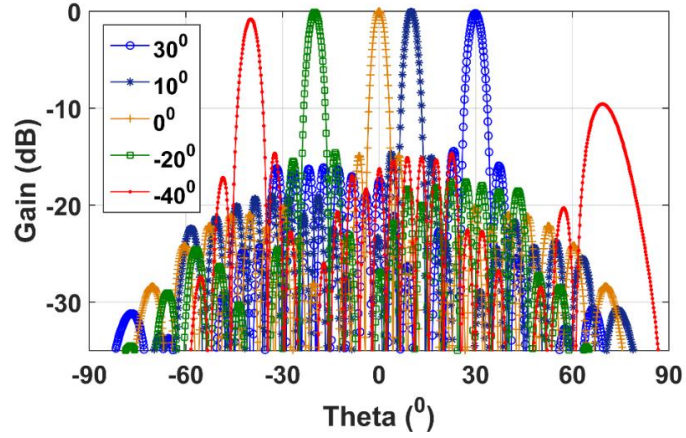


Figure 3.21: Far-field principle plane cuts of aperiodic array for various beam scans

TABLE – 3.6: NO. OF OBJECTIVE FUNCTION EVALUATIONS AND PEAK SLL FOR OPTIMIZATION ALGORITHMS

	Proposed Strip Projection Method	GA	PSO	Jaya
No. of Objective Function Evaluation	1801	564000	40500	30000
% increase	Reference	31%	22.49%	16.66%
Peak SLL achieved for -30° beam scan	-14.21	-10.17	-12.86	-12.93

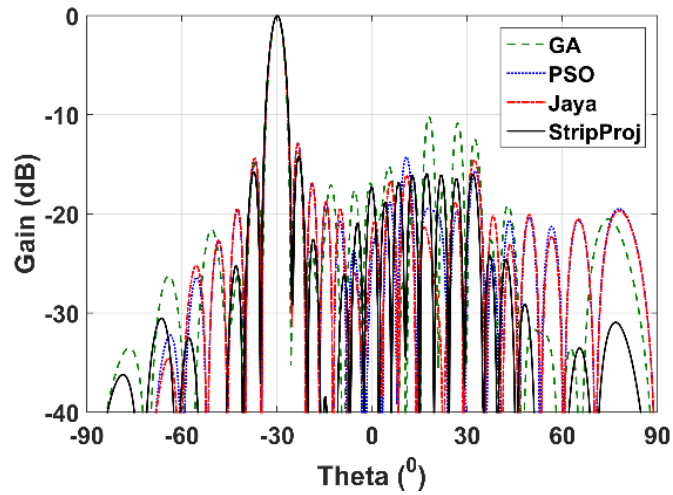


Figure 3.22: Comparisons of far-field pattern of aperiodic linear arrays generated by GA, PSO, Jaya algorithms and proposed SP method

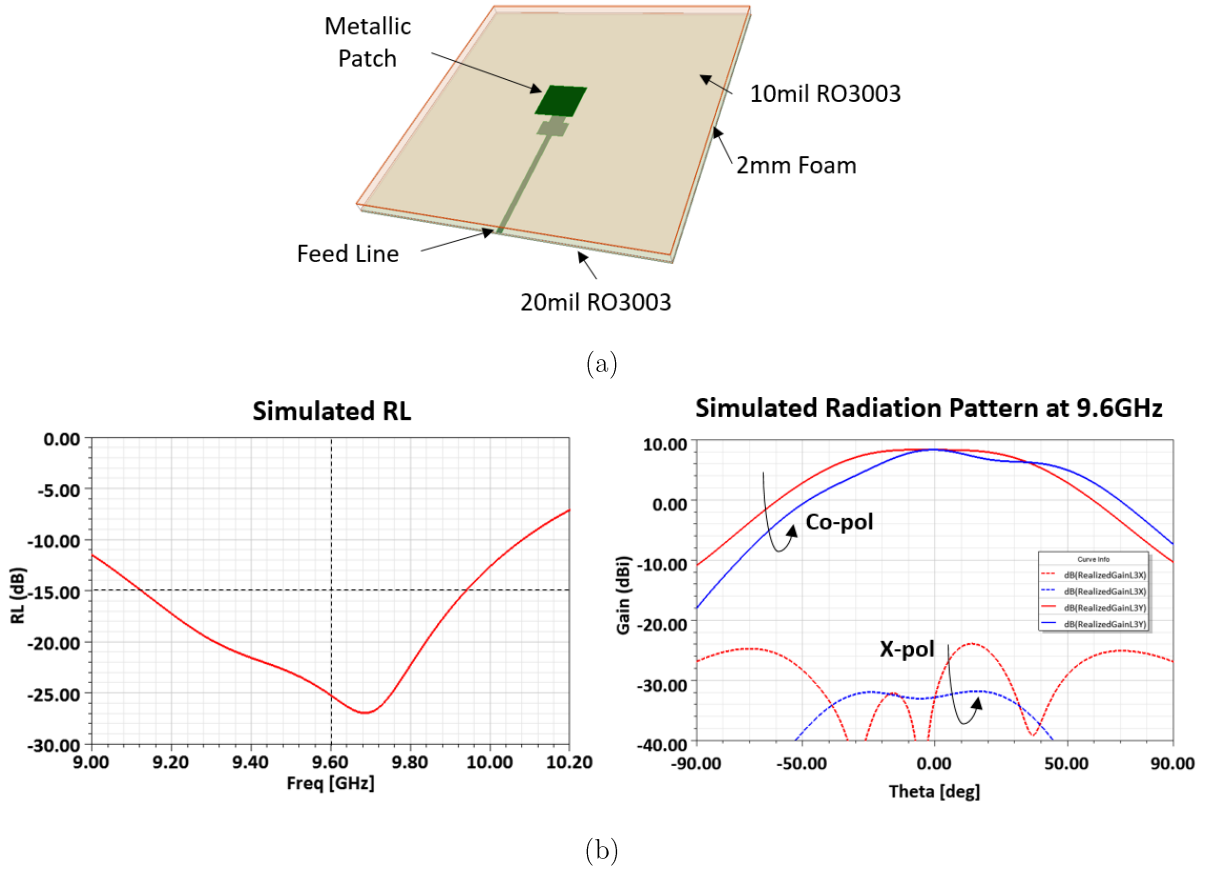


Figure 3.23: (a) X-Band Electromagnetically coupled (EMCP) microstrip single antenna element and (b) its simulated return loss and radiation pattern performance

To validate the proposed SP method, the 21 elements X-band microstrip patch-based aperiodic array antenna has been designed and simulated using the 3D finite element method (FEM) based electromagnetic simulator Ansys HFSS 20.0 [38]. Here, the electromagnetically coupled microstrip patch-based single element working at 9.6GHz has been designed to populate the aperiodic array lattice. The structure of the single element and its simulated performance is presented in Fig. 3.23. In order to provide the phase shift to the array elements for the beam scan, the high Dk substrate, i.e., Rogers TMM10i dielectric material having relative permittivity ($\epsilon_r = 9.8$) and loss tangent ($\tan \delta = 0.002$) is used on the microstrip line, as a phase shifting element. The structure of the same is shown in Fig. 3.24(a). Here, the length covered by the high Dk substrate over the microstrip line governs the generated differential phase shift ($\Delta\phi$). Fig. 3.24(b) shows the simulated performance of such a phase shifter at 9.6GHz. The populated structure of the X-band aperiodic array antenna, along with the dielectric-based phase shifting layer, is exhibited in Fig. 3.25(a). The four-separate phase-shifting layers have been designed to

demonstrate the array performance for 10° , 20° , 30° and 40° beam scans. The designed phase-shifting layout is also shown in Fig. 3.25(b).

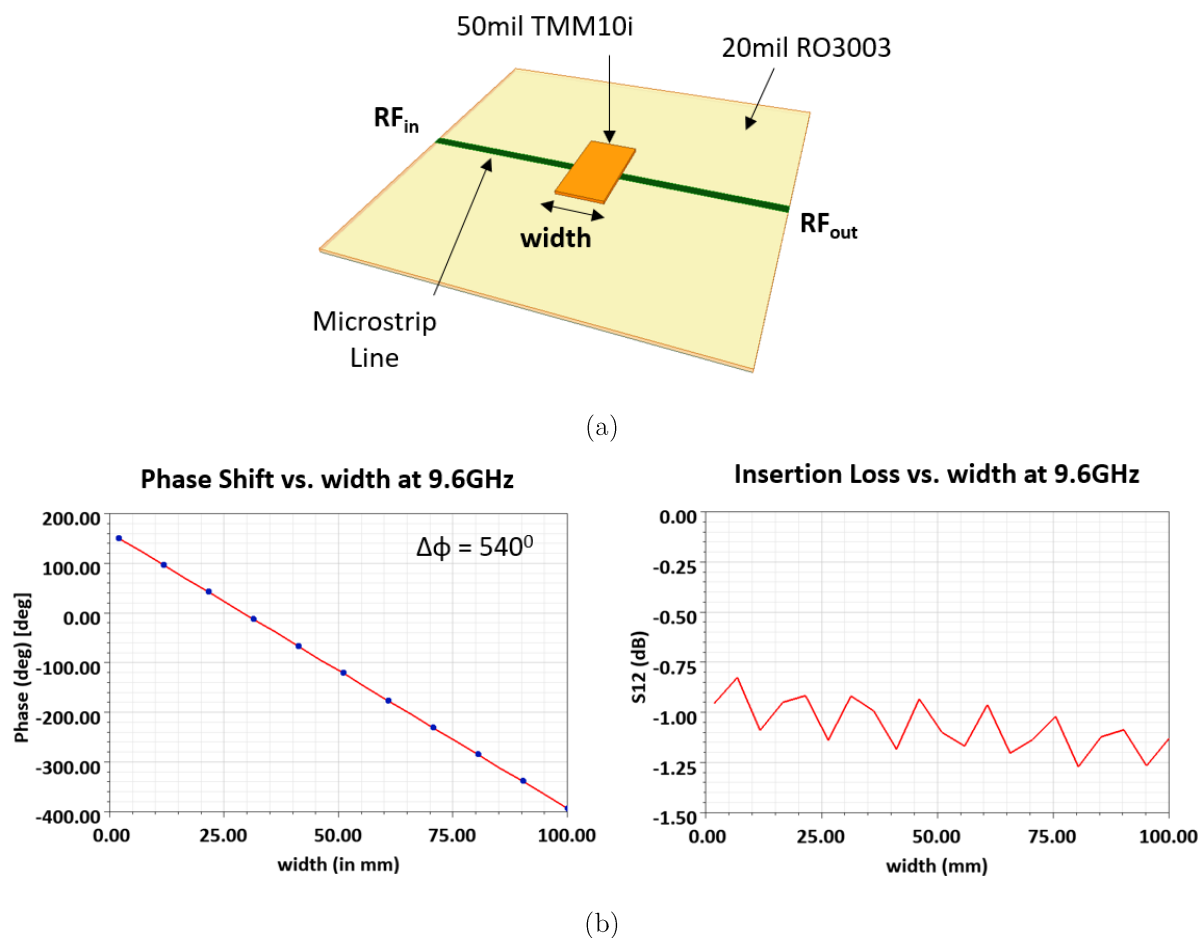


Figure 3.24: (a) Design of X band high Dk substrate (TMM10i) based phase shifter and (b) its simulated insertion phase and insertion loss performance by varying the width of TMM10i substrate

The designed X-band aperiodic array antenna has also been developed and characterized for various beam scans. Fig. 3.26(a) shows the developed model, mounted on the positioner of the anechoic chamber, for the farfield characterization. The 21 ports of the antenna have been combined using a 1:32 equi-phase power divider, where the 21 ports in sequence are connected with antenna ports and the remaining ports are terminated with matched loads. Fig. 3.27 presents the comparison of simulated, analyzed and measured performance of the proposed 21-element linear array antenna for various beam scans. From Fig. 3.27, it can be concluded that a good correlation has been achieved between the simulated and measured performance of the aperiodic linear array.

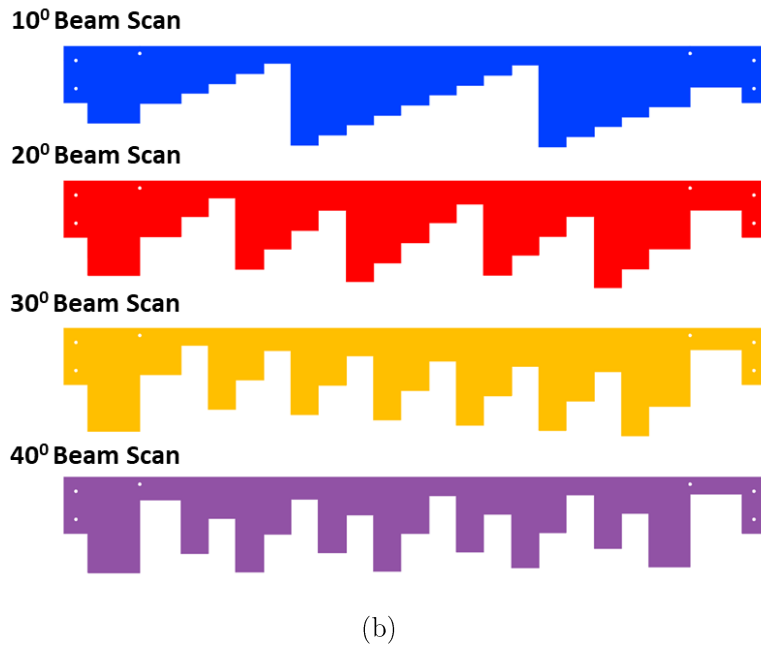
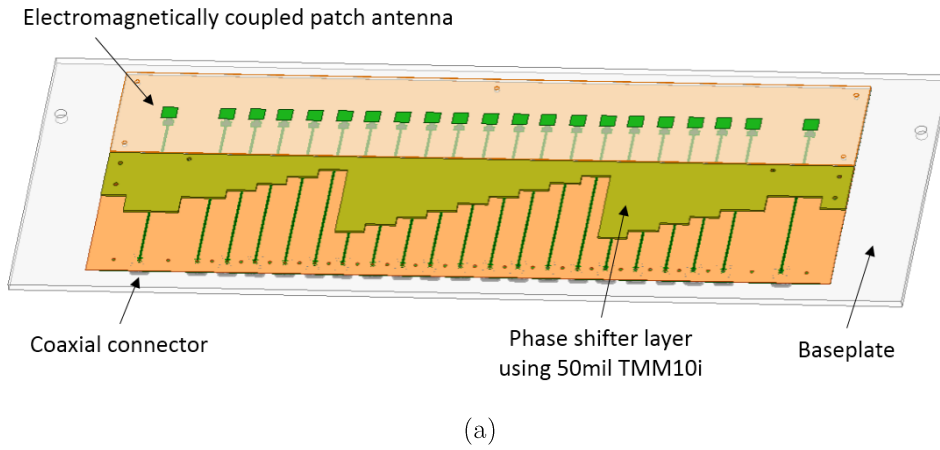


Figure 3.25: (a) Simulation model of X-band 21 elements aperiodic array antenna and (b) synthesized phase shifter layouts for various scan angles

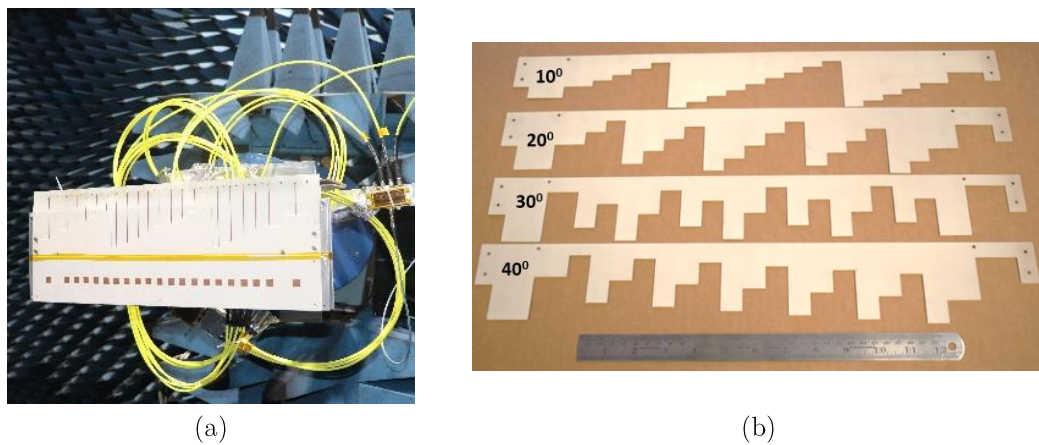


Figure 3.26: (a) Developed aperiodic array integrated with 1:21 equi-phase power divider and 10° phase shifter, and (b) developed phase shifter layers for various beam scans

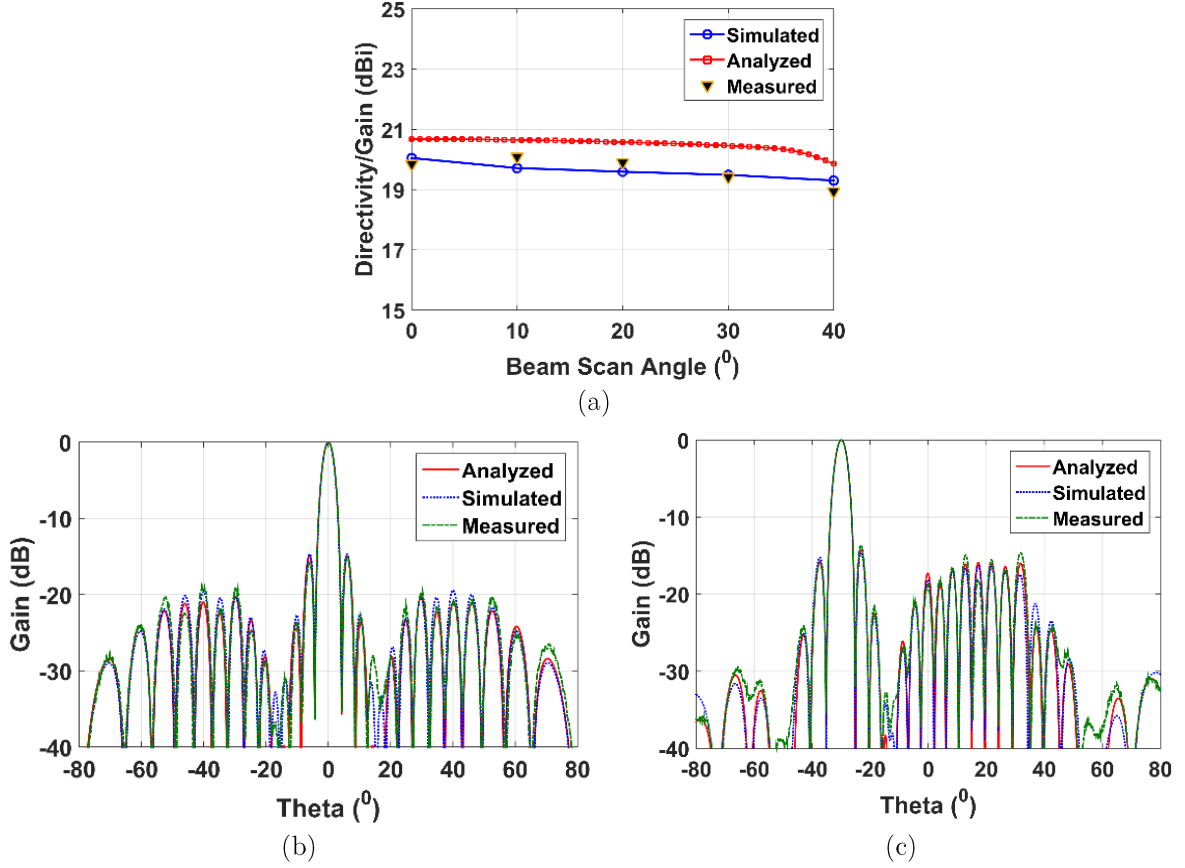


Figure 3.27: Comparison of analyzed, simulated and measured (a) gain/directivity variation with beam scan, (b) 0° scan radiation pattern and (c) -30° scan radiation pattern, for X-band 21 elements aperiodic array antenna

3.5.2 Design of Aperiodic Planar Array Antenna

The SP method described in the previous section is extended for the planar beam steerable array antennas. Here, the elements of a 3-dimensional (3D) lattice are projected onto a 2-dimensional (2D) lattice to form the planar array. For the demonstration of the SP method, a body-centric tetragonal lattice has been opted as a 3D lattice, where the inter-element spacing is 0.7λ ($\lambda =$ operating wavelength). The acceptance region (in this case, the acceptance volume) having dimensions $(W_x \times W_y \times W_z)$ is also defined in the lattice coordinate system. Fig. 3.28 shows the elements on the 3D lattice and the acceptance domain. The elements falling in the acceptance volume are projected on the X-Y aperture plane, which effectively forms the aperiodic planar lattice. As the 3D lattice can be rotated around any arbitrary vector \hat{n} , the element distribution on the X-Y aperture plane can be varied and optimized to achieve desired farfield performance with the beam scan. Rodrigue's Rotation Formula has been used to apply the rotation ' ψ ' to the 3D lattice w.r.t vector \hat{n} . The mathematical description of the SP method for

the generation of the planar aperiodic array is briefly described below,

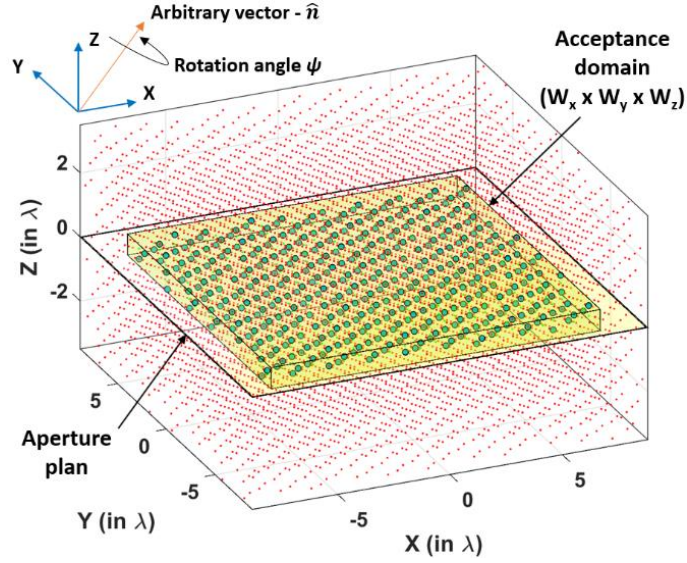


Figure 3.28: Modeling of SP method for planar aperiodic array, where rotated 3D lattice (red dots), acceptance domain (yellow box), lattice points enclosed by acceptance domain (green dots)

Primitive vectors

$$\vec{a}_1 = 0.7\lambda \cdot (1,0,0)^T, \vec{a}_2 = 0.7\lambda \cdot (0,1,0)^T, \vec{a}_3 = 0.35\lambda \cdot (0,0,1)^T \quad (3.2)$$

Rodrigue's Rotation Formula

$$\vec{a}'_i = \cos \psi \cdot \vec{a}_i + (1 - \cos \psi) \cdot (\vec{a}_i \cdot \hat{n}) \cdot \hat{n} + \sin \psi \cdot (\vec{a}_i \times \hat{n}) \quad (3.3)$$

Where $i = 1,2,3$

Set of 3D lattice points

$$\Gamma = \{(m\vec{a}'_1 + n\vec{a}'_2 + p\vec{a}'_3) | m, n, p \in \mathbb{Z}\}$$

Acceptance domain

$$\Omega = \{(x, y, z) | |x| \leq \frac{W_x}{2}, |y| \leq \frac{W_y}{2}, |z| \leq \frac{W_z}{2}\}$$

Set of the projected lattice points on the aperture plane

$$\Pi = \{(x, y) | \Gamma(x, y, z) \in \Omega\}$$

The vectors $\{\vec{a}_1, \vec{a}_2, \vec{a}_3\}$ are the primitive vector to define the elements in the unit cell of the 3D lattice. After applying Rodrigue's rotation formula, the vector $\{\vec{a}'_1, \vec{a}'_2, \vec{a}'_3\}$ are generated, which are translated to develop the 3D lattice. The elements belonging to set 'Π' forms the aperiodic planar lattice, whose farfield characteristics have been analyzed using Equation (3.4). Here, W_x, W_y, W_z, \hat{n} and ψ are the parameters optimized to improve the peak SLL for 30° beam scan in three principle planes ($\varphi = 0^\circ, \varphi = 45^\circ$ and $\varphi = 90^\circ$) and to reduce the number of array elements. Jaya algorithm based global optimization [39] has been used for the optimization. W_x and W_y parameters are fixed as per the required aperture dimensions. In the presented case, W_x and W_y parameters are 15λ . W_z is the crucial parameter which governs the distribution as well

as number of elements in the array. The optimization has been carried out by considering W_z, \hat{n} and ψ parameters as the optimization variable. The optimized values of W_z, \hat{n} and ψ are 0.63λ , $(-0.26, 0.46, -0.85)$ and 46.55° , respectively. The corresponding generated aperiodic array contains 378 elements (N_{sp}). Fig. 3.30 shows the antenna element distribution of the aperiodic planar array.

$$\vec{E}(\theta, \phi) = \vec{F}(\theta, \phi) \cdot \sum_{n=1}^N \omega_n \cdot e^{-j\vec{k}(\theta, \phi) \cdot \vec{r}_n} \quad (3.4)$$

Where,

$\vec{F}(\theta, \phi)$ = Element radiation pattern

N = No. of elements in Π (N_{sp})

\vec{r}_n = Element position (x, y) in array (Π_n)

$\vec{k}(\theta, \phi)$ = Wave vector $k_0 \cdot (\sin \theta \cdot \cos \phi, \sin \theta \cdot \sin \phi)$

ω_n = Excitation of n^{th} element $|\omega_n|e^{-j\theta_n}$

θ_n = Required phase for n^{th} element to scan beam in (θ_0, ϕ_0) direction $-\vec{k}(\theta_0, \phi_0) \cdot \vec{r}_n$

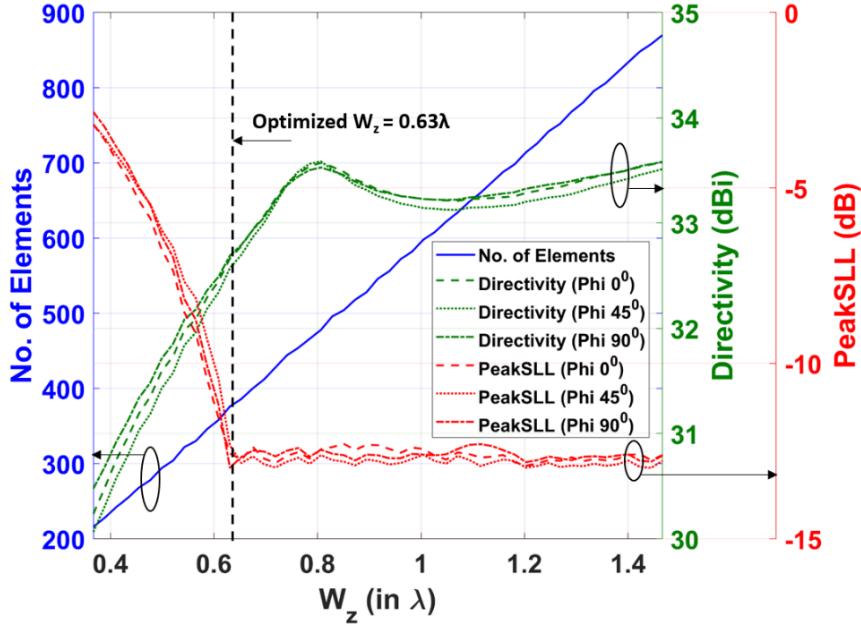


Figure 3.29: Variation of No. of Elements, directivity and peak SLL w.r.t W_z , for $(W_x, W_y) = (15\lambda, 15\lambda)$ aperture dimension

To achieve similar farfield performance, the number of elements required by the proposed optimized aperiodic array is 21.9% less than the periodic rectangular lattice. Moreover, the impact of the variation of W_z on the number of elements, directivity and peak

SLL has also been studied for the optimized \hat{n} and ψ . The plots of the same are presented in Fig. 3.29. From Fig. 3.29, it has been found that the proposed W_z is optimum for the specified beam scan requirement. Moreover, the distribution of the elements in the aperiodic array is quantified by taking the standard deviation of the element positions. The position standard deviation (σ_0) is defined as per Equation (3.5).

$$d_n = \min(\|\vec{r}_n - \vec{r}_i\|)$$

$$\sigma_0 = \sqrt{\frac{\sum_n (d_n - \bar{d}_0)^2}{N-1}} \quad (3.5)$$

where,

\bar{d}_0 = the average minimum interelement spacing

\vec{r}_n = position of n^{th} element

\vec{r}_i = position of i^{th} element

d_n = distance to the nearest element

\bar{d}_0 = average minimum interelement spacing of the array

N = Total number of elements

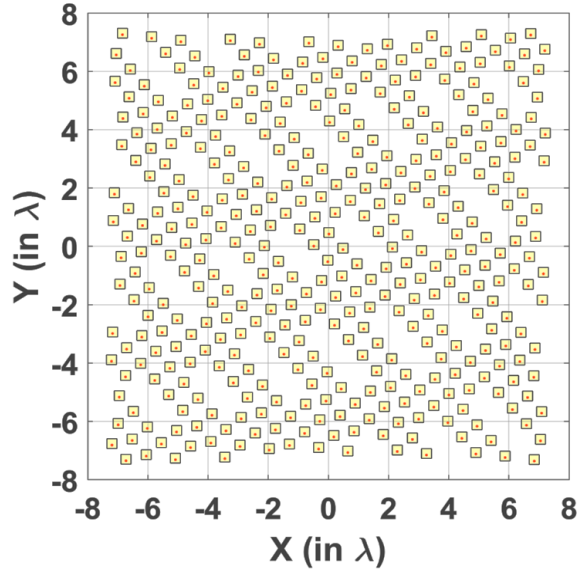


Figure 3.30: Aperiodic planar array generated using SP method

To compare the antenna performance of the aperiodic array generated by the SP method, Pinwheel based aperiodic array has also been generated. Pinwheel lattice has been generated by the substitution method where $(0, 0)$, $(0, 2\chi\lambda)$ and $(1\chi\lambda, 0)$ are the vertex of the base triangle [37]. χ is the scale factor and governs the number of array elements (N_{pw}) in the lattice. In general, large χ produces small N_{pw} , which offers poor directivity performance. Fig. 3.31 presents the variation of N_{pw} , directivity and peak SLL w.r.t χ . In this thesis, $\chi = 4.7$ is selected such

that $N_{pw} \approx N_{sp}$. For the selected χ , the number of array elements (N_{pw}) is 418, which is 15.78% less than the number of elements in the periodic array antenna. The Pinwheel lattice with element position is shown in Fig. 3.32(a). Fig. 3.32(b) shows the aperiodic array generated by placing the elements on the vertices of the Pinwheel triangles.

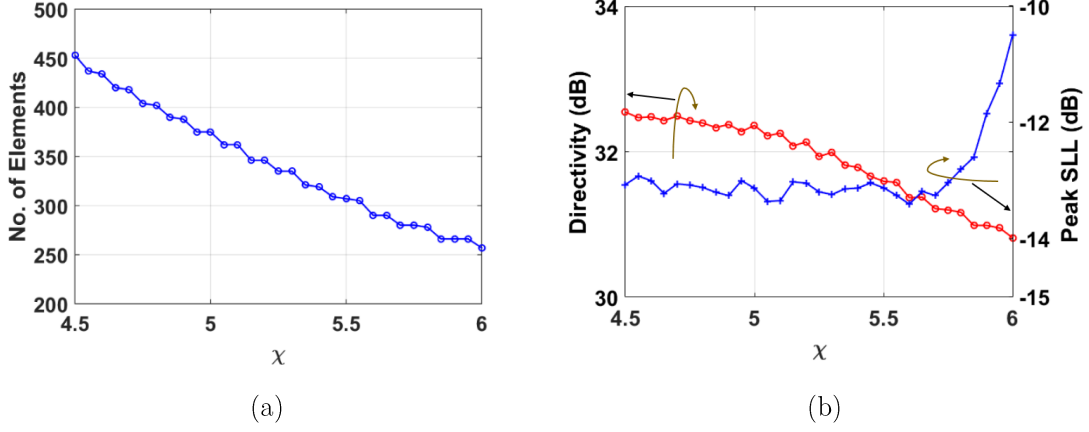


Figure 3.31: (a) Variation of number of element w.r.t χ and (b) Variation of directivity w.r.t χ , for $(15\lambda \times 15\lambda)$ pinwheel based aperiodic array

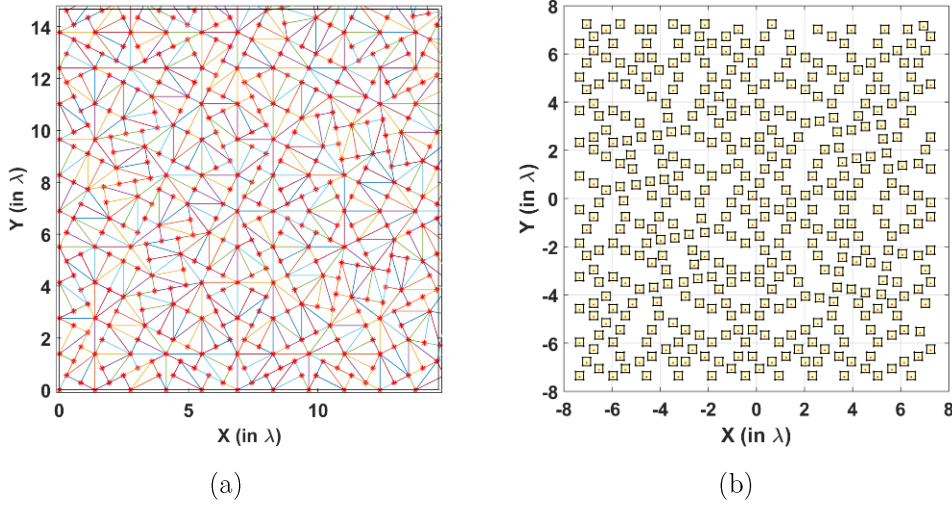


Figure 3.32: (a) Construction of pinwheel lattice and (b) designed pinwheel lattice based aperiodic array, for $(15\lambda \times 15\lambda)$ aperture dimension

The antenna array performance offered by both aperiodic array lattices has been simulated using the 3D electromagnetic simulator, i.e., Ansys HFSS 20.0. The aperiodic lattice points are populated with a dielectric resonator (DR) antenna operating at 2.2GHz [40]. The S-band cubic-shaped coax-fed DR antenna as the radiating element in the array has been opted to reduce the computational burden of 3D solver and speed up the simulation. Moreover, any printed broadside radiating element may be used to populate the proposed aperiodic array lattice and the desired scan performance can be ensured. Fig. 3.33 presents the DR structure and its

simulated performance. The populated structures of the proposed and Pinwheel based aperiodic array are exhibited in Fig. 3.34(a) and (b), respectively. The farfield performance of both aperiodic array antenna and equivalent periodic array antenna has been analyzed, simulated and evaluated at various beam scan angles. The UV radiation patterns of both types of the aperiodic array have been studied for various beam scans. Fig. 3.35 illustrates the analyzed and simulated UV radiation patterns of the proposed aperiodic array for -30° beam scan. The same for Pinwheel based aperiodic array has been illustrated in Fig. 3.36. The variation of directivity, peak SLL and beamwidth is also presented in Fig. 3.37. Table – 3.7 summarizes the results for -30° beam scan angle. Based on the UV radiation patterns, Fig. 3.37 and Table – 3.7, the following observations are derived,

- (1) The energy redistribution phenomenon has occurred, which has resulted in the improvement in peak SLL without affecting the main lobe shape. It has also been found out that the energy spread in the pinwheel-based array lattice is relatively large.
- (2) The proposed SP method based aperiodic array lattice has resulted in peak SLL < -11.36 dB over $\pm 30^\circ$ conical beam scan.
- (3) Directivity reduction of 0.94dB and 1.11dB in the boresight direction has been obtained in the case of the proposed array lattice and the pinwheel based array lattice, as compared to the periodic array.
- (4) There is a marginal impact on beamwidth performance. The beamwidth offered by the proposed aperiodic lattice is 0.08° wider than the pinwheel based aperiodic lattice and periodic lattice.
- (5) For the 30° beam scan, 0.56dB and 0.77dB directivity reduction can be observed in the SP method based and the pinwheel based array lattice, respectively.
- (6) Significant improvement in the scan loss performance has been achieved in both planar array lattices compared to the conventional periodic array lattice.
- (7) Although the proposed array lattice has been designed to achieve performance improvement at 30° beam scan, the functional scan range can be extended up to 40° with 1.8dB scan loss. The extended scan range of the aperiodic lattice can be attributed to the average inter-element spacing, i.e., 0.66λ for the SP based aperiodic array and 0.58λ for the pinwheel based aperiodic array.

The directivity reduction mentioned in observation (5) may be explained using position standard deviation (σ_0). Fig. 3.38 shows the distribution of the nearest element spacings for the SP based and Pinwheel based aperiodic arrays. From Fig. 3.38, it can be observed that the position spread is larger in the Pinwheel based array than in the SP based array. As a result, σ_0 for the SP based array is significantly less than σ_0 for the Pinwheel based array, as presented in Table-3.7. Alternatively, it can be interpreted as the large value of σ_0 implies high aperiodic content in the element position, resulting in the significant energy spread in the far field radiation pattern. Such an energy spread tends to reduce the directivity.

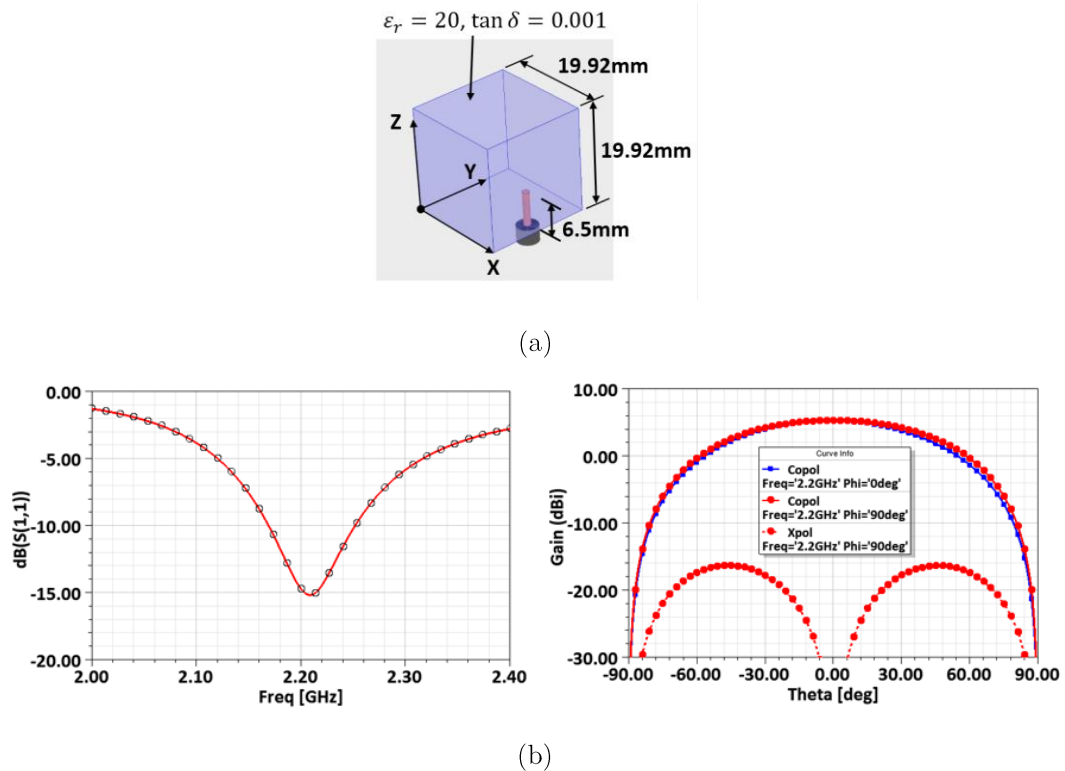


Figure 3.33: (a) S-band cubic shaped DR based radiating element, and (b) its simulated return loss and radiation pattern performance

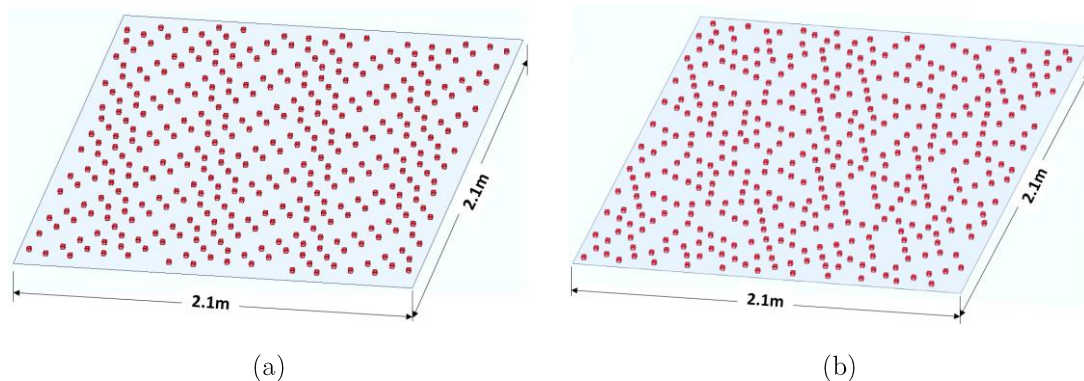


Figure 3.34: Simulated structures of (a) strip-projected planar aperiodic array and (b) pinwheel lattice based planar aperiodic array

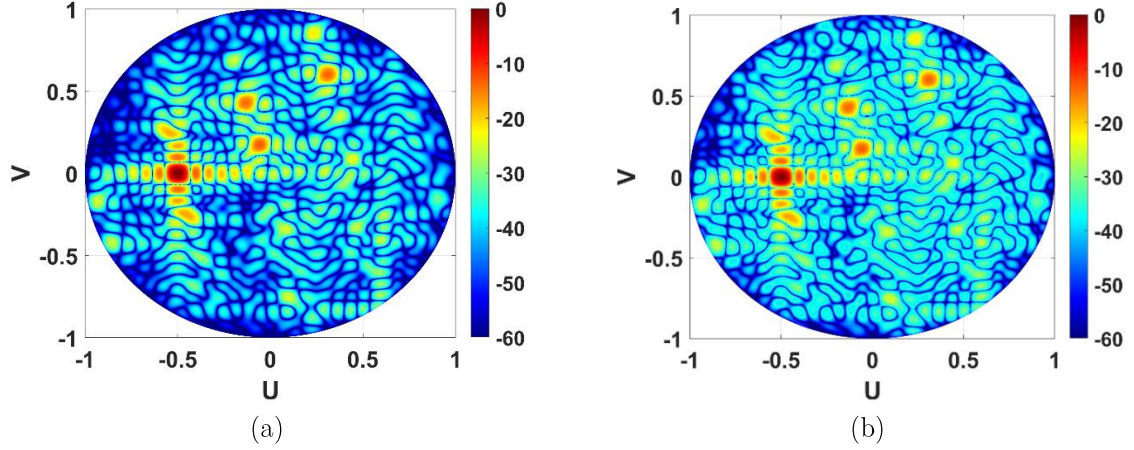


Figure 3.35: (a) Analyzed and (b) simulated UV radiation patterns of strip-projection method based planar aperiodic array, for -30° beam scan

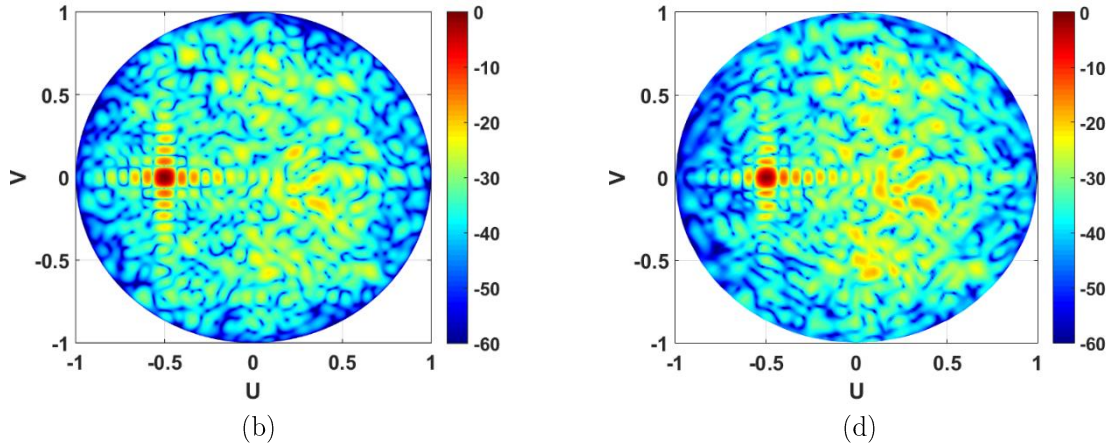


Figure 3.36: (a) Analyzed and (c) simulated UV radiation patterns of pinwheel lattice based planar aperiodic array, for -30° beam scan

It is important to compute the active reflection coefficient (active S_{11}) for the array elements of the simulated SP based and Pinwheel based aperiodic array. The computation of ARC has been carried out using the simulated passive S-parameters of the elements and fed them to Eq. (3.6) for each element [41]. Fig. 3.39 shows the element-wise active S_{11} of both types of aperiodic DRA antennas for various beam scans. From Fig. 3.39, it is evident that the proposed SP based DR array shows the improved active S_{11} over the beam scan, then the Pinwheel based DR array. This phenomenon is attributed to the average inter-element spacing of both types of aperiodic arrays. Since the average inter-element spacing (presented in Table-3.7) is larger in the case of SP based aperiodic array, the mutual coupling between the element is reduced, resulting in the improved active S_{11} .

$$(Active S_{11})_{mth\ element} = \sum_{n=1}^N S_{m,n} \frac{w_n}{w_m} \quad (3.6)$$

Where $S_{m,n}$ is the scattering parameter between m^{th} and n^{th} element and w_m and w_n are the excitation weight of m^{th} and n^{th} array elements.

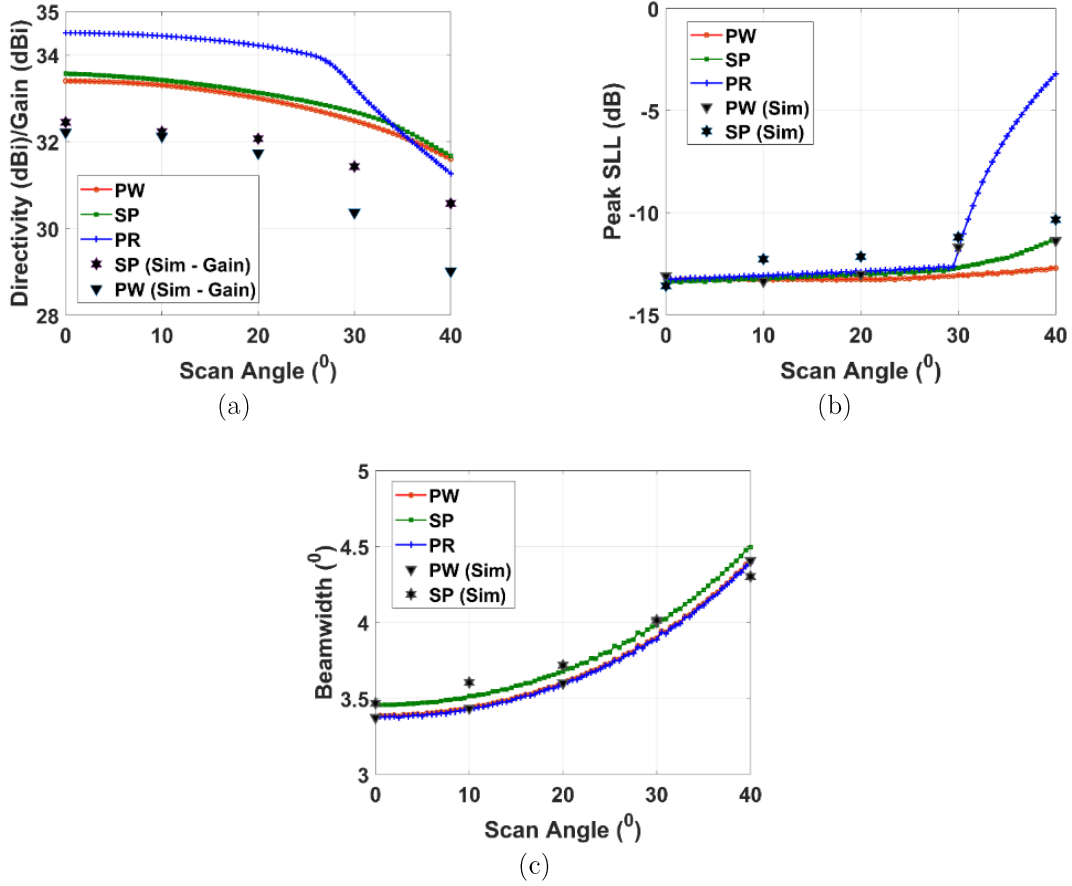


Figure 3.37: Variation of (a) directivity, (b) peak SLL and (c) beamwidth with scan angle for three types of array lattices (PW – Pinwheel based planar aperiodic array, SP – Strip-projection based planar aperiodic array, PR – Periodic planar array)

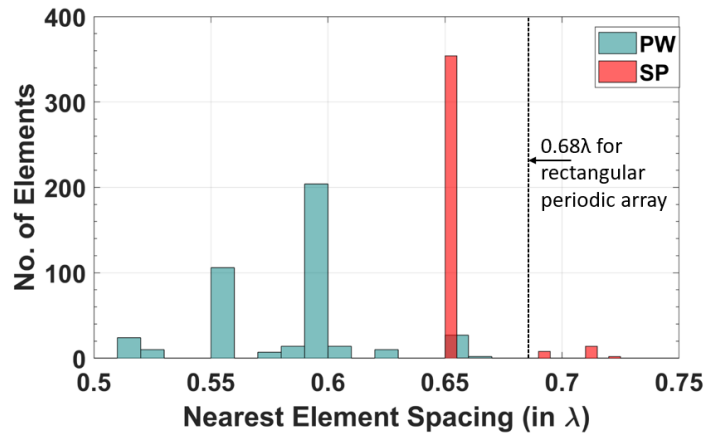
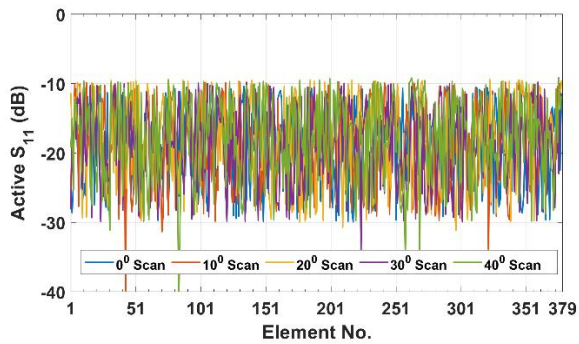


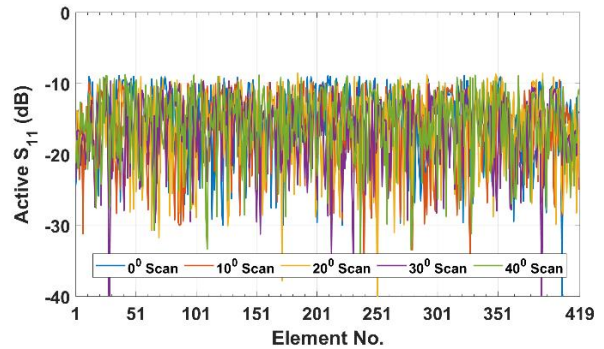
Figure 3.38: Distributions of the nearest element spacing for the planar aperiodic array lattices

TABLE – 3.7: FARFIELD PARAMETERS OF APERIODIC AND PERIODIC ARRAYS AT -30° BEAM SCAN

30° Beam Scan		Strip-projection based Aperiodic Array	Pinwheel base Aperiodic Array	Rect. Periodic Array
Average Inter-element spacing		0.66λ	0.58λ	0.68λ
No. of elements		378 (21.9% reduction)	418 (15.78% reduction)	484 (22 x 22)
Position Mean Deviation (in λ)		0.02	0.097	0
Position standard deviation σ_0 (in λ)		0.0131	0.0312	0
Peak SLL (dB)	$\theta = -30^\circ$ $\varphi = 0^\circ$	-12.81	-13.1	-11.95
	$\theta = -30^\circ$ $\varphi = 45^\circ$	-11.63	-12.83	-12.81
	$\theta = -30^\circ$ $\varphi = 90^\circ$	-12.84	-12.7	-11.95
Directivity (dB)	$\theta = -30^\circ$ $\varphi = 0^\circ$	32.69	32.5	33.26
	$\theta = -30^\circ$ $\varphi = 45^\circ$	32.59	32.48	33.86
	$\theta = -30^\circ$ $\varphi = 90^\circ$	32.71	32.5	33.26
Beamwidth ($^\circ$)	$\theta = -30^\circ$ $\varphi = 0^\circ$	3.98	3.90	3.89
	$\theta = -30^\circ$ $\varphi = 45^\circ$	4.01	3.97	3.96
	$\theta = -30^\circ$ $\varphi = 90^\circ$	3.95	3.90	3.89
Scan Loss (dB)		0.9	0.9	1.25



(a)



(b)

 Figure 3.39: Element wise active S_{11} of planar aperiodic DR array antenna using (a) the strip projection method and, (b) Pinwheel based method

The noteworthy feature of the proposed SP based aperiodic array is highlighted by computing the number of array elements with aperture size. Fig. 3.40 shows the same for three array lattices, namely, the SP based aperiodic array, conventional periodic rectangular array and Pinwheel based aperiodic array. From Fig. 3.40, it is evident that the number of the array element with an increase in aperture size remains significantly low in the case of the proposed aperiodic array, compared with the other two types of array. Table-3.8 shows the best-fit equations to compute the number of array elements w.r.t the aperture size. Here, the square aperture is assumed and the variable (x_λ) presents the aperture size in terms of operating wavelength and in the one direction. Moreover, Table – 3.9 compares the beam steerable proposed aperiodic array with published designs. It would be emphasized here that the literature contains various design methods of the aperiodic planar array antenna. However, most of the publications do not address equivalent beam scanning scenarios.

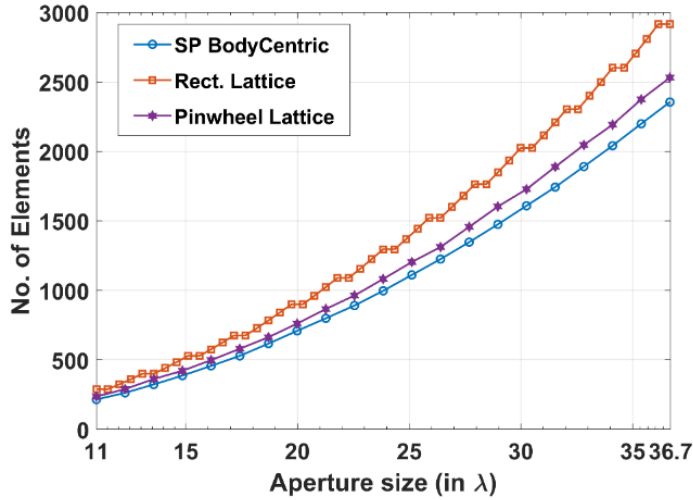


Figure 3.40: Comparison of the variation of the number of array elements with aperture size for various types of planar array lattices

TABLE – 3.8: BEST-FIT EQUATIONS FOR COMPUTATION OF NUMBER OF ELEMENTS

Lattice Type	Best-fit equation
Conventional periodic array	$x_\lambda^{2.212} + 125.3$
Pinwheel based aperiodic array	$x_\lambda^{2.171} + 86.05$
SP based aperiodic array	$x_\lambda^{2.151} + 66.39$

Where x_λ = aperture size in terms of operating wavelength

One of the major drawbacks of an aperiodic array is the lack of repetitive blocks in the arrays, which may lead to the design of an asymmetric beamforming network. Such an asymmetric beamforming network design requires special attention to maintain the amplitude

and phase at each array element with an asymmetric length of a transmission line. Therefore, an alternative approach of an active beam steerable antenna using RF beamforming (BF) ICs is proposed. Recent developments in the field of RF BFN ICs have literally revolutionized the field of Satellite-on-the-move (SOTM) and ground terminals for various applications. The RF BF ICs are equipped with low noise amplifiers (LNAs), power amplifiers (PAs), digital phase shifters (DPS) and digital attenuators (DA), and hence, making them a fully integrated solution that eliminates the need for discrete transceiver blocks. The application and development of the periodic array antennas with such RF BF ICs are described in the recently published manuscript by Jia-Chi Samuel Chieh et al. in [46]. The authors have shown the design and development of Ku- and Ka-band flat panel active phased array antenna using Anokiwave AWMF-0116 and AWMF-0117 RFICs. In [47], Xiaoxiong Gu et al. have also presented the development, implementation and characterization of 64 elements planar periodic phased array antenna using SiGe-based BiCMOS ICs.

TABLE – 3.9: SUMMARY OF THE PROPOSED APERIODIC ARRAY AND PUBLISHED ARRAY DESIGNS

	Aperture Size	No. of Elements	Max. Scan Angle	Peak SLL (dB)	Peak Directivity (dBi)	Average/Minimum Inter-element spacing
Proposed Aperiodic Array	$15\lambda \times 15\lambda$	378	30° conical	-11.63	32.59	0.66λ
[14] (Stage 6 terdragon fractile array)	-	308	45°	~ -18.8	29.8	$\sim 0.5\lambda$
[15]	-	344	30° conical	-9.71	25.27	0.805λ
[16]	-	431	$30^\circ, 60^\circ$	-15.76	27.1	0.72λ
[42]	-	1024	No Scan	-17.5	~ 30.0	Varied from 1λ to 10λ
[43] (Poisson array)	$15\lambda \times 15\lambda$	144	No scan	-13.83	-	-
[44]	$5\lambda \times 5\lambda$	9x9 (81)	No scan	-25.0	23.7	0.17λ (min. distance of the element)
[45]	$10\lambda \times 5\lambda$	108	No scan	-19.76	-	0.5λ (min. distance of the element)

In order to describe the beamforming of the proposed aperiodic array antenna, the author has considered the typical 8-channel RF receive (Rx) BF IC, as shown in Fig. 3.41. The typical internal block diagram of such IC is presented in Fig. 3.42. The elements of the aperiodic array are grouped such that each group contains the nearest 8 elements. Each group is connected with an 8-channel BF IC and each IC's output is connected using a binary feed network. Here, the main advantage is that the path length between the antenna port to RF_{in} port of the IC is not required to maintain constant for all elements. As each antenna element has an independent Rx chain containing DPS, the phase state of DPS is adjusted by adding the path length equivalent bias to the required phase for beam scanning. The results phase to be set by DPS is described below,

$$\Phi_{DPS_{element_i}} = \Phi_{(\theta,\varphi) \text{ beam scan}} + \Phi_{\text{pathlength correction for } i^{th} \text{ element}}$$

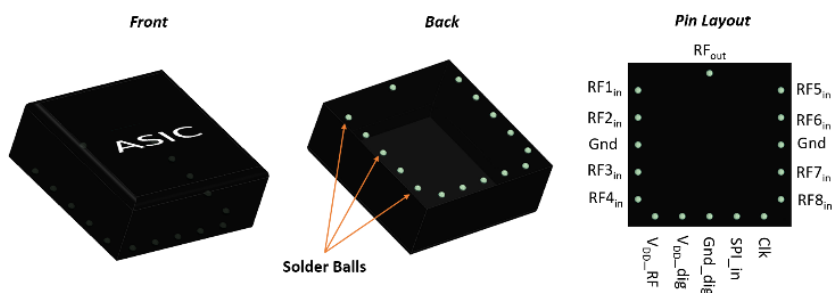


Figure 3.41: Typical layout of RF receiver BF IC

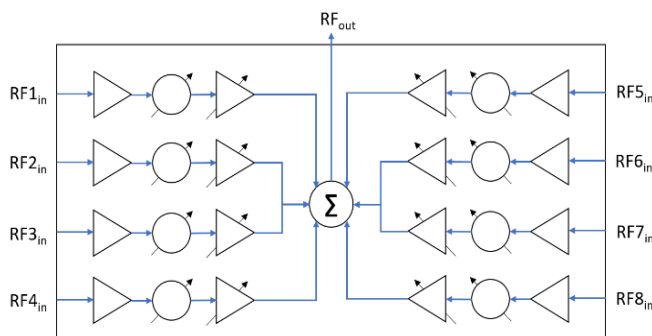


Figure 3.42: Typical RF block diagram of RF receiver BF IC

The grouping of the proposed aperiodic array antenna has been carried out by computing the Voronoi boundary around the element and then eliminating certain boundaries as per the grouping of the nearest elements. Fig. 3.43 shows the grouping of the elements in the proposed aperiodic array. The multilayer PCB has been used below the ground plane of DRA, which can support multilayer feed networks. Fig. 3.44 shows the feed network layout of the proposed

aperiodic array antenna. Moreover, Table – 3.10 presents the comparison between the proposed aperiodic array and the periodic array for the same beam scan capability. It can be observed that the aperiodic array layout requires 21.3% (13 ICs) less no. of BF ICs as compared to the periodic array. Moreover, such saving in the ICs shows significant design and cost advantages for the mass production of beam steerable array antennas.

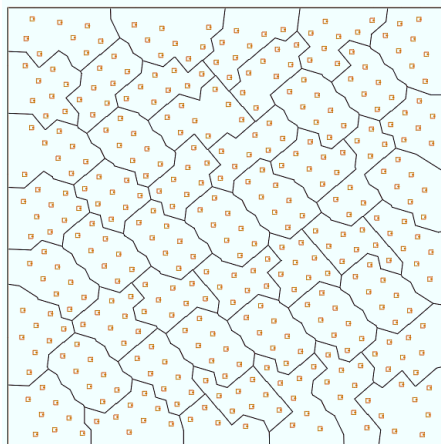


Figure 3.43: Proposed element grouping in the proposed planar aperiodic array antenna

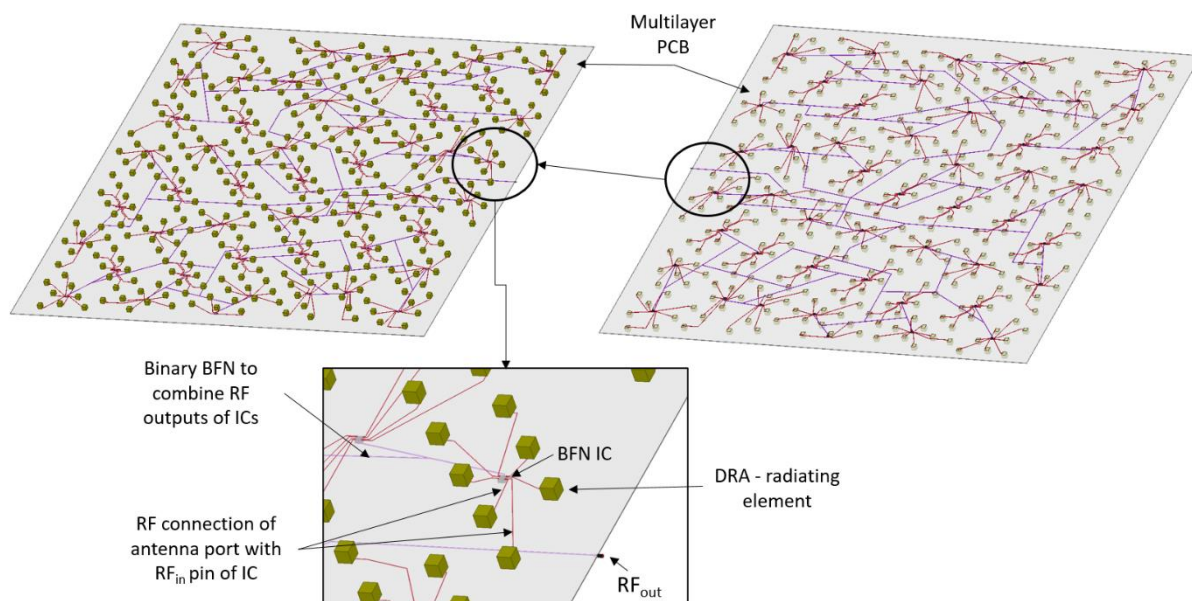


Figure 3.44: Feed network layout of the proposed aperiodic array antenna integrated with RF-ICs

TABLE – 3.10: COMPARISON BETWEEN THE PROPOSED APERIODIC AND PERIODIC ARRAY

	Proposed Aperiodic Array	Periodic Array
Beam Scan Capability	30 ^o conical	30 ^o conical
No. of elements	378	484
No. of 8-channel BFN ICs required	48	~61

3.6 Design of Quasi-periodic Planar Array Antenna using Projected Polyhedron based Approach

The projection-based concept has further been generalized where the vertices of a 3D-shaped regular convex polyhedron are projected on the 2D aperture plane to form the beam steerable aperiodic/quasi-aperiodic array. Such a polyhedron can be a family of 5 platonic solids [48], namely, tetrahedron, cube, octahedron, icosahedron, and dodecahedron. Fig. 3.45 shows the sample cases of the rotated dodecahedron and its projected vertices forming the quasi-periodic element distribution on the XY plane. Here, the rotation of the polyhedron can be altered and optimized to achieve the desired quasi-periodic distribution for the required farfield performance. However, Table-3.11 shows the number of vertices available in the platonic solids. Now, if the single polyhedron is used for the projection, the array elements are restricted by the number of vertices of the polyhedron. Therefore, the co-centric polyhedron-based approach has been adopted to increase or adjust the number of elements in the quasi-periodic array.

TABLE – 3.11: NO. OF VERTICES OF THE POLYHEDRONS

Type of Polyhedron	No. of Vertices
Tetrahedron	4
Octahedron	6
Cube	8
Icosahedron	12
Dodecahedron	20

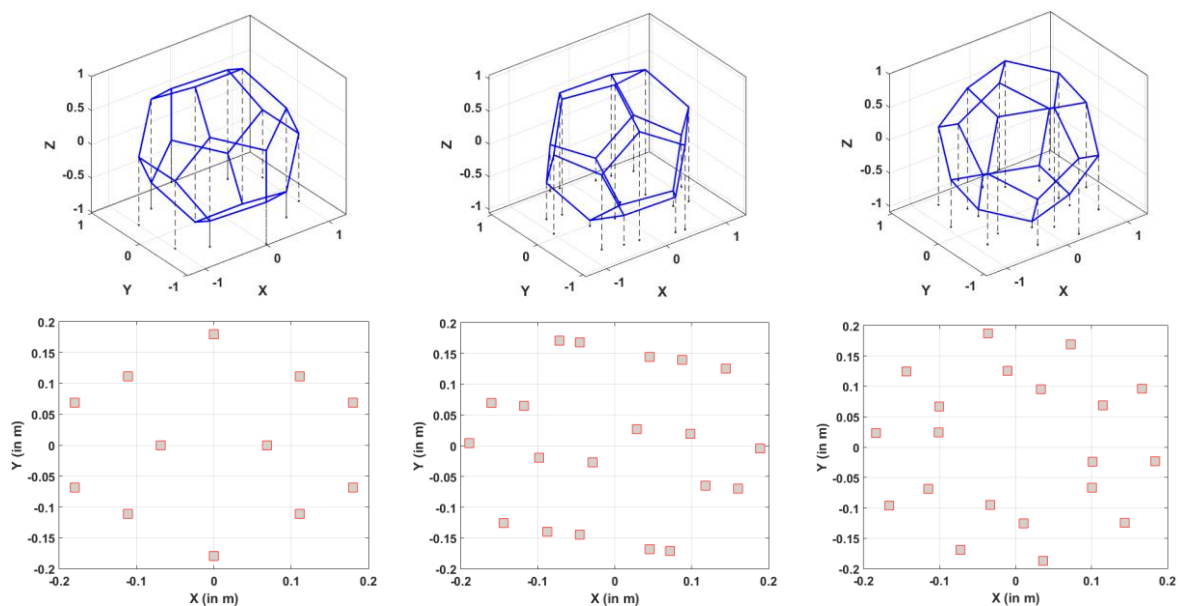


Figure 3.45: Sample cases of rotation of Dodecahedron and corresponding element positions, forming a planar quasi-periodic array

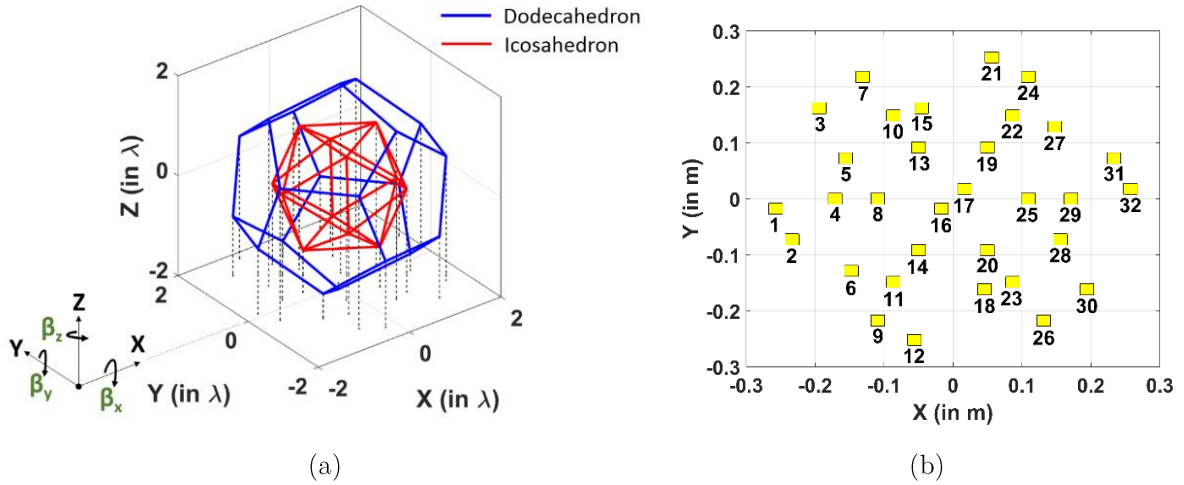


Figure 3.46: (a) Geometry of co-centric dodecahedron and icosahedron and (b) projection of vertices of co-centric polyhedrons on XY plane and corresponding array element positions ($\alpha_d = 0.25$, $\beta_{x,d} = 319.7^\circ$, $\beta_{y,d} = 218.9^\circ$, $\beta_{z,d} = 0^\circ$, $\alpha_i = 0.18$, $\beta_{x,i} = 0^\circ$, $\beta_{y,i} = 102.1^\circ$, $\beta_{z,i} = 0^\circ$, d = dodecahedron, i = icosahedron)

Here, the vertices of concentrically arranged two platonic solids, namely, dodecahedron and icosahedron, are projected on the 2-dimensional aperture plane (XY plane) to form a quasi-periodic array lattice. These two polyhedra combinedly form 32 element array. The angular position of these polyhedrons w.r.t three axes of Cartesian coordinates ($\beta_{x,d,i}, \beta_{y,d,i}, \beta_{z,d,i}$) are the variables that are optimized to form the quasi-periodic lattice offering improved SLL performance. Moreover, both polyhedrons have been assigned different scale factors, adjusted based on the required aperture dimensions. The modelling of co-centric dodecahedron and icosahedron is presented in Fig. 3.46(a). The farfield performance of the array has been analyzed by individually analyzing the array distribution of the individual polyhedron and superpositioning them for a combined performance. Equation (3.7) describes the modeling and analysis of such co-centric polyhedrons. Here, $\mathbf{F}(\theta, \varphi)$ represents the element radiation pattern, which is typically taken as $(\cos \theta)^q$. For a dielectric resonator antenna (DRA) based single element, $q=1.2$ is selected for ~ 7.00 dBi element gain.

$$\mathbf{E}(\theta, \varphi) = \mathbf{F}(\theta, \varphi) \cdot \left(\sum_{d=1}^D \omega_d \cdot e^{-jk(\theta, \varphi) \cdot \mathbf{r}_d} + \sum_{i=1}^I \omega_i \cdot e^{-jk(\theta, \varphi) \cdot \mathbf{r}_i} \right) \quad (3.7)$$

Where,

- D = No. of elements projected by dodecahedron
- I = No. of elements projected by icosahedron

$$\begin{aligned}
\mathbf{r}_{d,i} &= \begin{cases} \text{d}^{\text{th}} \text{ or } \text{i}^{\text{th}} \text{ element position } (x,y,0) \\ [\mathbf{P}_{xy}][\mathbf{R}_{xyz,d,i}](\alpha_{d,i} \cdot \mathbf{V}_{d,i}) \end{cases} \\
\mathbf{V}_{d,i} &= \begin{cases} \text{d}^{\text{th}} \text{ or } \text{i}^{\text{th}} \text{ vertex of polyhedron} \\ (x_{d,i}, y_{d,i}, z_{d,i})^T \end{cases} \\
\mathbf{k}(\theta, \varphi) &= \begin{cases} \text{wave vector} \\ k_0(\sin \theta \cos \varphi, \sin \theta \sin \varphi, \cos \theta) \end{cases} \\
[\mathbf{P}_{xy}] &= \text{Projection matrix } \begin{bmatrix} 1 & 0 & 0 \\ 0 & 1 & 0 \\ 0 & 0 & 0 \end{bmatrix} \\
[\mathbf{R}_{xyz,d,i}] &= \text{Rotation matrix } [\mathbf{R}_{z,d,i}][\mathbf{R}_{y,d,i}][\mathbf{R}_{x,d,i}] \\
[\mathbf{R}_{z,d,i}] &= \begin{bmatrix} \cos \beta_{z,d,i} & -\sin \beta_{z,d,i} & 0 \\ \sin \beta_{z,d,i} & \cos \beta_{z,d,i} & 0 \\ 0 & 0 & 1 \end{bmatrix} \\
[\mathbf{R}_{y,d,i}] &= \begin{bmatrix} \cos \beta_{y,d,i} & 0 & \sin \beta_{y,d,i} \\ 0 & 1 & 0 \\ -\sin \beta_{y,d,i} & 0 & \cos \beta_{y,d,i} \end{bmatrix} \\
[\mathbf{R}_{x,d,i}] &= \begin{bmatrix} 1 & 0 & 0 \\ 0 & \cos \beta_{x,d,i} & -\sin \beta_{x,d,i} \\ 0 & \sin \beta_{x,d,i} & \cos \beta_{x,d,i} \end{bmatrix} \\
\beta_{x,d,i} &= \text{Rotation w.r.t x-axis} \\
\beta_{y,d,i} &= \text{Rotation w.r.t y-axis} \\
\beta_{z,d,i} &= \text{Rotation w.r.t z-axis} \\
\omega_{d,i} &= \begin{cases} \text{Excitation of d}^{\text{th}} \text{ or i}^{\text{th}} \text{ element} \\ |\omega_{d,i}|e^{-j\varphi_{d,i}} \end{cases} \\
\varphi_{d,i} &= \begin{cases} \text{Excitation phase for d}^{\text{th}} \text{ or i}^{\text{th}} \text{ element} \\ -\bar{k}(\theta_0, \varphi_0) \cdot \bar{\mathbf{r}}_{d,i} \end{cases} \\
\alpha_{d,i} &= \text{Scale factor} \\
k_0 &= \text{Wave number } (2\pi/\lambda) \\
\lambda &= \text{Wavelength of operation} \\
i &= \text{Index for icosahedron} \\
d &= \text{Index for dodecahedron}
\end{aligned}$$

The quasi-periodic lattice is generated by optimizing angular orientations and scale factors of the dodecahedron and icosahedron. Here, the newly developed Jaya optimization algorithm has been used for the same. The optimization's objective function is defined for simultaneous minimization of peak SLL in 3D radiation pattern and maximization of minimum

inter-element spacing, for the required beam scan angle. The objective function of the inter-element spacing is included to maintain the developmental feasibility of the array.

$$\begin{aligned} W_{sll} &= \text{Peak SLL in 3D radiation pattern} \\ D_{ele} &= \text{Minimum inter - element distance} \end{aligned}$$

$$\text{objective } f_{obj}^n = \begin{cases} \min_{0 \leq (\beta_{z,d,i}, \beta_{y,d,i}, \beta_{x,d,i}) \leq 2\pi} (W_{sll}) \\ \max_{0 \leq (\beta_{z,d,i}, \beta_{y,d,i}, \beta_{x,d,i}) \leq 2\pi} (D_{ele}) \end{cases}$$

The flow chart showing the brief procedure of the design and optimization of the array lattice is shown in Fig. 3.47. The optimization of quasi-periodic array lattice has been carried out for peak SLL < -10dB for $\pm 30^\circ$ beam scan angle. The optimized array lattice is displayed in Fig. 3.46(b) with the optimized values of angular orientations and scale factors.

The optimized quasi-periodic array lattice has also been populated with 32 nos. S-band DRA elements, described in section 3.5.2. Fig. 3.48(a) exhibits the simulation model of the quasi-periodic array lattice. Each DRA has a phase shifter connected to it to apply the required phase to steer the beam in the desired beam scan direction. The DRA elements are then connected with a 1:32 equi-phase and equi-amplitude power divider. The system-level block diagram is presented in Fig. 3.49. The quasi-periodic array of DRA elements has been simulated using a 3D electromagnetic solver, namely, Ansys HFSS 20.0 [38]. From the simulation, the element-wise maximum mutual coupling has been studied and presented in Fig. 3.50. The red curve in Fig. 3.50 shows that 11 pairs of DRA elements have mutual coupling > -15dB. A simple metallic fence-based approach is used to improve the mutual coupling between the elements. As the quasi-periodic array lattice is not formed with periodic unit cells, the element boundaries for the metallic fence have been determined by computing the Voronoi diagram of the lattice [49]. The structure of the quasi-periodic array with metallic Voronoi boundary is shown in Fig. 3.48(b). The blue curve in Fig. 3.50 shows the element-wise maximum mutual coupling of an array antenna with the metallic Voronoi fence. Such a metallic fence has reduced the mutual coupling for four element pairs. The mutual coupling between the remaining pairs of elements has been improved by adding the decoupling network (DCN) between the elements. The DCN design presented in [50-51] has been adopted. The typical block diagram of the DCN is presented in Fig. 3.49(a). The simulation of a quasi-periodic DR based array with metallic fence and DCN has been carried out by integrating the schematic level design of DCN with a 3D modelled

structure of an array with the metallic fence. The simulation model of the same is shown in Fig. 3.51(b). The element-wise mutual coupling performance of the array with the metallic fence and DCN is added in the curve with black colour, presented in Fig. 3.50. It can be observed that the mutual coupling for all DRA elements is $< -15\text{dB}$. However, the introduction of the DCN adds an extra phase to the phase required for the array element for beam steering. Hence, additional phase correction at these element pairs is applied. The corresponding additional phase shifters are shown in blue colour in Fig. 3.49. During the practical implementation, the function of the phase shifter for beam steering and phase compensation for DCN may be combined into the single-phase shifter.

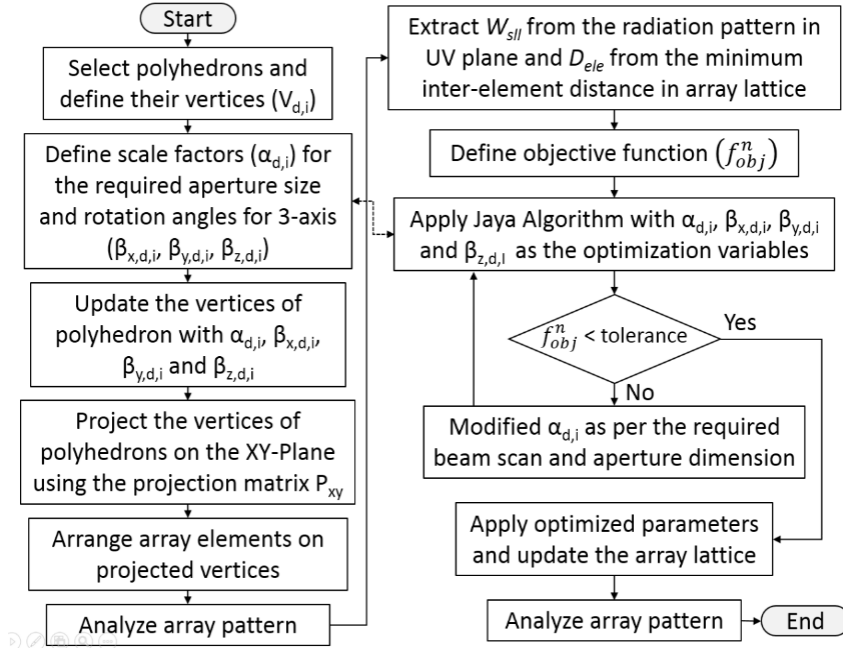


Figure 3.47: Flow chart for array lattice optimization using co-centric polyhedrons based approach

The proposed quasi-periodic array antenna has been analysed and its UV radiation pattern has been studied for 30° beam scan in $\varphi = 0^\circ$ and $\varphi = 90^\circ$ planes, respectively. Fig. 52(a) and (b) show the analysed UV radiation patterns for 30° beam scan in $\varphi = 0^\circ$ and $\varphi = 90^\circ$ planes, respectively. Fig. 52(c) and (d) present the simulated UV radiation patterns for 30° beam scan in $\varphi = 0^\circ$ and $\varphi = 90^\circ$ planes, respectively. From Fig. 52, it can be observed that a good match between analysed and simulated radiation pattern shapes has been achieved. Moreover, Fig. 3.53 shows the simulated radiation patterns for various scan angles in $\varphi = 0^\circ$ and $\varphi = 90^\circ$ planes. Fig. 3.55 presents the comparison plot of far-field parameters at various scan angles. From Fig. 3.55, a 0.8dB gain reduction in the simulation results can be observed. It is attributed to the

mutual coupling effect, losses introduced due to the 1:32 power divider and DCN in the simulation. The comparison between the proposed quasi-periodic array and periodic array says that a 4.2dB improvement in the peak SLL has been achieved by the quasi-periodic array. However, the quasi-periodic array shows a 0.5dB reduction in directivity as compared to the conventional periodic lattice. The directivity reduction has transpired as the presented quasi-periodic array lattice does not entirely cover the rectangular aperture generated by the periodic array.

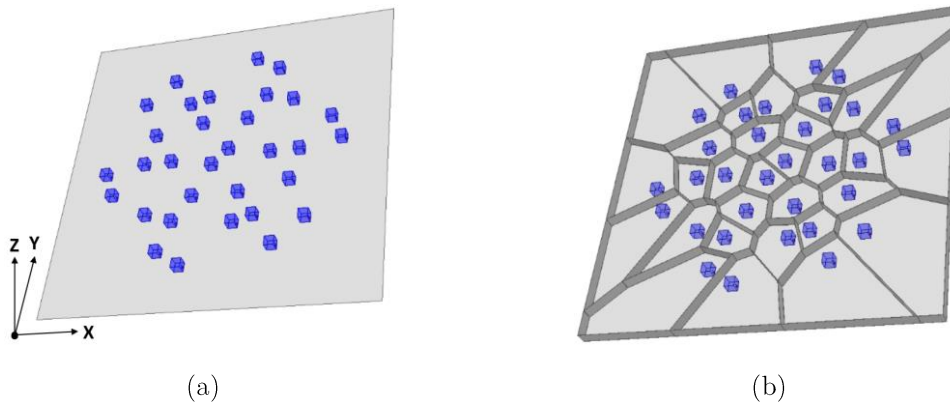


Figure 3.48: Simulation model of the planar quasi-periodic array of DRA (a) without Voronoi boundary and (b) with Voronoi boundary

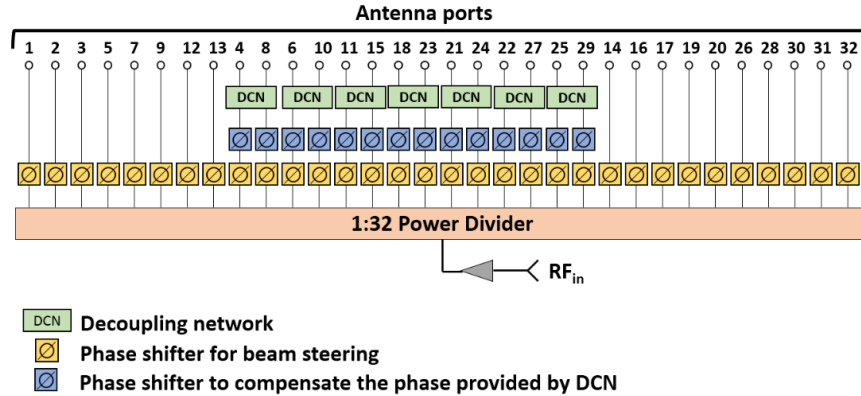


Figure 3.49: System schematic of feed network of quasi-periodic array of DRA

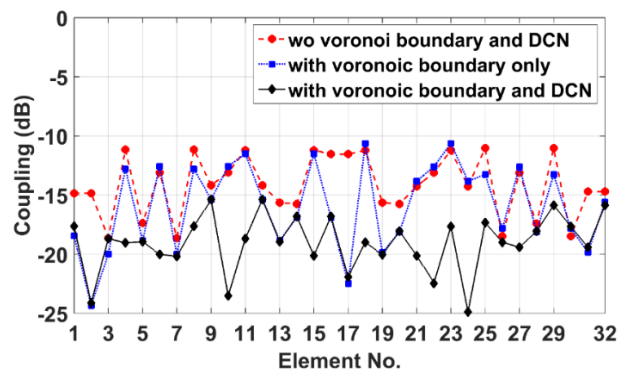
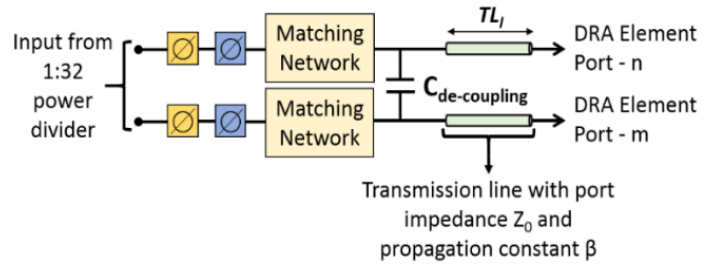
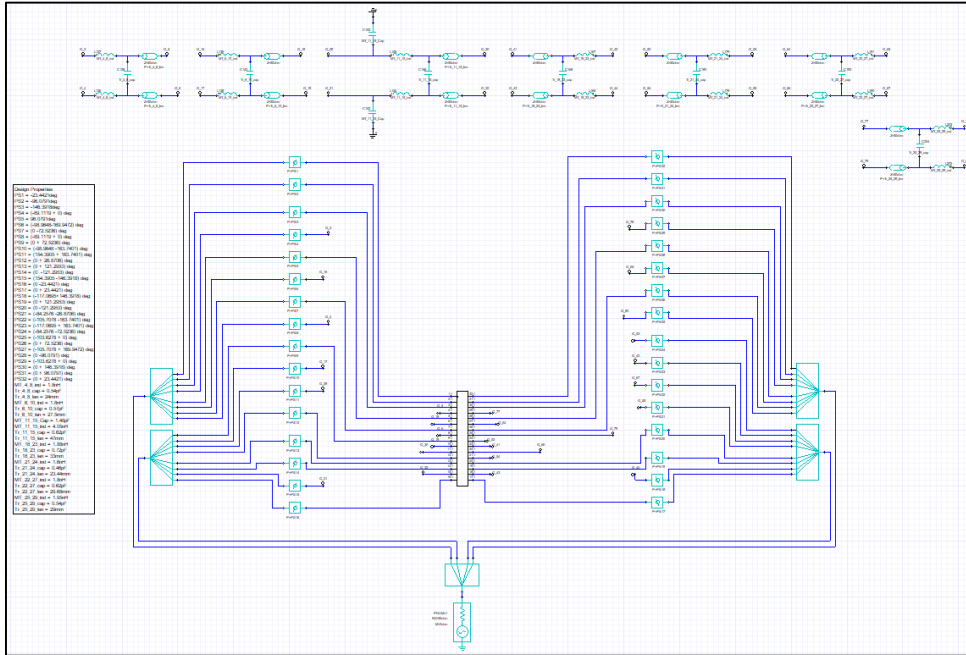


Figure 3.50: Element wise mutual coupling variation for various conditions of the planar quasi-periodic DRA array



(a)



(b)

Figure 3.51: (a) Block diagram of DCN and (b) schematic of simulation model of aperiodic array with DCN

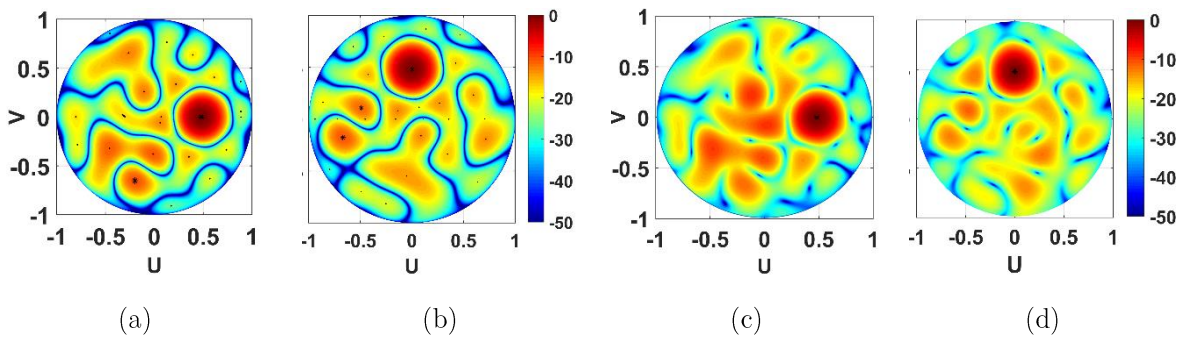


Figure 3.52: Analyzed UV radiation pattern for (a) ($\theta = 30^\circ$ and $\varphi = 0^\circ$), (b) ($\theta = 30^\circ$ and $\varphi = 90^\circ$), and simulated UV radiation pattern for (c) ($\theta = 30^\circ$ and $\varphi = 0^\circ$), (d) ($\theta = 30^\circ$ and $\varphi = 90^\circ$), of the planar quasi-periodic DRA array with Voronoi boundary and DCN

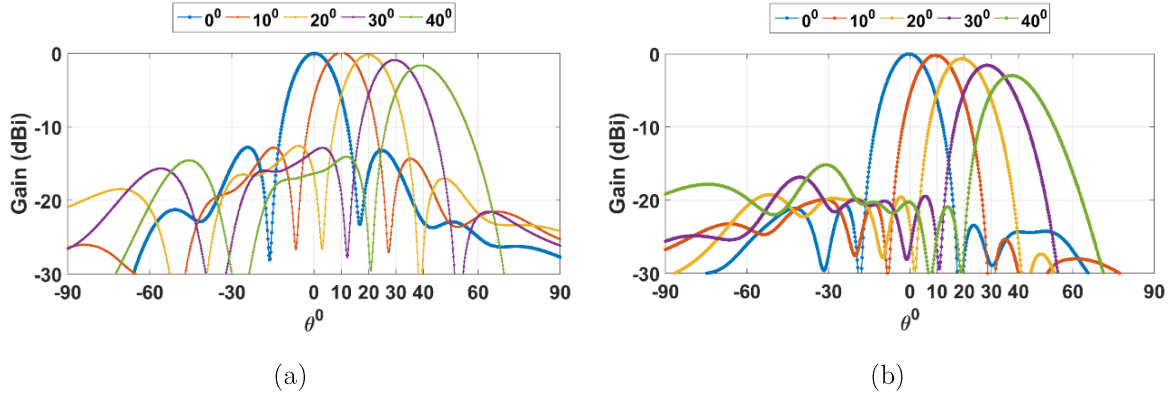


Figure 3.53: Simulated beam scan performance of co-centric polyhedrons based quasi-periodic array of DRA for beam scan in (a) $\varphi = 0^\circ$ and (b) $\varphi = 90^\circ$

To have a comparative assessment of the presented array lattice, the Pinwheel type of array lattice has also been generated as per the method described in section 3.5.2. The generated array lattice is shown in Fig. 3.54(a). The pinwheel lattice's aperture boundary is fixed by the convex hull of the projected polyhedrons-based array lattice. The analysis of the Pinwheel lattice has been carried out using a mathematical formulation similar to Equation (3.7) and the analysed UV radiation patterns for 30° beam scan in $\varphi = 0^\circ$ and $\varphi = 90^\circ$ planes are computed and presented in Fig. 54(b) and (c). It is also observed that the polyhedron-based array lattice shows a marginally improved performance compared to the pinwheel lattice-based array. The far-field parameters of the Pinwheel lattice are compared in Table-3.12 with that of the projected polyhedrons based quasi-periodic array lattice and conventional periodic array lattice. The significant difference in the beamwidths for beam scan in $\varphi = 0^\circ$ and $\varphi = 90^\circ$ is observed in Table-3.12. It is also observed that the polyhedron-based array lattice shows a marginally improved performance compared to the Pinwheel lattice-based array.

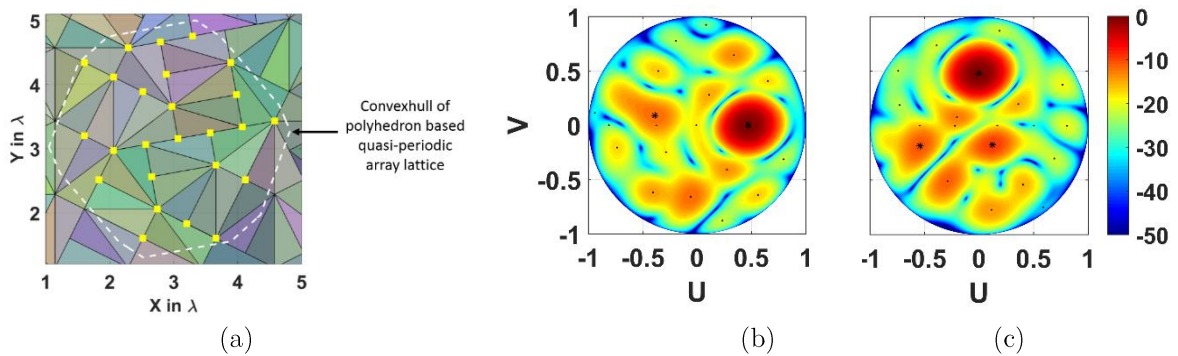


Figure 3.54: (a) Quasi-periodic Pinwheel lattice and its analysed beam scan performance for Pinwheel based array lattice for (a) $(\theta = 30^\circ$ and $\varphi = 0^\circ)$ beam scan, (b) $(\theta = 30^\circ$ and $\varphi = 90^\circ)$ beam scan

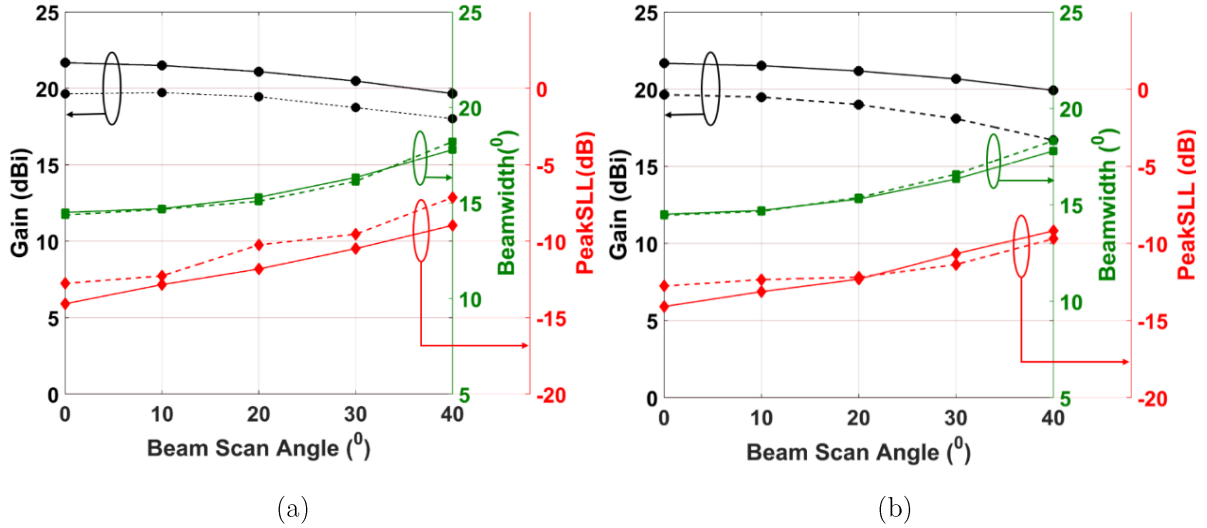


Figure 3.55: Comparison of far-field parameters (gain, beamwidth and peak SLL) for analyzed projected polyhedron based planar lattice and simulated planar quasi-periodic array of DRA with Voronoi boundary and DCN, for beam scan in (solid line – analyzed results, dotted line – simulated results) (a) $\varphi = 0^\circ$; and (b) $\varphi = 90^\circ$

Co-centric arrangement of dodecahedron and icosahedron results in an array lattice with 32 elements. Such arrangement can be generalized for any combination of platonic solids and polyhedrons, producing a variety of quasi-periodic lattices for required far-field performance. Table-3.13 shows the typical list of platonic solids and the number of array elements that can be obtained by their co-centric arrangement.

TABLE – 3.12: SUMMARY OF THE QUASI-PERIODIC ARRAYS

Description	Quasi-Periodic Array using		Periodic Array
	Projected Co-centric Dodecahedron and Icosahedron	Pinwheel lattice	25 elements (5 x 5) 0.7λ
No. of elements	32	32	25
Aperture Size	$4.4\lambda \times 4.4\lambda$	$4.4\lambda \times 4.4\lambda$	$3.5\lambda \times 3.5\lambda$
Peak SLL (dB)	-10.5	-9.2	-6.3
Beamwidth	16.3°	19.6° for ($\theta = 30^\circ$ and $\varphi = 0^\circ$), 17.5° for ($\theta = 30^\circ$ and $\varphi = 90^\circ$)	16.4°
Directivity (dBi)	20.7	19.44	21.2
Scan Loss (dB)	1.0	1.4	0.7

The polyhedron-based projection approach does not result in the significant improvement as in the case of an aperiodic SP method based planar array. However, the polyhedron based

aperiodic array is highly suitable for interferometric arrays, which are typically a multiplicative array. The subsequent section discusses the application of polyhedron-based projection in radio astronomy.

TABLE– 3.13: NO. OF ELEMENTS IN ARRAY FOR CO-CENTRIC PLATONIC SOLIDS

Polyhedrons	Vertices	No. of Elements				
		T	C	O	D	I
T	4	8	-			
C	8	12	16	-		
O	6	10	14	12	-	
D	20	24	28	26	40	-
I	12	16	20	18	32	24

T = Tetrahedron, C = Cube, O = Octahedron, D = Dodecahedron, I = Icosahedron.

CHAPTER 4

Application of Projection Based Aperiodic Arrays

Application A Design of Interferometric Array for Radio Astronomy

4.1 Introduction

The quasi-aperiodic and aperiodic arrays are widely used for radio interferometric arrays. The *very large baseline array* (VLA) in New Mexico, USA [52], the *Multi-Element Radio Linked Interferometer Network* (MERLIN), England [53], the *Australia Telescope Compact Array* (ATCA), Australia [54], The *Atacama Large Millimeter-Submillimeter Array* (ALMA), northern Chile [55], the *Giant Metrewave Radio Telescope* (GMRT), India [56] and The *Square Kilometre Array* (SKA) [57] are some of the widely popular interferometric arrays, developed for various types of astronomical imaging. Typically, the array configuration plays a vital role in achieving the desired image quality generated by the radio interferometers. The array also determines maximum resolution, a largest structure that can be images, side lobe levels in the image, and surface brightness sensitivity. The aperiodic array, along with earth rotation synthesis, generates the U-V distribution, which samples the frequency spectrum of the astronomical image. The sampled frequency response is later subjected to various corrections, including the instrumentation errors, and then, converted to the desired image using Fourier transform relationship.

The U-V distribution is basically the distribution of the baseline vectors, formed with the earth rotation, while observing the astronomical object at a specific declination (δ). The observation geometry is shown in Fig. 4.1. For N no. of antennas in the array, $N(N-1)$ baselines are generated. For good images, it is required to have adequate baselines, and their distribution with earth rotation should be optimized as per the required imaging. Followings are three major important aspects of U-V coverage, which are addressed and optimized while designing the array configuration,

1. Outer boundary of U-V coverage which governs the resolution limit and restricts the information on small scales.

2. Inner hole in U-V coverage which limits the information on the larger scale objects and also contributes to the sidelobe formation in the point spread function (PSF).
3. Irregular coverage between the above two boundaries, which effectively violates the sampling theorem and its inappropriate design, may cause the loss of information about the astronomical object.

Another critical aspect of U-V distribution is its related PSF, which effectively the response pattern of an interferometer. In practice, the measured sky brightness map (also called the dirty map) is the convolution between the true sky brightness map with the PSF of an interferometer [58-60]. Here, the true sky brightness map is usually derived by deconvolving the PSF from the dirty map. In practice, deconvolution is a complex, non-linear, and computationally intensive problem. Moreover, the noise in the image and the effect of atmospheric turbulence in the received signals further complicate the deconvolution process. In astronomy, CLEAN and Maximum entropy method are a few widely known deconvolution algorithms. There is always a fair chance that the adequately designed aperiodic array reduces the computation burden and omits the requirement of deconvolution. Hence, the role of U-V distribution and its related PSF is vital.

4.2 Application of Directly Projected Polyhedron based projection method in Radio Astronomy

As discussed in Chapter 3, the platonic solid-based polyhedrons can be used, and their vertices are projected on a 2D plane to form an aperiodic array. Here, the two nos. of such co-centric polyhedrons are used to create the array configuration. The rotation and scale factor of the polyhedrons are optimized to achieve desired U-V coverage. Fig. 4.2 shows the geometry of the co-centric polyhedrons, namely, icosahedron and dodecahedron and the projection of their vertices on the XY plane. Matlab codes are developed to compute U-V coverage by considering that the array is placed at fixed latitude 19.1° , operating at 1.42GHz frequency and for 12hr observation time. These specifications are kept the same as GMRT to make the performance comparison. The computed U-V coverage for various declinations (δ) is shown in Fig. 4.3.

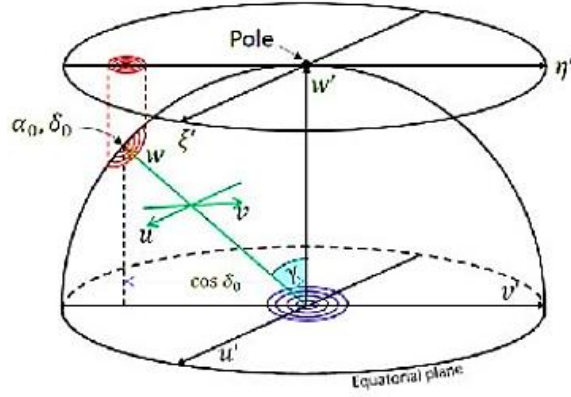


Figure 4.1: Coordinate definition and observation geometry for radio interferometry

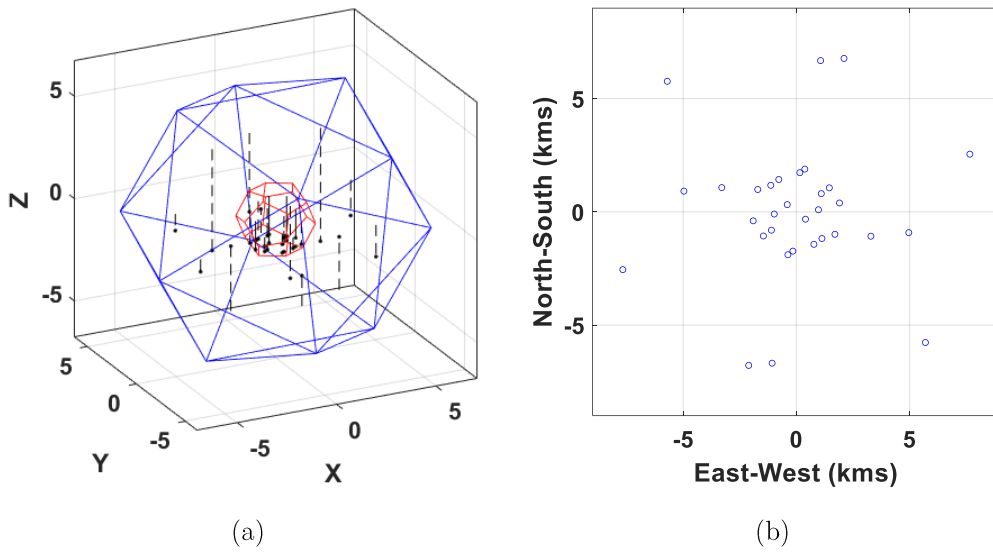


Figure 4.2: (a) Rotated and scaled co-centric polyhedrons, and (b) planar aperiodic array generated by projection of the vertices

The radio imaging flow has been implemented in Matlab to optimize the array configuration. Here, the sample model image has been taken as input and its frequency spectrum has been sampled as per the U-V coverage generated by the above array. The image is then recovered back. To quantify the quality of the observed image, the Fidelity index (FI) has been defined in Equation (4.1). Polyhedrons' rotation and scaling factors are optimized to achieve the highest FI value. The sample case is discussed and its process is shown in Fig. 4.4. Here, the sample image of the astronomical object, called a hydrogen cloud, spread over a $1'' \times 1''$ angular span, is used as a 'Model Image'. The U-V coverage has been generated for $\delta = -20^\circ$ and 12hrs observation time. As shown in Fig. 4.4(a), the frequency spectrum of the sample image is sampled by the U-V coverage and the recovered image is also presented. Fig. 4.4(b) shows the residual image. From Fig. 4.4, it can be observed that the recovered image is not exactly like the sample

image due to non-uniform sampling of the frequency spectrum of the sample image. Such loss of information may lead to dramatic changes in the discovery of astronomical objects.

$$Fidelity\ Index = \frac{Peak\ Intensity\ in\ observed\ image}{Residual\ RMS} \quad (4.1)$$

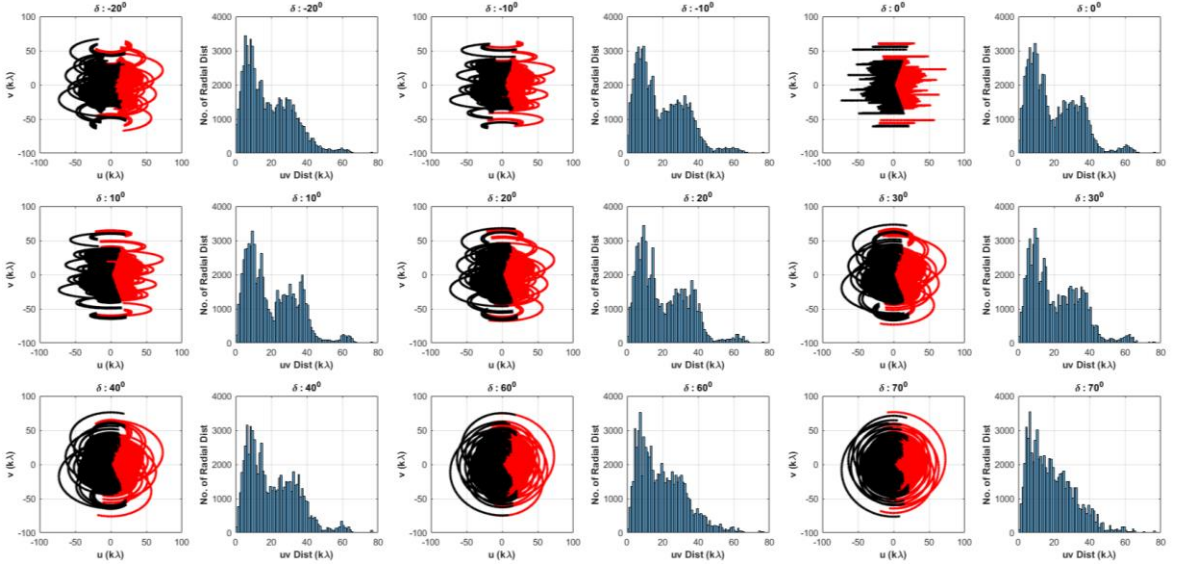
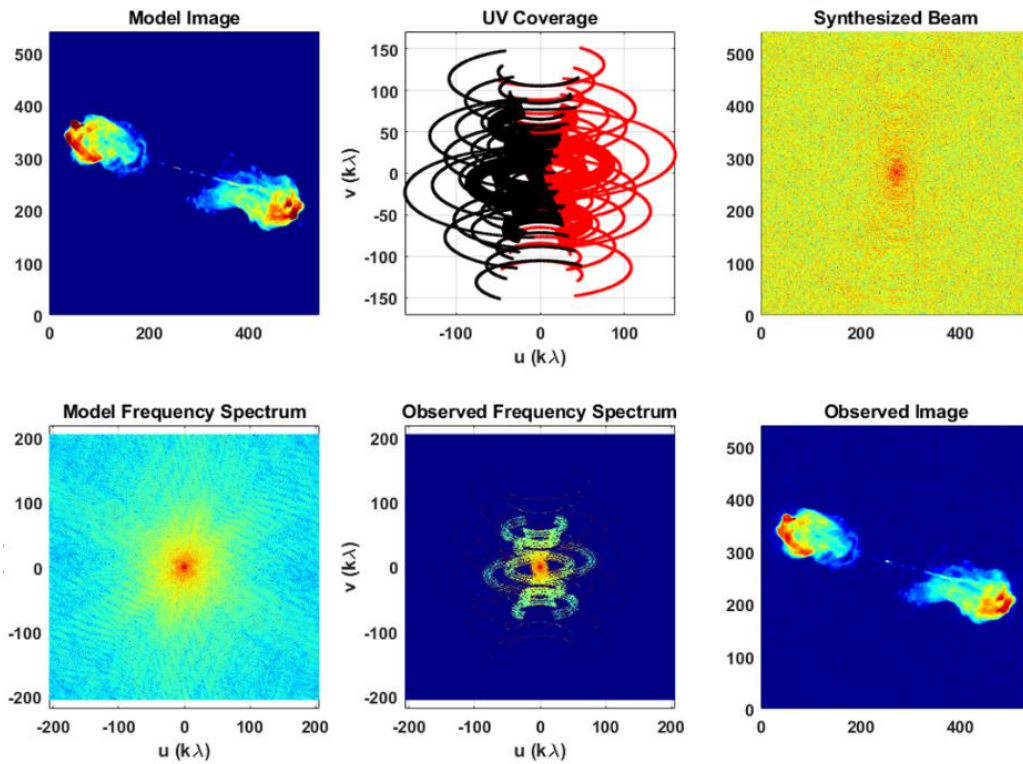


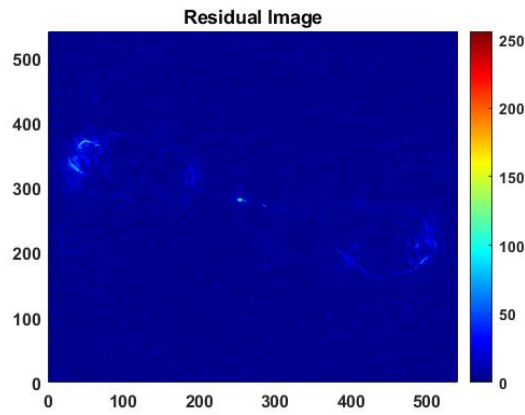
Figure 4.3: Computed UV Coverage using co-centric Polyhedron (icosahedron and dodecahedron) based Synthesized array for various declinations over 12hr observation

The co-centric polyhedrons are studied in detail to generate U-V coverage and it has been found that the U-V distribution generated by the array formed with the direct projection of the vertices of the polyhedron has large inner holes, which is not suitable, as the major frequency components of the image are usually centered around the low-frequency content. Fig. 4.5 shows the U-V coverage of the array generated by two different polyhedrons, i.e., icosahedron and dodecahedron. A similar observation has also been made for the array generated by the other three platonic solids: Cube, tetrahedron and octahedron. Hence, it is concluded that the approach to designing the aperiodic array generated by the direct projection of the vertices of the polyhedron needs the intermediate function, which can translate the vertices of the unit polyhedron to the infinite 2D space. This has been achieved using Stereographic projection, which is discussed in the subsequent section.

Declination = -20° , Observation Time = 12hrs, Latitude = 19.10, Sample Image Scale = $1''$



(a)



(b)

Figure 4.4: (a) Array Analysis, computation of U-V coverage and its impact on Image and (b) residual image, for co-centric Polyhedron (icosahedron and dodecahedron) based synthesized array

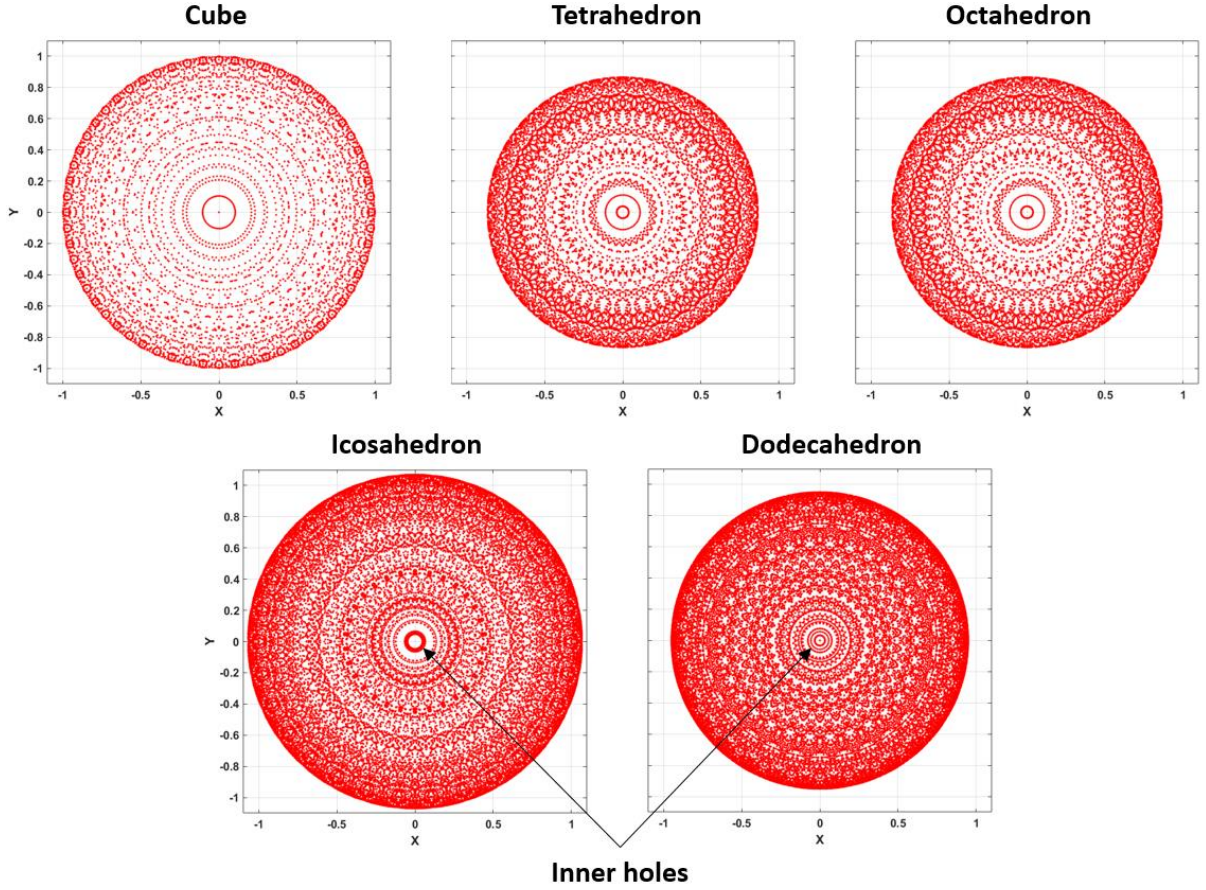


Figure 4.5: Inner holes in the U-V coverages of various polyhedron based arrays

4.3 Application of Stereographically project Polyhedron based Strip projection method in Radio Astronomy

As discussed in the above section, the U-V distribution of the aperiodic array, ideally, should not have any inner holes. However, due to the discretization of the array plane and the sphere shape of the earth, the occurrence of the inner hole is inherited. The aperiodic array can be designed to offer a minimum inner hole diameter in the U-V distribution. The aperiodic array generated by the polyhedron projection-based approach presented in the above section has the unavoidable large inner hole in the U-V distribution. In this section, the stereography-based project of the vertices of the unit polyhedron is proposed to reduce the size of the inner hole for the proposed sampling of the low-frequency content of the sample image.

The function which maps the points on a sphere onto a plane is called the stereographic projection function and is widely used in complex analysis [61]. In stereographic projection, the upper half of the sphere is mapped on the outer plane from the unit circle and the lower half is mapped on the inner plane from the unit circle. Thus, the complete 2D plane can be mapped

onto a sphere and vice versa. Equation (4.2) maps the points on the sphere to the 2D aperture plane.

$$x_{projected} = \frac{x_{poly}}{1-z_{poly}}, y_{projected} = \frac{y_{poly}}{1-z_{poly}} \quad (4.2)$$

Where (x_{poly}, y_{poly}) is the vertex of the polyhedron on the unit sphere and $(x_{projected}, y_{projected})$ is its mapping on the 2D aperture plane. Fig. 4.6 demonstrates the stereographic projection of the vertices of the polyhedron.

The U-V distributions of the array generated by the stereographic projection by the five platonic solids, are computed and presented in Fig. 4.7. From Fig. 4.7, it can be observed that the inner holes in both U-V distributions are filled. Such distributions can be used for interferometric imaging.

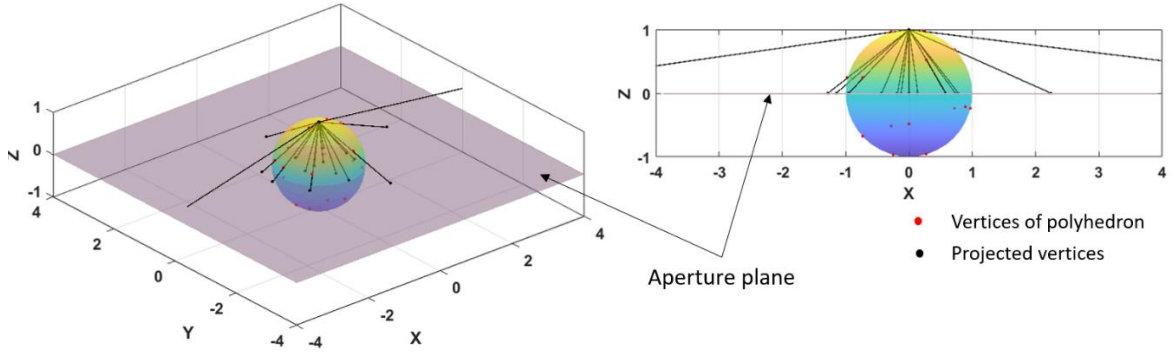


Figure 4.6: Stereographic projection of vertices of the polyhedrons and formation of planar aperiodic array

To design such an aperiodic array, the optimization-based approach is adopted. Here, as discussed in the previous chapter, the rotations of polyhedrons are considered the optimization variable and the cost function is defined to maximize the FI. The cost function is computed for various declinations and simultaneously maximized so that the array can be functional at the range of declinations without any physical modifications. Here, Jaya based optimization algorithm has been used. Fig. 4.8 shows the flow chart of the design process. The design of such an array has been carried out by fixing the number of array elements. Since the GMRT array having 30 elements has been opted as the reference, the combination of co-centric polyhedrons is selected such that the number of array elements in the designed array remains ~ 30 . Fig. 4.9 shows the array element distribution of the GMRT. Table – 4.1 shows the various polyhedron combination and their corresponding number of elements.

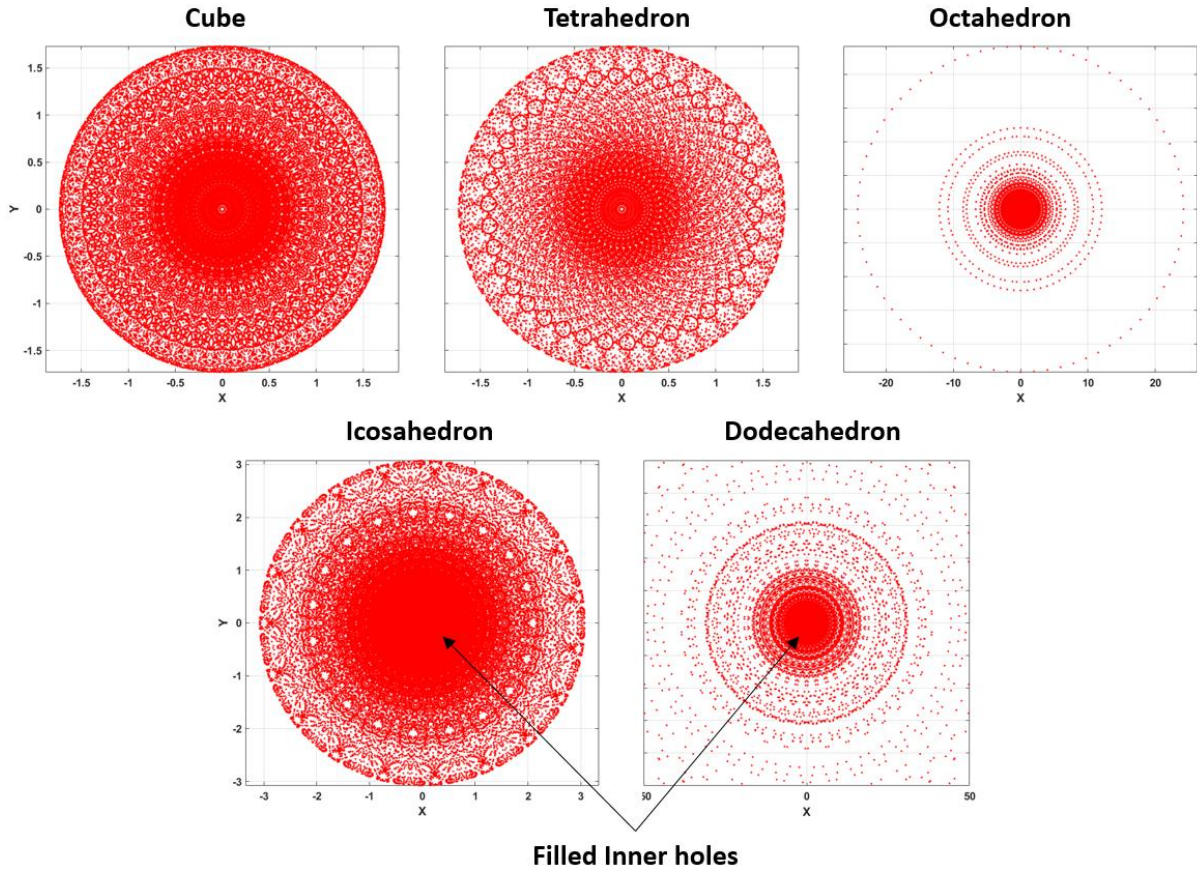


Figure 4.7: Filled inner holes in the U-V coverages of various polyhedron based arrays generated using stereographic projection

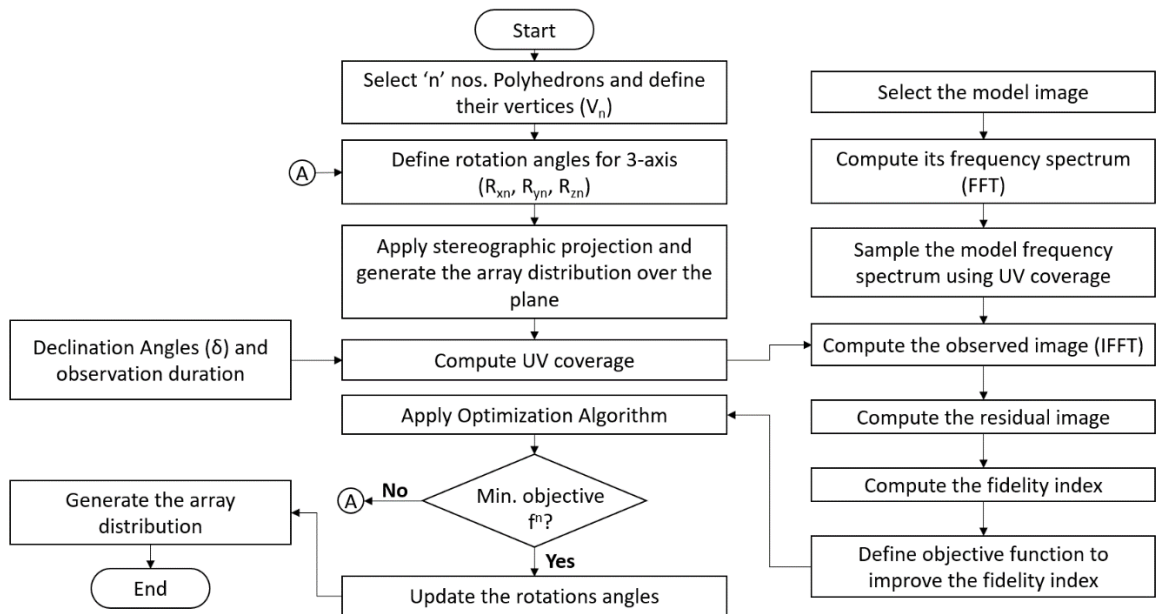


Figure 4.8: Design flow chart of the aperiodic interferometric array using stereographic projection

The design process described in Fig. 4.8 has been applied to all 10 cases described in Table – 4.1. The optimized array distributions for all cases are presented in Fig. 4.10. The FI

values of all designed arrays have been computed over the declination range and compared with that of the GMRT array. Fig. 4.11 presents the variation of FI values for 10 designed arrays and the GMRT array. From Fig. 4.11, it can be observed that case – 4 (1 nos. Dodecahedron + 1 nos. Octahedron + 1 nos. Tetrahedron) and case – 8 (1 nos. Icosahedron + 3 nos. Octahedron) offer better performance than the GMRT array over the declination angles. Fig. 4.12 shows the histogram of the baseline of the case – 4 for $\delta = -50^\circ$ and $\delta = 70^\circ$. From the histogram, the high baseline density at short baselines and no occurrence of the inner hole can be interpreted. The sample cases of image generation for the case – 4 array are also presented in Fig. 4.13 and Fig. 4.14 for $\delta = -50^\circ$ and 70° , respectively. Here, the spiral galaxy-based image spanning over a $1'' \times 1''$ angular range has been used for the demonstration.

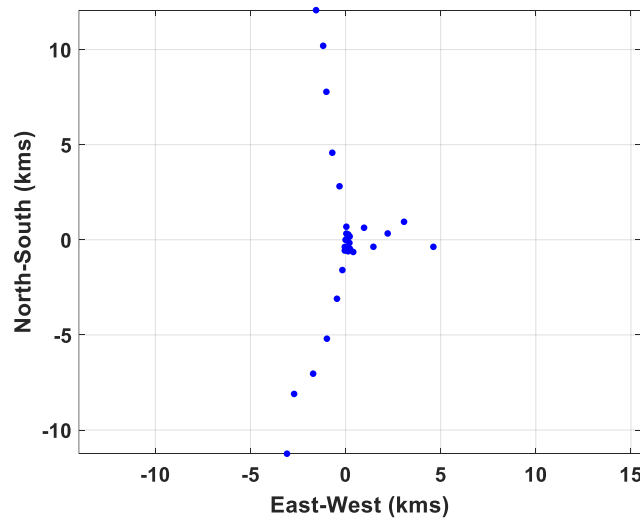
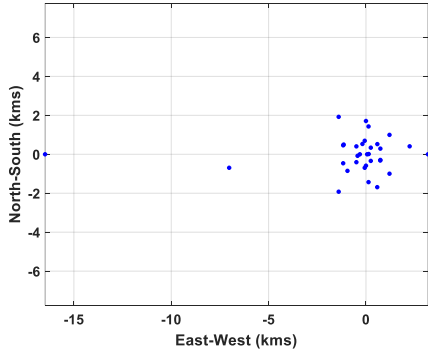


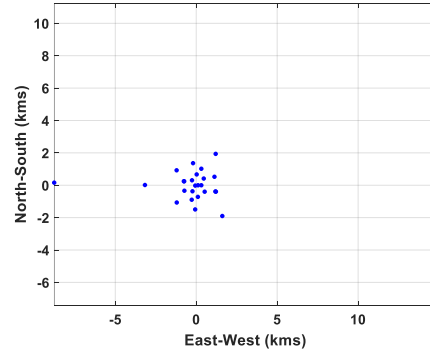
Figure 4.9: Array Distribution of GMRT (No. of Array Elements = 30)

TABLE – 4.1: VARIOUS CASES OF POLYHEDRON COMBINATIONS

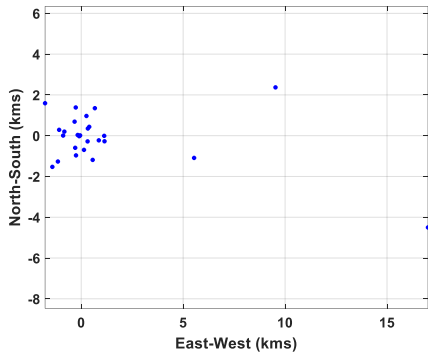
Case No.	Polyhedron Combination	Total No. of Antennas
1	Dodecahedron + Icosahedron	32
2	Dodecahedron + Octahedron	26
3	Cube + Octahedron + Icosahedron	26
4	Dodecahedron + Octahedron + Tetrahedron	30
5	Cube + Octahedron + Icosahedron + Tetrahedron	30
6	Dodecahedron + Cube + Tetrahedron	32
7	2 Cube + 2 Octahedron	28
8	Icosahedron + 3 Octahedron	30
9	3 Tetrahedron + Dodecahedron	32
10	2 Icosahedron + Octahedron	30



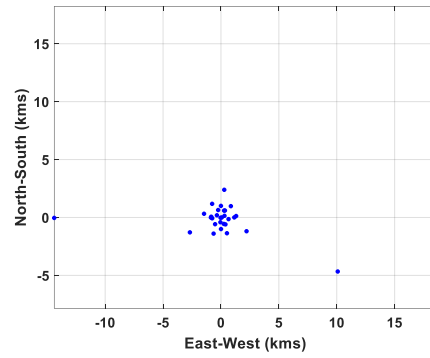
(a)



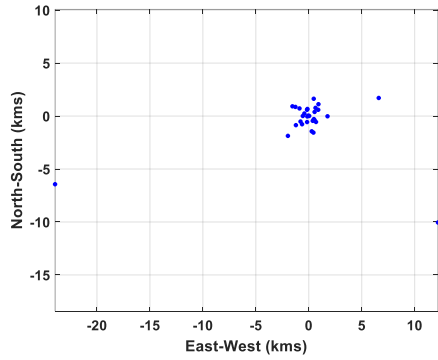
(b)



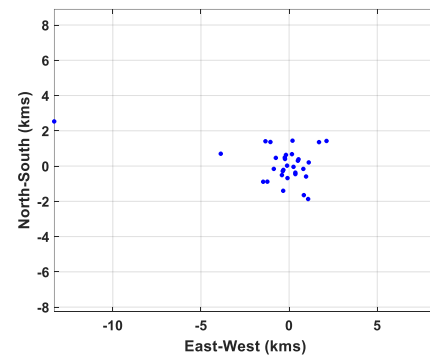
(c)



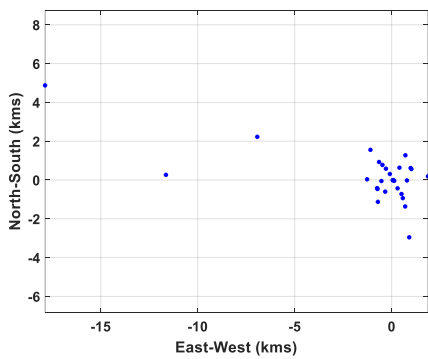
(d)



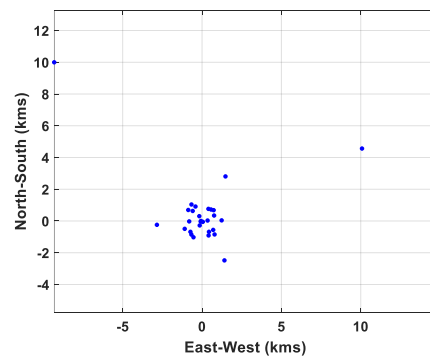
(e)



(f)



(g)



(h)

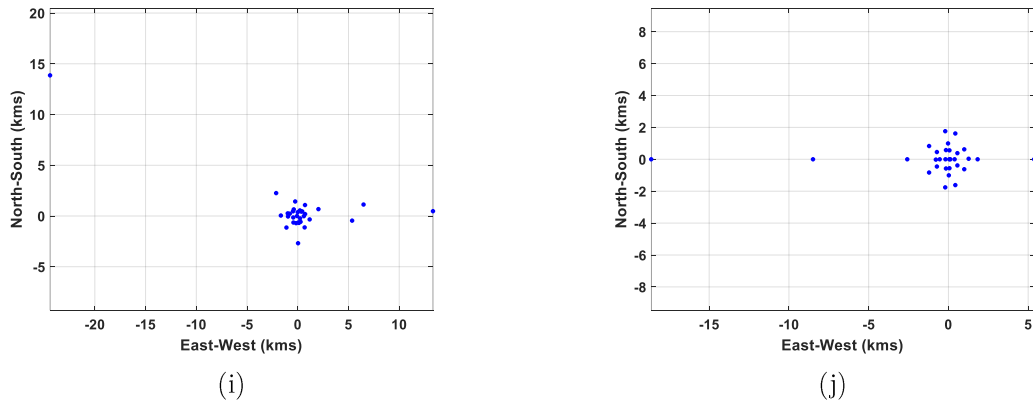


Figure 4.10: Array distributions of (a) case-1, (b) case-2, (c) case-3, (d) case-4, (e) case-5, (f) case-6, (g) case-7, (h) case-8, (i) case-9 and (j) case-10

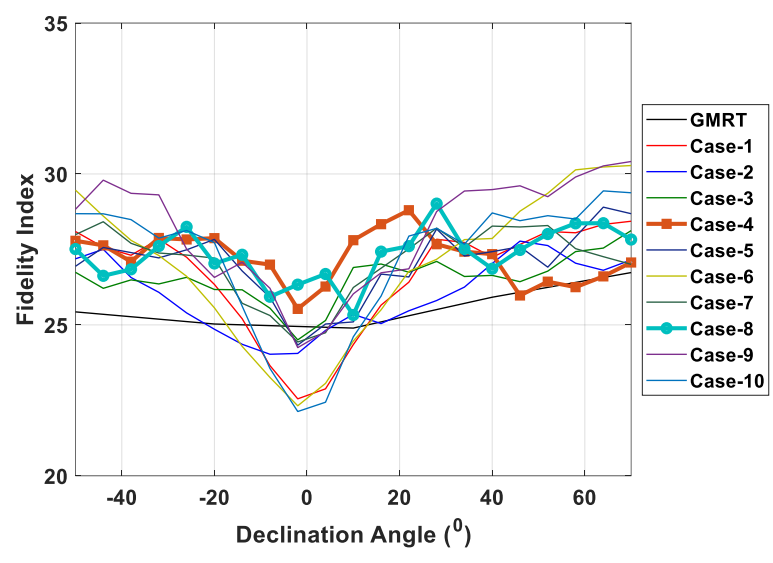


Figure 4.11: Fidelity Index for various declination angles for various cases of aperiodic arrays and GMRT array

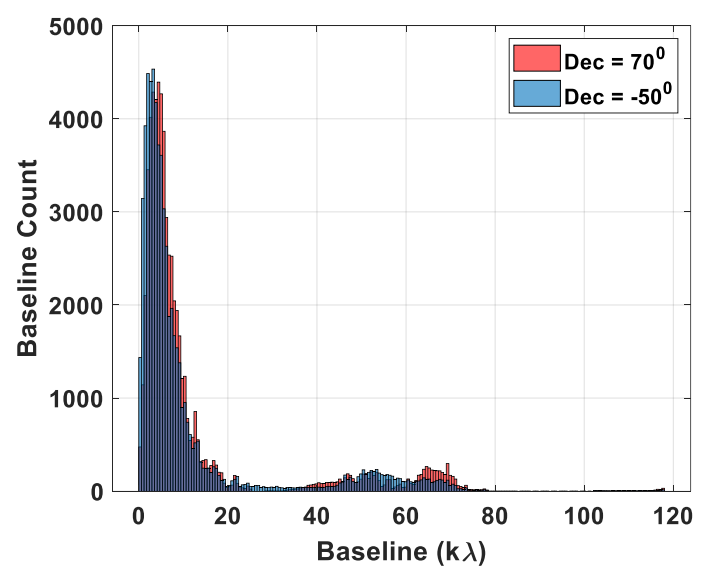
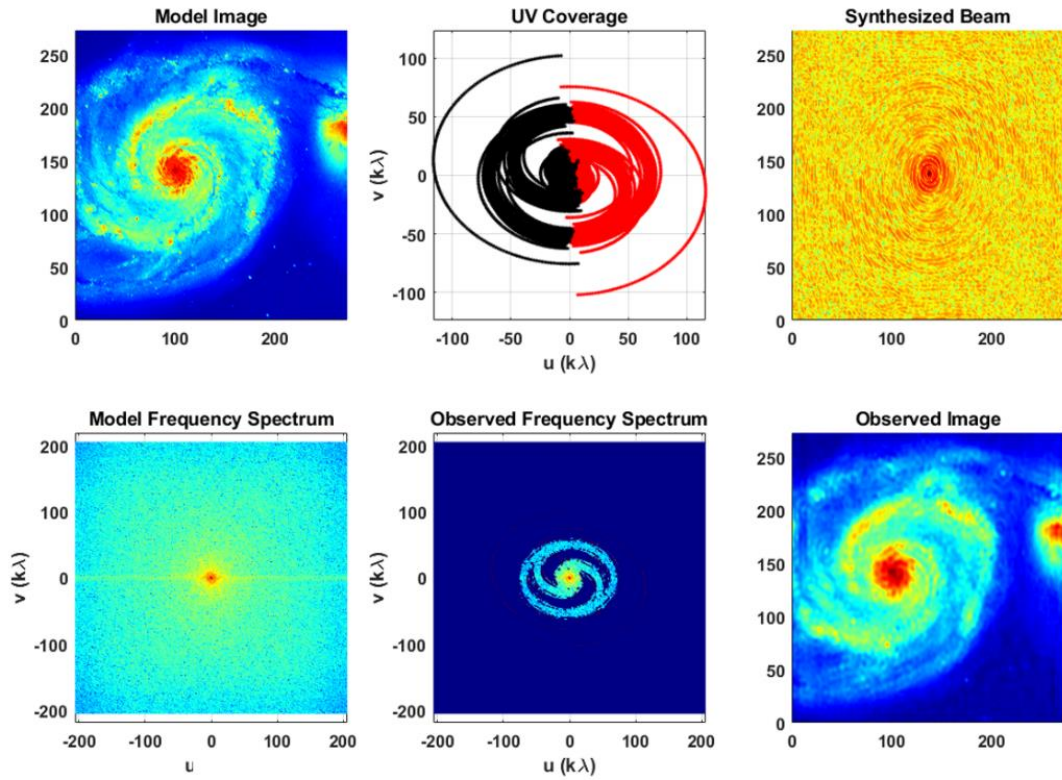
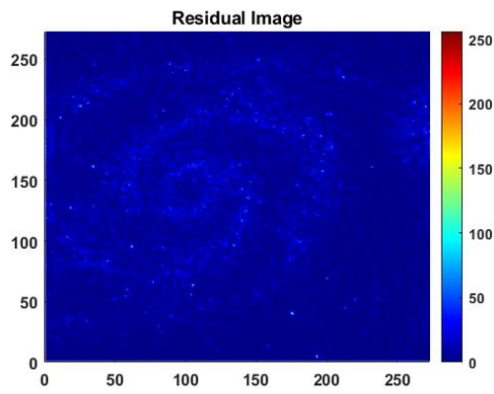


Figure 4.12: Histogram of baselines for Case-4 (Dodecahedron + Octahedron + Tetrahedron) and for -50° and 70° declination angles

Case 4: declinations = -50° , over 12hr observation, 1" image span



(a)



(b)

Figure 4.13: (a) Image sampling and generation using aperiodic array from the case – 4 and (b) residual image, for -50° declination angle

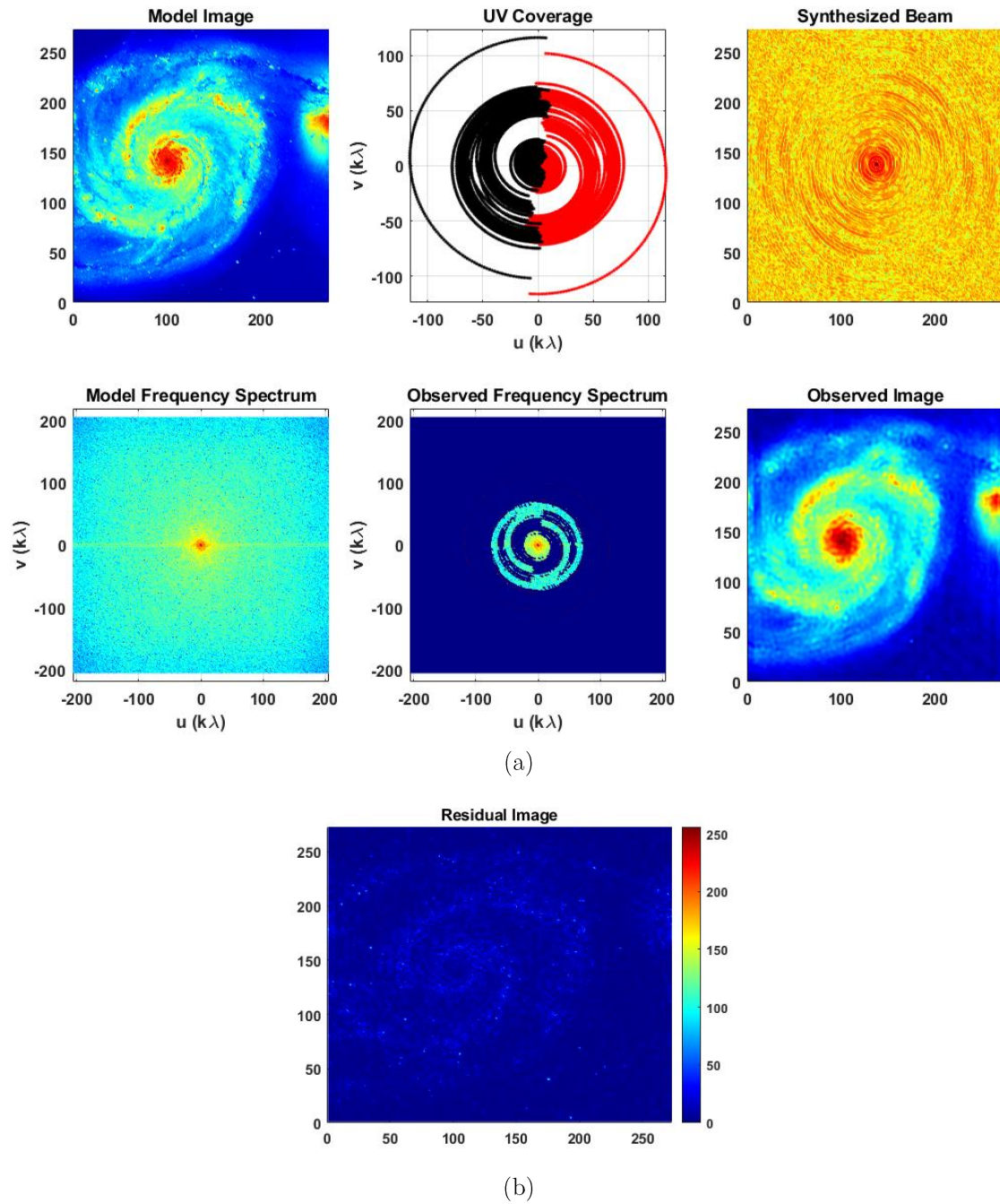


Figure. 4.14: (a) Image sampling and generation using aperiodic array from the case – 4 and (b) residual image, for 70° declination angle

Application B Direction of Arrival (DoA) using MVDR technique using proposed Aperiodic Array

Beamformers are, nowadays, the widely researched area in the field of communication, radar, acoustics, and sonar. The beamformers typically use the signal processing technique to compute the antenna weight factors by statistically evaluating the signal and noise, which forms the main lobe in the desired direction and nulls in the interference direction. Various types of

fundamental beamformers and their variants are studied in the literature [62]. To evaluate the performance of the proposed aperiodic array antenna presented in Chapter – 3, the minimum variance distortionless response (MVDR) type of beamformer has been adopted and used to implement the direction of arrival (DoA) estimate. The MVDR algorithm was offered by J. Capon in 1969 [63] and is currently a widely utilized adaptive beamforming algorithm. The concept of the algorithm is to minimize the variance of the residual noise at the output while constraining that the signals from the desired angular direction experience no distortion [64]. The such algorithm works very well in the high SNR and low noise scenario.

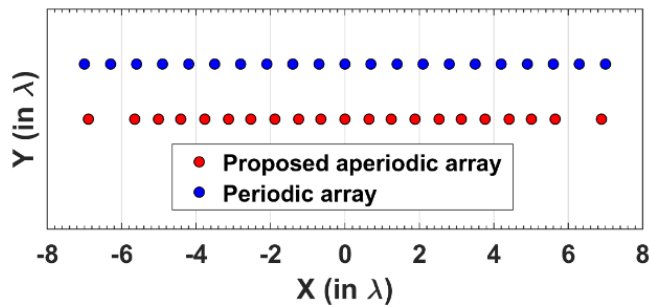


Figure 4.15: Proposed strip projection based aperiodic linear array and conventional periodic linear array

Here, Matlab codes have been developed to implement the MVDR-based DoA estimation using aperiodic and periodic linear arrays. The linear lattices of the proposed aperiodic and conventional periodic arrays are represented in Fig. 4.15 for reference. Fig. 4.16 shows the DoA estimation performance of the proposed strip projection-based aperiodic linear array and conventional periodic linear array, assuming the signal sources are at -20° and 30° with $\text{SNR} = 0\text{dB}$ at 9.6GHz . From Fig. 4.16, it can be observed that the proposed aperiodic linear array identified the signal sources unambiguously, whereas the conventional periodic array shows the signal source at -70° in addition to the desired two signal sources. The undesired lobe in the DoA estimation of the periodic array has transpired due to the periodic 0.7λ inter-element spacing. The addition of aperiodicity in the element positions has helped to remove such lobes. This proves that the proposed strip projection-based aperiodic linear array has strong potential to be used for beamformers.

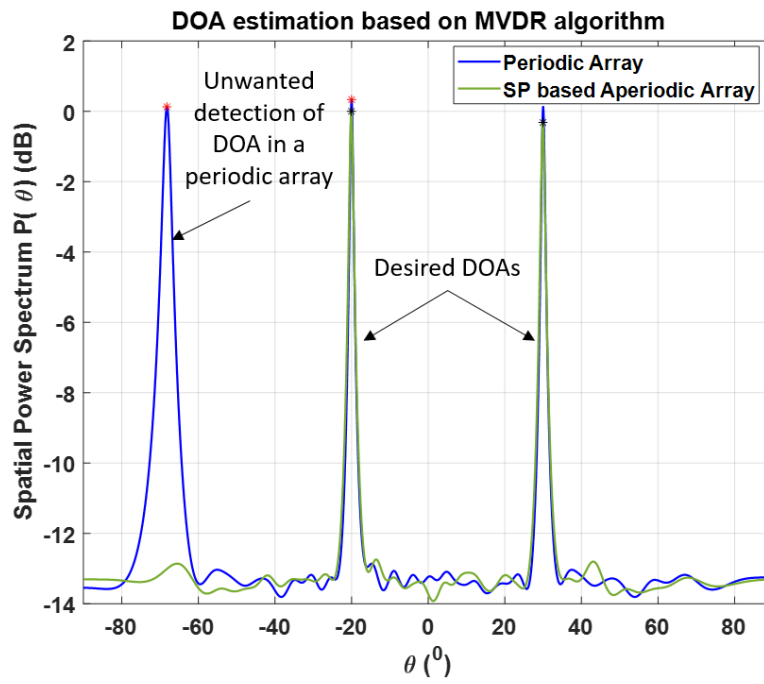


Figure 4.16: Angular plot of DoA estimation carried out by the proposed SP based aperiodic array and conventional aperiodic array

CHAPTER 5

Conclusion and Future Work

5.1 Conclusion

The thesis work mainly focuses on the aperiodic array design for the beam steerable antenna, offering farfield performance at par with the periodic array or better than it. The work has been initiated with the literature survey and understanding of the use of aperiodicity. The effect of aperture tapering on the grating lobe performance has been studied in detail by considering various types of aperture distributions. It has been concluded that the aperture tapering significantly impacts on the sidelobe performance. However, it has no noticeable effect on the grating lobe. To understand the effect of aperiodicity in the periodic environment, the subarray displacement concept has been studied for an 8 x 8 periodic array antenna, where 2 x 2, 3 x 3 and 4 x 4 element arrays are used as the array elements. In the 3D radiation pattern of the array with beam scan, it has been observed that the null lines are rotated and pass through the grating lobe peak, effectively dividing the energy in the grating into two lobes. Therefore, at-least 3-dB improvement in the peak SLL can be achieved. Furthermore, the aperiodic grouping has also been studied by implementing the Pinwheel based clustering of the 8 x 8 array antenna. The Pinwheel pattern has been generated and mapped on the array to form the aperiodic group. The grouping has been optimized for 10^0 beam scan and 20^0 beam scan. It has been found that 3.8dB and 6.6dB improvements in SLL performance have been achieved over the conventional 8 x 8 periodic array with a 2 x 2 subarray.

Taking inspiration from crystallography, the new strip-projection (SP) based method has been proposed to design an aperiodic beam steerable linear and planar array antenna. The SP method is discussed extensively, where the higher dimensional (3D) lattice points are projected on, the lower dimension (2D), which forms the aperiodic distribution on the 2D plane. The aperiodic distribution on the 2D plane varied with the rotation of the 3D lattice around any arbitrary vector. The rotation angle and arbitrary vector are optimized to achieve the desired farfield performance during the beam scan. Based on the formulation, analysis and results discussed in the thesis, it can be concluded that the proposed method is fast and efficient for the

design as it aids the optimization process and reduces the number of times the objective function is evaluated, offering the following advantages over other methods,

1. Unlike other optimization techniques, the SP method does not increase the number of optimization variables with aperture size. As discussed in the manuscript, w_h and θ_{Rot} are the two optimization variables for any length of the linear aperiodic array, which results in a significant benefit when the large beam steerable linear arrays are designed.
2. The synthesized aperiodic array layout using the SP method has improved peak SLL performance for 30° beam scan, as opposed to the aperiodic array layouts generated by GA, PSO and Jaya.
3. Implementing the SP method is relatively simpler and easier than the complex equation-based method.

To demonstrate the SP method for linear array, 21 elements aperiodic array having 15λ aperture length has been designed and optimized with the goal to achieve improved peak SLL performance up to 30° beam scan, as compared to the 21 elements periodic array. The designed array showed a 5.72dB improvement in peak SLL and 0.36dB improvement in scan loss for $\pm 30^\circ$ beam scan range without significantly impacting other far-field parameters. The designed aperiodic linear array has been populated with X-band electromagnetically coupled patch antennas and simulated. The antenna has also been developed and practically demonstrated the farfield performance in an anechoic chamber. The measured and analysed results are found to be in close agreement.

The SP method also has been implemented to design an aperiodic planar array antenna. Here, a 3D periodic body-centric tetragonal lattice has been used and its elements are projected on a 2D aperture plane. Rodrigue's rotation formula has been used to rotate a 3D lattice around any arbitrary vector. The optimization has been carried out to improve the peak SLL up to 30° beam scan and reduce the number of elements. It is interesting to note that a 21.9% element reduction has been achieved. The pinwheel based aperiodic array has also been designed and presented to compare with the proposed aperiodic planar array antenna. Both aperiodic array lattices have been populated with S-band cubic-shaped DR elements and simulated using a 3D electromagnetic finite element-based solver. The quantity called position standard deviation (σ_0) has been defined and computed to quantify the aperiodicity in the element distribution. It has

been concluded that the relatively large variance of the pinwheel lattice has resulted in significant energy spread in the radiation pattern.

As a variant of the SP method, the project concept has been generalized and applied for the projection of the vertices of the co-centric polyhedrons to form the aperiodic array for SLL improvement for $\pm 30^\circ$ beam scan. Here, two platonic solids, i.e., dodecahedron and icosahedron, have been placed co-centrally and their vertices have been projected on the aperture plane to form the quasi-periodic array lattice. The optimization of the array lattice for the peak SLL improvement has been carried out by optimizing the 3-axis angular orientations and scale factors of two polyhedrons. The analysis results of the optimized array lattice have shown a 4.2dB improvement in the peak SLL for $\pm 30^\circ$ beam scan. The presented design of the quasi-periodic array lattice has also been compared with the pinwheel type quasi-periodic array lattice and showed superior far-field performance for $\pm 30^\circ$ beam scan. S-band cubic-shaped coaxially fed dielectric resonator (DR) based array antenna has been modeled and simulated using the generated quasi-periodic array lattice. The quasi-periodic DR array antenna has been incorporated with a Voronoi boundary-based metallic fence and DCN for mutual coupling improvement between the array elements.

The concept of projection of the co-centric polyhedron has been explored further to design an interferometric array for radio astronomy. The required framework for the evaluation of the aperiodic array for astronomical observation has been developed in Matlab. The fidelity index (FI) has been defined to quantify the effectiveness of the array and the array has been optimized to achieve maximum FI value for the accurate recovery of the observed image. The aperiodic array distributions have been generated by the direct project and using stereographic projection. The FI values of the proposed aperiodic arrays have been computed for various combinations of polyhedrons and declination angles. The proposed aperiodic arrays have been compared to the existing GMRT array. It has been observed that case – 4 where the array designed using three co-centric polyhedrons, namely, Dodecahedron, Octahedron and Tetrahedron, offers better FI variation with declination for the recovery of 1" image observed over a 12hr timespan at 1.42GHz frequency.

In this thesis, the application of the aperiodic array antenna has also been addressed for the MVDR type beamformers. The proposed aperiodic linear array has been evaluated for DoA

estimation using the MVDR technique, and the results are compared with the conventional periodic linear array having 0.7λ inter-element spacing. It has been demonstrated that the periodic array detects the unwanted direction when the target direction is increased beyond $\pm 30^\circ$. Such lobes are significantly suppressed using the proposed aperiodic linear array for the same target detection range. Thus, the aperiodic array has showcased the significant possibilities for its use in such beamformers.

5.2 Future Work

The proposed SP method is highly versatile and straightforward to implement. In addition, the designer has the flexibility to select any higher dimensional lattice and project it onto lower dimensions and can design a variety of aperiodic arrays. In the thesis, the rotation angles of the lattice have been varied. In the future, the presented design flow can be used by introducing the linear offset to the lattice, and the rotation, which adds another degree of freedom to the design.

Currently, several active array-based Satcom terminals are available in the commercial market. The typical requirement of the array is to have a large conical scan angle $\sim \pm 50^\circ$. The majority of active arrays are designed using uniform array lattices. The design of an aperiodic array antenna using RF-IC has already been proposed and discussed, which has strong potential to replace such uniform array lattice based active arrays. The presented aperiodic planar array antenna may be further designed for practical applications like Satcom terminals.

The co-centric polyhedron-based approach presented for the design of an interferometric array is also versatile. It may be expanded by considering various other aspects of radio imaging, including quality of point spread function (PSF), multi-frequency operation, masking of real estate, the minimum length for the fiber connectivity and the possibility of on-site reconfigurability. Moreover, the proposed aperiodic array has also been presented as a promising candidate for various state-of-the-art beamformers, which are being developed for various applications, including communication, radar, acoustics, and sonar. Therefore, the scope of future work can also be defined to design the aperiodic array integrated with the beamformer using the proposed SP method.

References

- [1] F. Rusek, D. Persson, B. K. Lau, E. G. Larsson, T. L. Marzetta, and F. Tufvesson, "Scaling up MIMO: opportunities and challenges with very large arrays," *IEEE Signal Processing Magazine*, vol. 30, no. 1, pp. 40–60, 2013.
- [2] W. Wirth, *Radar techniques using array antennas*. London: The Institution of Engineering and Technology, 2013.
- [3] J. Kraus, A. Räsänen and M. Tiuri, *Radio astronomy*. Powell, Ohio: Cygnus-Quasar Books, 1986.
- [4] H. Unz, *Linear Arrays with Arbitrarily Distributed Elements*, November 1956.
- [5] H. Unz, "Linear arrays with arbitrarily distributed elements," *IRE Trans. on Antennas and Propagation*, vol. AP-8, pp. 222-223, March 1960.
- [6] D. D. King, R. F. Packard and R. K. Thomas, "Unequally spaced broad-band antenna arrays," *IRE Trans. on Antennas and Propagation*, vol. AP-8, pp. 380-385, July 1960.
- [7] R. Harrington, "Sidelobe reduction by nonuniform element spacing," *IRE Transactions on Antennas and Propagation*, vol. 9, no. 2, pp. 187-192, March 1961.
- [8] M. G. Bray, D. H. Werner, D. W. Boeringer and D. W. Machuga, "Optimization of Thinned Aperiodic Linear Phased Arrays using Genetic Algorithms to Reduce Grating Lobes During Scanning," *IEEE Transactions on Antennas and Propagation*, vol. 50, pp. 1732-1742, December 2002.
- [9] V. Pierro, V. Galdi, G. Castaldi, I. M. Pinto, L. B. Felsen, "Radiation Properties of Planar Antenna Arrays Based on Certain Categories of Aperiodic Tilings," *IEEE Transactions on Antennas and Propagation*, vol. 53, pp. 635-644, February 2005.
- [10] T. Isernia, M. Durso, and O. Bucci, "A Simple Idea for an Effective Sub-Arraying of Large Planar Sources," *IEEE Antennas and Wireless Propagation Letters*, vol. 8, pp. 169–172, 2009.
- [11] W. C. Barott and P. G. Steffes, "Grating Lobe Reduction in Aperiodic Linear Arrays of Physically Large Antennas," *IEEE Antennas and Wireless Propagation Letters*, vol. 8, pp. 406-408, 2009.

- [12] T. Azar, "Overlapped Subarrays: Review and Update [Education Column]," *IEEE Antennas and Propagation Magazine*, vol. 55, no. 2, pp. 228–234, 2013.
- [13] A. Kedar, "Deterministic Synthesis Approach for Linear Sparse Array Antennas," *IEEE Transactions on Antennas and Propagation*, vol. 68, no. 9, pp. 6667-6674, Sept. 2020.
- [14] D. H. Werner, W. Kuhirun and P. L. Werner, "Fractile arrays: a new class of tiled arrays with fractal boundaries," *IEEE Transactions on Antennas and Propagation*, vol. 52, no. 8, pp. 2008-2018, Aug. 2004.
- [15] T. G. Spence, D. H. Werner and J. N. Carvajal, "Modular Broadband Phased-Arrays Based on a Nonuniform Distribution of Elements Along the Peano-Gosper Space-Filling Curve," *IEEE Transactions on Antennas and Propagation*, vol. 58, no. 2, pp. 600-604, Feb. 2010.
- [16] T. G. Spence and D. H. Werner, "Design of Broadband Planar Arrays Based on the Optimization of Aperiodic Tilings," *IEEE Transactions on Antennas and Propagation*, vol. 56, no. 1, pp. 76-86, Jan. 2008.
- [17] Y. Lo, "A mathematical theory of antenna arrays with randomly spaced elements," *IEEE Transactions on Antennas and Propagation*, vol. 12, no. 3, pp. 257-268, May 1964.
- [18] V. D. Agrawal and Y. T. Lo, "Distribution of sidelobe level in random arrays," *Proceedings of the IEEE*, vol. 57, no. 10, pp. 1764-1765, Oct. 1969.
- [19] B. Steinberg, "The peak sidelobe of the phased array having randomly located elements," *IEEE Transactions on Antennas and Propagation*, vol. 20, no. 2, pp. 129-136, March 1972.
- [20] B. Steinberg, "Comparison between the peak sidelobe of the random array and algorithmically designed aperiodic arrays," *IEEE Transactions on Antennas and Propagation*, vol. 21, no. 3, pp. 366-370, May 1973.
- [21] M. Donvito and S. Kassam, "Characterization of the random array peak sidelobe," *IEEE Transactions on Antennas and Propagation*, vol. 27, no. 3, pp. 379-385, May 1979.
- [22] W. J. Hendricks, "The totally random versus the bin approach for random arrays," *IEEE Transactions on Antennas and Propagation*, vol. 39, no. 12, pp. 1757-1762, Dec. 1991.

- [23] K. C. Kerby and J. T. Bernhard, "Sidelobe level and wideband behavior of arrays of random subarrays," *IEEE Transactions on Antennas and Propagation*, vol. 54, no. 8, pp. 2253-2262, Aug. 2006.
- [24] Giovanni Buonanno and Raffaele Solimene, "Large Linear Random Symmetric Arrays," *Progress In Electromagnetics Research M*, Vol. 52, 67-77, 2016.
- [25] Y. Chow, "Comparison of some correlation array configurations for radio astronomy," *IEEE Transactions on Antennas and Propagation*, vol. 18, no. 4, pp. 567-569, 1970.
- [26] N. Treloar, "Investigation of Array Configuration for An Aperture Synthesis Radio Telescope," *J. Roy. Astron. Soc. Can.*, vol. 83, no. 2, pp. 92-104, 1989.
- [27] E. Keto, "The Shapes of Cross-Correlation Interferometers," *The Astrophysical Journal*, vol. 475, no. 2, pp. 843-852, 1997.
- [28] Y. Su, R. Nan, B. Peng, N. Roddis and J. Zhou, "Optimization of interferometric array configurations by 'sieving' $u - v$ points," *Astronomy & Astrophysics*, vol. 414, no. 1, pp. 389-397, 2004.
- [29] M. de Villiers, "Interferometric array layout design by tomographic projection," *Astronomy & Astrophysics*, vol. 469, no. 2, pp. 793-797, 2007.
- [30] N. Patra, N. Kanekar, J. Chengalur et al., "The expanded Giant Metrewave Radio Telescope," *Monthly Notices of the Royal Astronomical Society (MNRAS)*, pp. 3007-3021, 2019.
- [31] W. Montlouis and P.-R. J. Cornely, "Direction of Arrival and Angular Velocities (DOAV) Estimation using Minimum Variance Beamforming," *2007 IEEE Radar Conference*, Waltham, MA, USA, 2007, pp. 641-646.
- [32] T. Ohira and K. Gyoda, "Electronically steerable passive array radiator antennas for low-cost analog adaptive beamforming," *Proceedings 2000 IEEE International Conference on Phased Array Systems and Technology (Cat. No.00TH8510)*, 2000.
- [33] R. Qian, M. Sellathurai and D. Wilcox, "A Study on MVDR Beamforming Applied to an ESPAR Antenna," *IEEE Signal Processing Letters*, vol. 22, no. 1, pp. 67-70, Jan. 2015.

- [34] X. Wang and M. Amin, "Design of optimum sparse array for robust MVDR beamforming against DOA mismatch," *2017 IEEE 7th International Workshop on Computational Advances in Multi-Sensor Adaptive Processing (CAMSAP)*, , 2017.
- [35] Y. V. Krivosheev, A. V. Shishlov and V. V. Denisenko, "Grating Lobe Suppression in Aperiodic Phased Array Antennas Composed of Periodic Subarrays with Large Element Spacing," *IEEE Antennas and Propagation Magazine*, vol. 57, no. 1, pp. 76-85, Feb. 2015.
- [36] M. Marder, "Order versus symmetry in pinwheel tilings of the plane," *Physical Review B*, vol. 48, no. 18, pp. 13971–13973, Nov. 1993.
- [37] N. P. Frank and M. F. Whittaker, "A Fractal Version of the Pinwheel Tiling," *The Mathematical Intelligencer*, vol. 33, no. 2, pp. 7–17, May 2011.
- [38] <https://www.ansys.com/products/electronics/antennas>.
- [39] H. M. Pandey, "Jaya a novel optimization algorithm: What, how and why?," *2016 6th International Conference - Cloud System and Big Data Engineering (Confluence)*, 2016.
- [40] A. A. Kishk, "Dielectric resonator antenna elements for array applications," *IEEE International Symposium on Phased Array Systems and Technology, 2003.*, 2003, pp. 300-305.
- [41] R. C. Hansen, *Phased array antennas*. New York: Wiley, 2009.
- [42] L. H. Gabrielli and H. E. Hernandez-Figueroa, "Aperiodic Antenna Array for Secondary Lobe Suppression," in *IEEE Photonics Technology Letters*, vol. 28, no. 2, pp. 209-212, 15 Jan.15, 2016.
- [43] P. L. T. Bui, P. Rocca and R. L. Haupt, "Aperiodic Planar Array Synthesis Using Pseudo-Random Sequences," *2018 International Applied Computational Electromagnetics Society Symposium - China (ACES)*, 2018, pp. 1-2.
- [44] T. N. Kaifas, D. G. Babas and J. N. Sahalos, "Design of Planar Arrays With Reduced Nonuniform Excitation Subject to Constraints on the Resulting Pattern and the Directivity," *IEEE Transactions on Antennas and Propagation*, vol. 57, no. 8, pp. 2270-2278, Aug. 2009.
- [45] R. L. Haupt, "Thinned arrays using genetic algorithms," *IEEE Transactions on Antennas and Propagation*, vol. 42, no. 7, pp. 993-999, July 1994.

- [46] J.-C. S. Chieh et al., "Development of Flat Panel Active Phased Array Antennas Using 5G Silicon RFICs at Ku- and Ka-Bands," *IEEE Access*, vol. 8, pp. 192669–192681, 2020.
- [47] X. Gu et al., "Development, Implementation, and Characterization of a 64-Element Dual-Polarized Phased-Array Antenna Module for 28-GHz High-Speed Data Communications," *IEEE Transactions on Microwave Theory and Techniques*, vol. 67, no. 7, pp. 2975–2984, Jul. 2019.
- [48] P. Cromwell, *Polyhedra*. Cambridge: Cambridge University Press, 2008.
- [49] F. P. Preparata and M. I. Shamos, *Computational Geometry*. Springer Science & Business Media, 2012.
- [50] J. Andersen and H. Rasmussen, "Decoupling and descattering networks for antennas," *IEEE Transactions on Antennas and Propagation*, vol. 24, no. 6, pp. 841–846, November 1976.
- [51] S.-C. Chen, Y.-S. Wang and S.-J. Chung, "A Decoupling Technique for Increasing the Port Isolation Between Two Strongly Coupled Antennas," *IEEE Transactions on Antennas and Propagation*, vol. 56, no. 12, pp. 3650–3658, Dec. 2008.
- [52] <https://www.vla.nrao.edu/>
- [53] <https://www.e-merlin.ac.uk/>
- [54] <https://www.narrabri.atnf.csiro.au/>
- [55] <https://www.almaobservatory.org/en/home/>
- [56] <http://www.gmrt.ncra.tifr.res.in/>
- [57] <https://www.skatelescope.org/the-ska-project/>
- [58] J. D. Kraus, M. E. Tiuri, Räsänen Antti V., and T. D. Carr, *Radio astronomy*. Durham: Cygnus-Quasar, 2005.
- [59] T. L. Wilson, K. Rohlfs, and S. Hüttemeister, *Tools of radio astronomy*. Berlin, Heidelberg: Springer Berlin Heidelberg, 2009.
- [60] A. R. Thompson, J. M. Moran, and G. W. Swenson, *Interferometry and synthesis in radio astronomy*. New York: Wiley, 2001.
- [61] E. Saff, *Fundamentals of Complex Analysis with Applications to Engineering*. Harlow: Pearson, 2013.

- [62] V. T. H. L., *Optimum array processing: Part IV of detection, estimation and modulation theory*. New York: John Wiley & Sons, 2002.
- [63] J. Capon, “High-resolution frequency-wavenumber spectrum analysis,” *Proceedings of the IEEE*, vol. 57, no. 8, pp. 1408–1418, 1969.
- [64] C. Pan, J. Chen, and J. Benesty, “Performance Study of the MVDR Beamformer as a Function of the Source Incidence Angle,” *IEEE/ACM Transactions on Audio, Speech, and Language Processing*, vol. 22, no. 1, pp. 67–79, Jan. 2014.

List of Publications

International Journals

- [1] P. Mevada, S. Gupta, S. Chakrabarty and M. Mahajan, "Design of Beam-Steerable Aperiodic Linear Array Antenna With Improved Peak SLL Using Strip-Projection Method," in *IEEE Transactions on Antennas and Propagation*, vol. 70, no. 7, pp. 5430-5436, July 2022.
- [2] P. Mevada, S. Gupta, S. Chakrabarty and M. Mahajan, "A novel approach for design of beam steerable aperiodic planar array antenna with reduced number of elements", in *Journal of Electromagnetic Waves and Applications*, vol. 36, no. 6, pp. 748-766, 2021.

International Conferences

- [3] P. Mevada, S. Gupta, S. Kulshreshtha, S. Chakrabarty and M. Mahajan, "Analysis of Pinwheel type Aperiodic Clustering for Sidelobe level Improvement in Phased Array Antenna," *2020 IEEE International Symposium on Antennas and Propagation and North American Radio Science Meeting*, 2020, pp. 351-352.
- [4] P. Mevada, S. Gupta, S. Kulshrestha, S. Chakrabarty and M. Mahajan, "Study of Effect of Aperture Tapering on Grating Lobe in Array Antenna," *2019 IEEE Indian Conference on Antennas and Propagation (InCAP)*, 2019, pp. 1-4.

ANNEXURE A

List of Element Locations in the Proposed Aperiodic Planar Array

1			2			3			4			5			6			7			8		
Elem. No.	X(λ)	Y(λ)	Elem. No.	X(λ)	Y(λ)	Elem. No.	X(λ)	Y(λ)	Elem. No.	X(λ)	Y(λ)	Elem. No.	X(λ)	Y(λ)	Elem. No.	X(λ)	Y(λ)	Elem. No.	X(λ)	Y(λ)	Elem. No.	X(λ)	Y(λ)
1	6.73	7.3	51	2.19	4.75	101	-0.85	6.32	151	-3.51	5.46	201	-2.35	2.2	251	-1.66	-0.51	301	-4.31	-1.38	351	-3.91	-6.69
2	6.95	5.12	52	2.69	5.17	102	-2.33	6.03	152	-4.48	5.58	202	-3.32	2.33	252	-2.63	-0.39	302	-3.81	-0.96	352	-3.4	-6.27
3	6.48	5.65	53	1.72	5.29	103	-1.82	6.44	153	-3.97	5.99	203	-2.82	2.74	253	-2.13	0.02	303	-4.78	-0.84	353	-2.9	-5.86
4	6.99	6.07	54	2.23	5.7	104	-2.79	6.57	154	-4.94	6.11	204	-3.79	2.86	254	-3.1	0.15	304	-4.28	-0.43	354	-4.37	-6.15
5	6.02	6.19	55	0.75	5.41	105	-2.29	6.98	155	-4.44	6.53	205	-3.28	3.28	255	-2.6	0.56	305	-5.25	-0.3	355	-3.87	-5.74
6	6.52	6.6	56	1.26	5.82	106	-3.26	7.1	156	-5.41	6.65	206	-4.25	3.4	256	-4.07	0.27	306	-4.74	0.11	356	-4.84	-5.62
7	5.55	6.72	57	1.76	6.24	107	6.83	-4.43	157	-4.9	7.07	207	-3.75	3.81	257	-3.57	0.68	307	-6.22	-0.18	357	-4.34	-5.2
8	6.06	7.14	58	0.29	5.94	108	6.36	-3.9	158	-5.87	7.19	208	-4.72	3.93	258	-3.06	1.1	308	-5.71	0.23	358	-5.31	-5.08
9	4.58	6.85	59	0.79	6.36	109	6.87	-3.48	159	-6.85	7.31	209	-4.22	4.35	259	-4.54	0.8	309	-5.21	0.65	359	-4.8	-4.67
10	5.08	7.26	60	1.29	6.77	110	5.9	-3.36	160	7.05	-6.61	210	-5.69	4.06	260	-4.03	1.22	310	-6.68	0.35	360	-5.77	-4.54
11	7.17	2.94	61	-0.18	6.48	111	6.4	-2.95	161	6.59	-6.08	211	-5.19	4.47	261	-3.53	1.63	311	-6.18	0.77	361	-5.27	-4.13
12	6.2	3.06	62	0.32	6.89	112	5.43	-2.83	162	7.09	-5.66	212	-4.68	4.88	262	-5	1.34	312	-5.68	1.18	362	-6.74	-4.42
13	6.71	3.47	63	-0.65	7.02	113	5.93	-2.41	163	6.12	-5.54	213	-6.16	4.59	263	-4.5	1.75	313	-7.15	0.89	363	-6.24	-4.01
14	7.21	3.89	64	7.11	-1.84	114	4.96	-2.29	164	6.62	-5.13	214	-5.65	5.01	264	-5.47	1.88	314	-6.65	1.3	364	-5.74	-3.59
15	5.74	3.59	65	6.65	-1.3	115	5.47	-1.88	165	5.65	-5.01	215	-6.62	5.13	265	-4.96	2.29	315	-7.11	1.84	365	-7.21	-3.89
16	6.24	4.01	66	7.15	-0.89	116	4.5	-1.75	166	6.16	-4.59	216	-6.12	5.54	266	-5.93	2.41	316	0.65	-7.02	366	-6.71	-3.47
17	6.74	4.42	67	5.68	-1.18	117	5	-1.34	167	4.68	-4.88	217	-7.09	5.66	267	-5.43	2.83	317	-0.32	-6.89	367	-6.2	-3.06
18	5.27	4.13	68	6.18	-0.77	118	3.53	-1.63	168	5.19	-4.47	218	-6.59	6.08	268	-6.4	2.95	318	0.18	-6.48	368	-7.17	-2.94
19	5.77	4.54	69	6.68	-0.35	119	4.03	-1.22	169	5.69	-4.06	219	-7.05	6.61	269	-5.9	3.36	319	-1.29	-6.77	369	-5.08	-7.26
20	4.8	4.67	70	5.21	-0.65	120	4.54	-0.8	170	4.22	-4.35	220	6.85	-7.31	270	-6.87	3.48	320	-0.79	-6.36	370	-4.58	-6.85
21	5.31	5.08	71	5.71	-0.23	121	3.06	-1.1	171	4.72	-3.93	221	5.87	-7.19	271	-6.36	3.9	321	-0.29	-5.94	371	-6.06	-7.14
22	4.34	5.2	72	6.22	0.18	122	3.57	-0.68	172	3.75	-3.81	222	4.9	-7.07	272	-6.83	4.43	322	-1.76	-6.24	372	-5.55	-6.72
23	4.84	5.62	73	4.74	-0.11	123	4.07	-0.27	173	4.25	-3.4	223	5.41	-6.65	273	3.26	-7.1	323	-1.26	-5.82	373	-6.52	-6.6
24	3.87	5.74	74	5.25	0.3	124	2.6	-0.56	174	3.28	-3.28	224	4.44	-6.53	274	2.29	-6.98	324	-0.75	-5.41	374	-6.02	-6.19
25	4.37	6.15	75	4.28	0.43	125	3.1	-0.15	175	3.79	-2.86	225	4.94	-6.11	275	2.79	-6.57	325	-2.23	-5.7	375	-6.99	-6.07
26	2.9	5.86	76	4.78	0.84	126	2.13	-0.02	176	2.82	-2.74	226	3.97	-5.99	276	1.82	-6.44	326	-1.72	-5.29	376	-6.48	-5.65
27	3.4	6.27	77	3.81	0.96	127	2.63	0.39	177	3.32	-2.33	227	4.48	-5.58	277	2.33	-6.03	327	-2.69	-5.17	377	-6.95	-5.12
28	3.91	6.69	78	4.31	1.38	128	1.66	0.51	178	2.35	-2.2	228	3.51	-5.46	278	0.85	-6.32	328	-2.19	-4.75	378	-6.73	-7.3
29	2.43	6.39	79	3.34	1.5	129	2.17	0.93	179	2.85	-1.79	229	4.01	-5.04	279	1.36	-5.91	329	-3.16	-4.63			
30	2.94	6.81	80	3.85	1.91	130	1.2	1.05	180	1.38	-2.08	230	2.53	-5.34	280	1.86	-5.49	330	-2.66	-4.21			
31	3.44	7.22	81	2.88	2.03	131	1.7	1.46	181	1.88	-1.67	231	3.04	-4.92	281	0.39	-5.79	331	-3.63	-4.09			
32	1.97	6.93	82	3.38	2.45	132	0.73	1.58	182	2.39	-1.25	232	3.54	-4.51	282	0.89	-5.37	332	-3.12	-3.68			
33	6.89	0.34	83	1.91	2.16	133	1.23	2	183	0.91	-1.55	233	2.07	-4.8	283	1.4	-4.96	333	-4.09	-3.56			
34	6.42	0.88	84	2.41	2.57	134	-0.24	1.7	184	1.42	-1.13	234	2.57	-4.39	284	-0.08	-5.25	334	-3.59	-3.14			
35	6.93	1.29	85	2.91	2.98	135	0.26	2.12	185	1.92	-0.72	235	1.6	-4.26	285	0.43	-4.84	335	-5.06	-3.44			
36	5.96	1.41	86	1.44	2.69	136	0.77	2.53	186	0.45	-1.01	236	2.11	-3.85	286	-0.55	-4.71	336	-4.56	-3.02			
37	6.46	1.83	87	1.94	3.11	137	-0.71	2.24	187	0.95	-0.6	237	1.14	-3.73	287	-0.04	-4.3	337	-4.05	-2.61			
38	5.49	1.95	88	0.97	3.23	138	-0.2	2.66	188	-0.02	-0.48	238	1.64	-3.31	288	-1.01	-4.18	338	-5.53	-2.9			
39	6	2.36	89	1.48	3.64	139	-1.17	2.78	189	0.49	-0.06	239	0.67	-3.19	289	-0.51	-3.76	339	-5.02	-2.48			
40	5.02	2.48	90	0.51	3.76	140	-0.67	3.19	190	-0.49	0.06	240	1.17	-2.78	290	-1.48	-3.64	340	-6	-2.36			
41	5.53	2.9	91	1.01	4.18	141	-1.64	3.31	191	0.02	0.48	241	0.2	-2.66	291	-0.97	-3.23	341	-5.49	-1.95			
42	4.05	2.61	92	0.04	4.3	142	-1.14	3.73	192	-0.95	0.6	242	0.71	-2.24	292	-1.94	-3.11	342	-6.46	-1.83			
43	4.56	3.02	93	0.55	4.71	143	-2.11	3.85	193	-0.45	1.01	243	-0.77	-2.53	293	-1.44	-2.69	343	-5.96	-1.41			
44	5.06	3.44	94	-0.43	4.84	144	-1.6	4.26	194	-1.92	0.72	244	-0.26	-2.12	294	-2.91	-2.98	344	-6.93	-1.29			
45	3.59	3.14	95	0.08	5.25	145	-2.57	4.39	195	-1.42	1.13	245	0.24	-1.7	295	-2.41	-2.57	345	-6.42	-0.88			
46	4.09	3.56	96	-1.4	4.96	146	-2.07	4.8	196	-0.91	1.55	246	-1.23	-2	296	-1.91	-2.16	346	-6.89	-0.34			
47	3.12	3.68	97	-0.89	5.37	147	-3.54	4.51	197	-2.39	1.25	247	-0.73	-1.58	297	-3.38	-2.45	347	-1.97	-6.93			
48	3.63	4.09	98	-0.39	5.79	148	-3.04	4.92	198	-1.88	1.67	248	-1.7	-1.46	298	-2.88	-2.03	348	-3.44	-7.22			
49	2.66	4.21	99	-1.86	5.49	149	-2.53	5.34	199	-1.38	2.08	249	-1.2	-1.05	299	-3.85	-1.91	349	-2.94	-6.81			
50	3.16	4.63	100	-1.36	5.91	150	-4.01	5.04	200	-2.85	1.79	250	-2.17	-0.93	300	-3.34	-1.5	350	-2.43	-6.39			